ORTA DOĞU TEKNİK ÜNİVERSİTESİ
FEN BİLİMLERİ ENSTİTÜSÜ MÜDÜRLÜĞÜ

TEZ ŞABLONU ONAY FORMU
THESIS TEMPLATE CONFIRMATION FORM

1. Şablonda verilen yerleşim ve boşluklar değiştirilmemelidir.
2. Jüri tarihi Başlık Sayfası, İmza Sayfası, Abstract ve Öz'de ilgili yerlere yazılmalıdır.
3. İmza sayfasında jüri üyelerinin unvanları doğru olarak yazılmalıdır.
4. Tezin son sayfasının sayfa numarası Abstract ve Öz'de ilgili yerlere yazılmalıdır.
5. Bütün chapterlar, referanslar, ekler ve CV sağ sayfada başlamalıdır. Bunun için **kesmeler** kullanılmıştır. **Kesmelerin kayması** fazladan boş sayfaların oluşmasına sebep olabilir. Bu gibi durumlarda paragraf (¶) işaretine tıklayarak kesmeleri görünür hale getirin ve yerlerini **kontrol edin**.
6. Figürler ve tablolar kenar boşluklarına taşmamalıdır.
7. Şablonda yorum olarak eklenen uyarılar dikkatle okunmalı ve uygulanmalıdır.
8. Tez yazdırılmadan önce PDF olarak kaydedilmelidir. Şablonda yorum olarak eklenen uyarılar PDF dokümanında yer almamalıdır.
9. **Bu form aracılığıyla oluşturulan PDF dosyası arkalı-önlü baskı alınarak tek bir spiralli cilt haline getirilmelidir.**
10. Spiralli hale getirilen tez taslağınızdaki ilgili alanları imzalandıktan sonra, Tez Juri Atama Formu ile birlikte bölüm sekreterliğine teslim edilmelidir.
11. Tez taslağınız bölüm sekreterliğiniz aracılığıyla format ve görünüm açısından kontrol edilmek üzere FBE'ye ulaştırılacaktır.
12. FBE tarafından kontrol işlemleri tamamlanan tez taslakları, öğrencilere teslim edilmek üzere bölüm sekreterliklerine iletilecektir.
13. Tez taslaklarının kontrol işlemleri tamamlandığında, bu durum öğrencilere METU uzantılı öğrenci e-posta adresleri aracılığıyla duyurulacaktır.
14. Tez taslakları bölüm sekreterlikleri tarafından öğrencilere iletileceği için öğrencilerimizin tez taslaklarını enstitümüzden elden alma konusunda ısrarcı olmamaları beklenmektedir.
15. Tez yazım süreci ile ilgili herhangi bir sıkıntı yaşarsanız, **Sıkça Sorulan Sorular (SSS)** sayfamızı ziyaret ederek yaşadığınız sıkıntıyla ilgili bir çözüm bulabilirsiniz.

1. Do not change the spacing and placement in the template.
2. Write defense date to the related places given on Title page, Approval page, Abstract and Öz.
3. Write the titles of the examining committee members correctly on Approval Page.
4. Write the page number of the last page in the related places given on Abstract and Öz pages.
5. All chapters, references, appendices and CV must be started on the right page. **Section Breaks** were used for this. **Change in the placement** of section breaks can result in extra blank pages. In such cases, make the section breaks visible by clicking paragraph (¶) mark and **check their position.**
6. All figures and tables must be given inside the page. Nothing must appear in the margins.
7. All the warnings given on the comments section through the thesis template must be read and applied.
8. Save your thesis as pdf and Disable all the comments before taking the printout.
9. **Print two-sided the PDF file that you have created through this form and make a single spiral bound.**
10. Once you have signed the relevant fields in your thesis draft that you spiraled, submit it to the department secretary together with your Thesis Jury Assignment Form.
11. Your thesis draft will be delivered to the GSNAS via your department secretary for controlling in terms of format and appearance.
12. The thesis drafts that are controlled by GSNAS, will be sent to the department secretary to be delivered to the students.
13. This will be announced to the students via their METU students e-mail addresses when the control of the thesis drafts has been completed.
14. As the thesis drafts will be delivered to the students by the department secretaries, we are expecting from our students no to insist about getting their theses drafts from the Institute.
15. If you have any problems with the thesis writing process, you may visit our **Frequently Asked Questions (FAQ)** page and find a solution to your problem.

☒ **Yukarıda bulunan tüm maddeleri okudum, anladım ve kabul ediyorum. / I have read, understand and accept all of the items above.**

Name : **Ozan**
Surname : **Adıgüzel**
E-Mail : **ozan.adiguzel@metu.edu.tr**
Date : **03.09.2020**
Signature : _____

STRUCTURAL OPTIMIZATION OF A JET TRAINER WING STRUCTURE UNDER STRENGTH AND STIFFNESS RELATED CONSTRAINTS

A THESIS SUBMITTED TO
THE GRADUATE SCHOOL OF NATURAL AND APPLIED SCIENCES
OF
MIDDLE EAST TECHNICAL UNIVERSITY

BY

OZAN ADIGÜZEL

IN PARTIAL FULFILLMENT OF THE REQUIREMENTS
FOR
THE DEGREE OF MASTER OF SCIENCE
IN
AEROSPACE ENGINEERING

SEPTEMBER 2020

Approval of the thesis:

THESIS TITLE

submitted by **OZAN ADIGÜZEL** in partial fulfillment of the requirements for the degree of **Master of Science** i**n Aerospace Engineering, Middle East Technical University** by,

Prof. Dr. Halil Kalıpçılar
Dean, Graduate School of **Natural and Applied Sciences** _____

Prof. Dr. İsmail Hakkı Tuncer
Head of the Department, **Aerospace Engineering** _____

Assoc. Prof. Dr. Melin Şahin
Supervisor, **Aerospace Engineering, METU** _____

Examining Committee Members:

Prof. Dr. Altan Kayran
Aerospace Engineering, METU _____

Assoc. Prof. Dr. Melin Şahin
Aerospace Engineering, METU _____

Prof. Dr. Serkan Özgen
Aerospace Engineering, METU _____

Assoc. Prof. Dr. Ercan Gürses
Aerospace Engineering, METU _____

Prof. Dr. Erdem Acar
Mechanical Engineering, TOBB –
University of Economics and Technology
_____

Date: 03.09.2020

I hereby declare that all information in this document has been obtained and presented in accordance with academic rules and ethical conduct. I also declare that, as required by these rules and conduct, I have fully cited and referenced all material and results that are not original to this work.

Name, Last name : Ozan Adıgüzel

Signature :

ABSTRACT

STRUCTURAL OPTIMIZATION OF A JET TRAINER WING STRUCTURE UNDER STRENGTH AND STIFFNESS RELATED CONSTRAINTS

Adıgüzel, Ozan
Master of Science, Aerospace Engineering
Supervisor: Assoc. Prof. Dr. Melin Şahin

September 2020, 148 pages

This thesis presents structural optimization studies for a jet trainer aircraft wing structure. The main purpose is to select the most convenient rib/spar layout for T-38 wing like geometry which consists of metallic and composite components by using a finite element modeling and analysis tool of MSC NASTRAN optimization capabilities. In this study, in order to decrease the number of design variables and as well as to be able to obtain smooth thickness transitions between adjacent zones, design variable linking method is used by applying different shape functions.

First of all, after creating the outer geometry in CATIA, the finite element model (FEM) is prepared using MSC PATRAN. Similarly, all design zones where design variables are free to change are designated. To be able to link the thicknesses of the components to each other with regards to their locations on the wing, all coordinates of design zones are transformed to natural coordinate system as their center points are positioned as located between 0 and 1 in span-wise direction and -0.5 and 0.5 in chord-wise direction using scripts coded in Python. Aerodynamic loads are then calculated by using MSC FLDS (FlightLoads) tool and summed in predefined

monitor stations to distribute onto the structure using rigid body elements. Obtained shear force and bending moment distributions are also compared with another method called as Schrenk's Approximation.

In the optimization studies, thicknesses of the metallic structures and principal composite ply thicknesses are considered as design variables. There are five design constraints which are von Mises stress for the metallic structures, failure index for strength check of composite structures, global buckling, damping and natural frequencies which are used to control the flutter speed. The objective in this research is to obtain a minimum weight in design while providing predefined constraints via investigating various design candidate geometries having different layouts but same outer geometry. Finally, by using the scripts developed within this thesis study, the design variable linking method used according to the locations of the design zones become suitable also for the Nastran Sol 200 users.

Keywords: Structural Optimization, Composite Structures, Design Variable Linking Method, Mode Separation, Aeroelastic Tailoring

ÖZ

BİR JET EĞİTİM UÇAĞI KANADININ DAYANIM VE DİRENGENLİK KISITLARI ALTINDA YAPISAL ENİYİLEMESİ

Adıgüzel, Ozan
Yüksek Lisans, Havacılık ve Uzay Mühendisliği
Tez Yöneticisi: Doç. Dr. Melin Şahin

Eylül 2020, 148 sayfa

Bu tezde, bir jet eğitim uçağı kanadı için yapılan eniyileme çalışmaları sunulmuştur. Metal ve kompozit yapılardan oluşan T-38 kanat geometrisine benzer bir kanat yapısı için, MSC NASTRAN yazılımının sonlu elemanlar modelleme ve eniyileme kabiliyetleri kullanılarak en uygun kaburga/kiriş (rib/spar) yerleşimi bulunması amaçlanmıştır. Hem toplam tasarım değişkeni sayısını azaltmak hem de komşu tasarım bölgeleri arasında düzgün kalınlık geçişleri elde etmek amacıyla, farklı şekil fonksiyonları kullanarak tasarım değişkenlerini birbirine bağlama metodu uygulanmıştır.

Öncelikle, CATIA yazılımı kullanarak dış geometri oluşturulduktan sonra, MSC PATRAN yazılımı kullanılarak sonlu elemanlar modeli oluşturulmuştur. Benzer şekilde, tasarım değişkenlerinin eniyileme sürecinde değişebileceği bölgeler belirlenmiştir. Yapısal eleman kalınlıklarını, kanat üzerindeki konumlarına göre birbirlerine bağlayabilmek için, daha önceden belirlenen tasarım bölgelerinin merkez noktaları, açıklık boyunca 0 ve 1 arasında, veter doğrultusunda ise -0.5 ve 0.5 arasında konumlanacak şekilde, Python yazılımda hazırlanan komut dizisi yardımıyla doğal koordinat sistemine dönüştürülmüştür. Aerodinamik yükler MSC FLDS aracı kullanılarak hesaplanmış ve bütün yapıya rijit elemanlar ile dağıtmak

amacıyla belirlenen istasyonlarda toplatılmıştır. Elde edilen kesme kuvveti ve eğilme momenti dağılımları, Schrenk yaklaşımı isimli farklı bir metot ile de karşılaştırılmıştır.

Metal yapıların ve kompozit yapılarda kullanılan katmanların kalınlıkları, eniyileme çalışmasındaki tasarım değişkenleri olarak belirlenmişlerdir. Eniyileme çalışmasında kullanmak üzere, metal yapılar için von Mises gerilimi, kompozit yapılar için hasar kriteri, genel burkulma ve çırpınma hızını kontrol etmek için sönümleme ve doğal frekanslar olmak üzere toplam beş farklı kısıt bulunmaktadır. Farklı iç yerleşimli ama aynı dış geometriye sahip olarak tasarlanan birbirinden farklı kanat adayları için, belirlenen çok disiplinli bütün kısıtları sağlayan en hafif ağırlığı elde etmek, bu çalışmanın amacı olarak belirlenmiştir. Son olarak, bu çalışma için geliştirilen komut dizisi yardımıyla, tasarım değişkenlerini birbirine tasarım bölgelerinin kanat üzerinde bulundukları konuma göre bağlanması metodu MSC NASTRAN Sol 200 kullanıcıları için de uygun hale gelmiştir.

Anahtar Kelimeler: Yapısal Optimizasyon, Kompozit Yapılar, Tasarım Değişkenlerini Birbirine Bağlama Metodu, Modları Ayırma Yöntemi, Aeroelastik Performans İyileme

To my family

ACKNOWLEDGMENTS

I would like to express my deepest gratitude to my supervisor Assoc. Prof. Dr. Melin Şahin for his valuable advice, assistance, giving me opportunity to work with him and patience through this study.

I am grateful to Deniz Can Erdayı from Turkish Aerospace Industries for giving me an idea of this thesis study, supporting me patiently about all technical subjects throughout the study and for all contributions to my entire engineering skills.

I would like to thank to my previous and present chief engineers Can Kurgan and Mehmet Efruz Yalçın for all contributions to my engineering career and letting me use the computational capabilites of Turkish Aerospace Industries.

I would like to thank to my colleagues Zafer Eker, Çağrı Koçan, Fırat Şentürken and Oğuzhan Dede, also Mesut Mert, Berk Kaplanlıoğlu, İnanç Gürbüz and Barış Gider who are my first mentors in working life, for their all precious supports throughout this thesis study.

I also would like to thank to Ahmet Barutçu, Okan Ergün and Yavuz Alp Çavuşoğlu for their strong friendships.

Finally, I would like to present my deepest thanks to my parents Hatice Adıgüzel, Erdoğan Adıgüzel, my brother Utku Adıgüzel and my dear family for their endless supports in my whole life.

TABLE OF CONTENTS

LIST OF TABLES

TABLES

LIST OF FIGURES

FIGURES

CHAPTER 1

INTRODUCTION

1.1 Background and Motivation of the Study

Generally, providing structural strength criteria in aerospace structures is inadequate. It is also required to study related with weight reduction with the purpose of increasing maneuverability and payloads or reducing the fuel consumption and CO_2 emission. In this sense, integrating structural optimization into design process especially in preliminary design stages is a significant issue to bring down the expected cost in the production after a detail design.

As the subject which should be included in the early phases of the fighter wings is the aeroelastic stability of the components such as wing and horizontal tail of the aircrafts, a wing structure of a fighter aircraft is aimed to be optimized by also considering these subjects in this thesis. Additionally, flutter is the most critical and dangerous phenomena from aeroelastic stability point of view since it may lead to loss of whole aircraft. In general, as it is not receiving the required attention and is a very complex phenomena, the local changes may not be sufficient to produce a flutter-free structure in detail design stage. Therefore, it should be included in the structural optimization studies of a preliminary design stage to prevent costly failures.

However, including various disciplines simultaneously in the optimization process increases the complexity of the problem. Therefore, this type of optimization

applications is also known as multidisciplinary optimization requiring automated tools that minimize the iteration time. There are various methods to be integrated into structural optimization studies; however, each optimization method cannot be used effectively in all structural optimization problems. While one method provides sufficient results in any design problem, it may not converge to the desired values or may not be cost effective for another problem. Therefore, it is also an important issue to choose the optimization method prior to the design studies. A crucial subject that increase the significance of the selection of the optimization method is said to be the total number of design variables used in the optimization and the available capabilities related with the constraints. A detailed structural optimization of a wing structure may result in thousands of design variables and therefore complexity of the problem increases equally; however, by implementing a method so-called design variable linking method into the optimization, all of the properties of the structural components could be tailored with fewer number of variables, besides smooth thickness transitions between design zones may also be obtained. Therefore, in order to evaluate different layouts on the wing in a short time, design variable linking method is the one preferred in this particular study.

1.2 Objectives of the Study

The main objective of this thesis is to determine to the most convenient layout for a wing of a jet trainer aircraft via optimization tool with implementing design variable linking method so as to decrease the number of design variables and obtain smooth thickness transitions on the wing.

All objectives of this thesis are summarized below as;

- Designing seven different wings with different layouts through investigating the wings of similar other aircrafts.
- Creating detailed finite element models for each of the candidate designs.

- Performing modal analysis to obtain the natural frequencies and the corresponding mode shapes of the wing geometry.
- Constructing a trim model to obtain aerodynamic loads acting on the wing via MSC FLDS and verifying the obtained loads with another method called as Schrenk's Approximation through the distribution of shear force and bending moments.
- Transforming all of the coordinates of design zones into natural coordinate system to make them suitable for the use of variable linking method.
- Optimizing all of the candidates with strength-only constraints and following that by controlling the sized wings whether they satisfy the requirement for minimum flutter speed according to MIL-A-8870C Military Specification.
- Finally, performing structural optimizations including flutter and frequency constraints to obtain minimum weight in design which satisfies all of the defined constraints.

1.3 Limitations of the Study

The major limitations of this thesis are listed as follows;

- Flanges of the ribs and spars are not modelled.
- Only two load cases of pull-up maneuver are included where one of them is subsonic and the other is supersonic.
- The aeroelastic trim analysis is performed with rigid trim method.
- Only symmetric and balanced composite laminates which consists of 0°, ±45° and 90° plies are used.
- Control surfaces are not included into optimization model.

1.4 Outline of the Thesis

This thesis includes mainly eight chapters and organization scheme is listed as below, respectively.

In Chapter 2, jet trainer aircrafts are introduced briefly and similar specifications of their wing geometries are investigated as guide-line while creating the geometry of the wing in research. After that, different structural optimization methods are mentioned which are used commonly in aerospace structures and categorized into two main titles as gradient-based and gradient-free methods. Considering the advantages and disadvantages of both types, the optimizer which will be used in this study is decided. Multidisciplinary methods are also introduced with sample studies performed in the area of aerospace. Briefly, the background of the flutter phenomena is presented with general equations and finally, an alternative method to postpone the flutter speed of the structures is presented.

In Chapter 3, firstly the outer geometry of the wing used in this thesis is presented with its dimensions. Then, the main load carrying structural components are mentioned regarding their general purposes in the wing structure. To determine the internal layout of the wing structure, multi-rib and multi-spar concepts are compared with each other and by selecting the multi-spar concept, seven different candidate layouts are prepared by investigating the previously tried concepts in similar aircrafts.

In Chapter 4, structural finite element models are created and mesh convergence study is performed to determine the most efficient mesh size to be cost effective in the optimization studies. Having introduced the material properties and the boundary conditions, modal analysis is performed to obtain the vibration characteristics of the wing geometry.

In Chapter 5, like for the structural analyses, aerodynamic loads are also calculated through the finite element analyses and therefore the trim model which includes aero models in addition to the structural finite element models is constructed. The theory

of the trim analyses is also presented shortly to provide a theoretical background. Then, the aerodynamic loads acting on the wing are calculated via two different methods and the results are the compared with each other using shear-moment diagrams.

In Chapter 6, first, isoparametric elements are mentioned and the importance of them in the area of design variable linking method is presented. Then, the coordinate transformation method applied while transforming the coordinates of the design zones from Cartesian to the natural coordinate system is shown item by item. Design variable linking method is then introduced elaborately and the success of the method in decreasing the total number of variables are presented with an example. All constraints used in the study are presented with brief theoretical backgrounds and finally the steps followed for the optimization studies through this thesis is summarized by a flowchart.

In Chapter 7, first of all, shape functions affecting the performance of the design variable linking method are compared with each other over one of the candidate layouts. After determining the shape functions which are used for ribs, spars and skin, all abovementioned methods are practiced in the previously created seven different candidate wings and the results of the optimizations are shown by considering strength-only constraints. After that, flutter speeds of all sized wings are calculated by using of MSC NASTRAN Sol 145 and wings which cannot satisfy the minimum speed requirement for the flutter are subjected to an optimization via two different methods. Finally, all the results are investigated especially from the weight reduction point of view.

In Chapter 8, the summary of all the obtained results through this thesis study are presented and recommendations are provided for future studies.

CHAPTER 2

LITERATURE REVIEW

2.1 Introduction

Nowadays, the structural optimization methods are used in the area of aerospace more than ever before. The companies which realize the advantages of the optimization tools, especially the ones which include multiple disciplines are started to incorporate these tools into early design phases. After a brief introduction with general geometric specifications of jet trainer wings, in this chapter, optimization methods are compared and multidisciplinary methods are then presented with their contributions to past studies performed in these particular areas.

2.2 General Geometric Specifications of Jet Trainer Wing Structures

The fighter aircrafts are becoming complex, therefore use of these advanced jets are being increasingly expensive in the recent years. While the hourly cost of operating of an F-35 is $18000, this can be reduced to approximately $4000 in T-38 [1]. In addition to the cost advantage, the need to avoid potential crashes as a results of student pilots has led to increase of market share of the jet trainer aircrafts [2].

Today, most of the jet trainer aircraft are able to fly in supersonic speeds and can be used as light attack aircraft by the countries. Therefore, wings of them are designed with sweepback geometry with thin airfoils to delay the shock waves occurred in supersonic flight regimes.

Another reason why the jet trainer aircrafts use the swept wing is that they are subjected to a high bending moment. It should be obvious that any vertical force results in moment in the structures if it applies with respect to the fixed reference point having a distance from location of applied force. In the aircraft wing structures, lift is the dominant vertical force which is assumed as located in the center of pressure and simply multiplying the lift force with distance to the root of the wing creates bending moment on the wing root. The bending moment results in a significant in-plane load for the wing structures where the upper side is under compression resulting hazardous instability modes and the lower side is under tensile loads which are also critical for fatigue issues. Besides, high bending moment in the root section aggravates the design of wing to fuselage connection fittings. Using swept geometries for the wing structures, the location of the center of pressure can be get closer to the root section resulting a decrease in the bending moment.

In this research, T-38 wing like geometry having thin airfoil and sweepback geometry (Figure 2-1) is used in the optimization studies.

T - 38 Talon *Boeing T - 7 Red Hawk*

Figure 2-1 Representation of Swept Jet Trainer Aircraft Wings [3], [4]

2.3 Structural Optimization Methods for the Wing Structures

Basically, optimization is an efficient engineering method that changes the parameters affecting the objective function with the expectation to reach the best design, in other words, is the process of achieving the best solution of given objective

or objectives while satisfying predetermined restrictions. There are several optimization methods and they are categorized in two groups. Those using gradient information to get optimum results are known as gradient-based and the others are the gradient-free methods [5]. Each method has advantages and disadvantages; according to problem, and therefore the most appropriate method may show an alteration. There are numerous studies which use these optimization methods for the structural optimization applications through the history of aircraft industry. In the following section, these methods will be compared and the best method to use in this study will be selected and applied.

2.3.1 Gradient-Based vs Gradient-Free Methods

Generally, in the optimization problems which have smooth functions namely have a unique defined first derivative (i.e. slope or gradient) at every point as shown in Figure 2-2, gradient-based methods are used. Gradient information is used to determine the direction to go and to update parameters in order to get best results in the optimization process. Basic working principle is summarized as follows in Equation 2.1 [6],

$$x^{(k+1)} = x^{(k)} + \alpha^{(k)}.\, s^{(k)} \text{ and } k = 0,1,2 \ldots \quad (2.1)$$

where, superscript k refers to iteration number, $x^{(k)}$ is initial point, $x^{(k+1)}$ is new design point at iteration number $k + 1$, $\alpha^{(k)}$ is step size at iteration k and $s^{(k)}$ is the search direction.

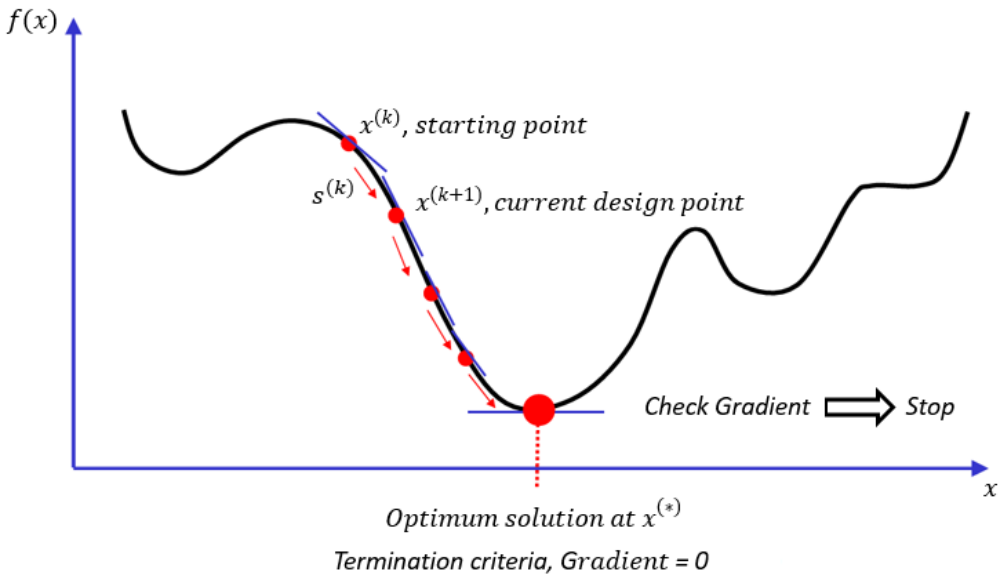

Figure 2-2 Approaches of Gradient-Based Optimization Methods

The iterative procedure in Equation 2.1 starts with a current design point at an iteration and after determining the search direction and step size, the process continues until stopping criteria is satisfied. Differences in the methods lie in the selection of the search direction. The most common methods in this category are said to be,

- Steepest descent method
- Newton's method
- Marquard's method

Most of the aircraft companies use gradient-based optimization tools such as ASTROS and MSC NASTRAN Sol 200. Automated STRuctural Optimization System (ASTROS) is a multidisciplinary optimization tool based on MICRODOT code which uses a modified feasible direction method with a polynomial interpolation [7]. Having capabilities such as applying flutter constraint and linking of design variables, ASTROS is completely sufficient optimization tool for the aircrafts at the preliminary design stage.

In short, general features of these methods are listed below as;

- Exploiting the derivative information
- Providing usually fast converges to optimum
- Being efficient for problems where derivative information is available.

However, while converging to optimum quickly, the main disadvantage in these types of methods is to find a local optimum instead of guaranteeing a global one. Furthermore, the optimization solution may be influenced by the initial design point.

The other optimization type is gradient-free method which does not need any gradient information and driven by only the function values [8]. In the literature, the most known methods may be listed as [9],

- Genetic algorithm
- Simulated annealing
- Particle swarm optimization
- Ant colony optimization

Generally, these algorithms are found out by engineers who are inspired from the real-life examples such as genetic algorithms which are developed based on Darwin's natural selection theory. Similarly, ant colony optimization method is found by observing the movements of the ants while seeking for the food.

Zheng [10] performed a two-step study that optimizes thickness and stacking sequence of the composite wing structure. In the first step, ply thicknesses and in the next step orientation of the plies are optimized. Both strength and aeroelastic constraints such as maximum displacement and flutter speed are considered. Genetic algorithm-based code is developed to use in the optimization process. The results obtained through this particular study show that the weight of the composite wing structure of interest may be decreased by 28.8%.

In another study, four different gradient-free methods are tried to increase the flutter and divergence speed of the simple rectangular composite wing structure [11]. Four different biological inspired methods (namely; binary genetic algorithm, continuous

genetic algorithm, particle swarm optimization and ant colony optimization) are tried to determine optimum ply orientations by Cooper. Besides, a statistical investigation has been performed to investigate the variation of the design variables. After using 100 solution set for each method, results are found to be very similar with a few exceptions.

Briefly, specification of gradient – free methods can be listed as;

- No need for gradient information
- Capable of finding the global optimum instead of a local one.
- Computational time may also increase due to the need for evaluating the interest functions multiple times.

2.3.2 Selection of the Optimizer

In this study, it is decided to be used MSC NASTRAN Sol 200 as an optimizer which is based on gradient-based methods. Being available as an open source package program, the easiness of applying the design variable linking method by using the cards already available in the MSC NASTRAN and the capabilities including the constraints related with flutter and frequency are said to be most influential factors while selecting the optimizer to be used in this study.

2.3.3 The Optimization Methodology of MSC NASTRAN Sol 200

Especially in aerospace applications, airframe structures become progressively complicated to provide effective load paths through carrying components, therefore optimizing existing structures turn out be more compelling issue for the engineers. While design optimality performed, an engineer must always be sure in terms of structural strength under maneuvers which are encountered during the flight. At this stage, MSC NASTRAN provides engineers precious support such that using MSC NASTRAN Sol 200 where more efficient structures could be designed with many

available constraint capabilities and trade-off studies may be performed quickly to achieve design objectives such as weight, stress, aeroelastic responses [12].

As mentioned before, MSC NASTRAN Sol 200 optimization algorithm uses gradient-based optimization methods. Briefly, process of the optimization starts by defining the initial point which is found in design space. By calculating the gradients of the constraints and objective function, the search direction is then determined. Following this, the optimizer proceeds in the determined search direction for each design cycle until it comes across with one of the predefined boundary of the constraints. Finally, this process continues iteratively until it is not possible to make no further progress in the objective function along with satisfying all of the constraints.

Generally, the gradient-based optimization methods are differed from each other with applied search direction method. At the starting of the optimization if none of the constraints are violated, MSC NASTRAN Sol 200 uses the steepest descent method to determine the search direction and goes in that direction until it encounters with the constraint boundary. After that point, if there are no further improvement by using steepest descent method, the optimizer starts to use more efficient methods to determine the search direction and it uses modified method of feasible direction as a default. The method of feasible direction uses only the first order derivatives of the constraints and always providing feasible designs if the initial design is feasible. For that reason, the method of feasible directions are commonly used especially in structural optimization and according to [13], the most efficient method of feasible direction is found as the modified method of feasible direction which is also adopted by MSC NASTRAN.

In Figure 2-3, the flowchart of the optimization process for MSC NASTRAN Sol 200 can be seen.

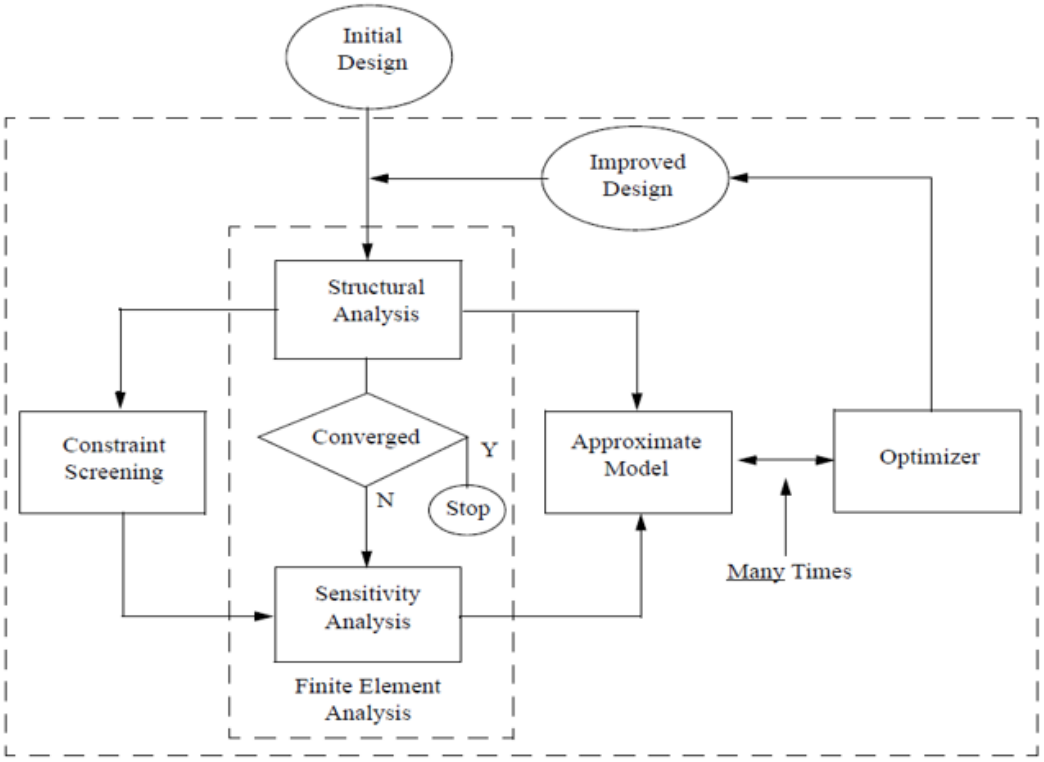

Figure 2-3 MSC NASTRAN Execution of Structural Optimization [12]

Optimization process in Sol 200 starts with the initial design provided by the user. After finite element model is created, structural analysis, which depends on expected response type, is mandatory to investigate the obtained results. After the results are obtained from the structural analysis, sensitivity analyses are performed in which the rate of change of the constraints are calculated with respect to the change in the design variables. To define a new point, the optimizer also requires high number of function evaluations in each step in addition to the derivative information and using finite element analyses for these function evaluations is an expensive process. Therefore, MSC NASTRAN applies some approximations to avoid these difficulties. The adopted methods for approximation by MSC NASTRAN can be investigated in three steps. The first one is determining the most efficient combination of the design variables which is also known as “design variable linking”. The second method is “constraint deletion”. In this method, MSC NASTRAN ignores some of the constraints temporarily which are not critical for that iteration. Finally, parametric

studies are performed by using formal approximations and these studies can be used by the optimizer instead of the costly finite element analyses. The approximate model is created in the basis of the finite element analyses by using the approximation methods described above. It should be noted that, constraint deletion and parametric studies by using formal approximations are performed automatically by MSC NASTRAN while the design variable linking is constituted by the user if it is required [12].

After many iterations performed by the optimizer, improved design is finally obtained. To determine for the structure whether it is the optimum, two convergence check methods are available in NASTRAN Sol 200 [12]. These are soft and hard convergence tests. The improved design is the new starting design for the finite element analysis and the soft convergence check is performed at this stage. It compares the design responses obtained from the approximate model and previous finite element analysis. This test does not stop the optimization unless the user activates the parameter of SOFTEXIT which is an available card in MSC NASTRAN used for exit when the soft convergence is satisfied. On the other hand, the hard convergence compares the results of the last two performed finite element analyses and since this test deals with the exact results of the analyses, it is used as a default test for determining whether or not to finish the design process.

Although, the soft convergence is not conclusive as the hard convergence, it may also be sufficient when the solution of the finite element analysis is costly and if there is no significant alteration in the design variables.

The flowchart for the decision of soft convergence which is followed by MSC NASTRAN can be seen in below Figure 2-4. The decision for exit according to soft convergence check is given with respect to SOFTCV parameter. Design process is finished if SOFTCV is true and SOFTEXIT is activated. As similar to the soft convergence test, there is also a flowchart for the hard convergence test in MSC NASTRAN and can be seen in below Figure 2-5. The parameters in Figure 2-4 and Figure 2-5 are summarized in Table 2-1.

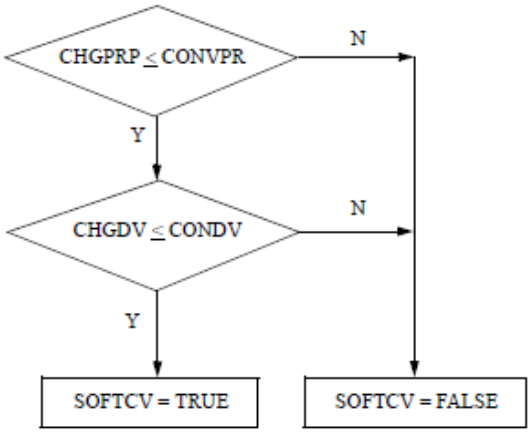

Figure 2-4 Logic for the Soft Convergence Decision [12]

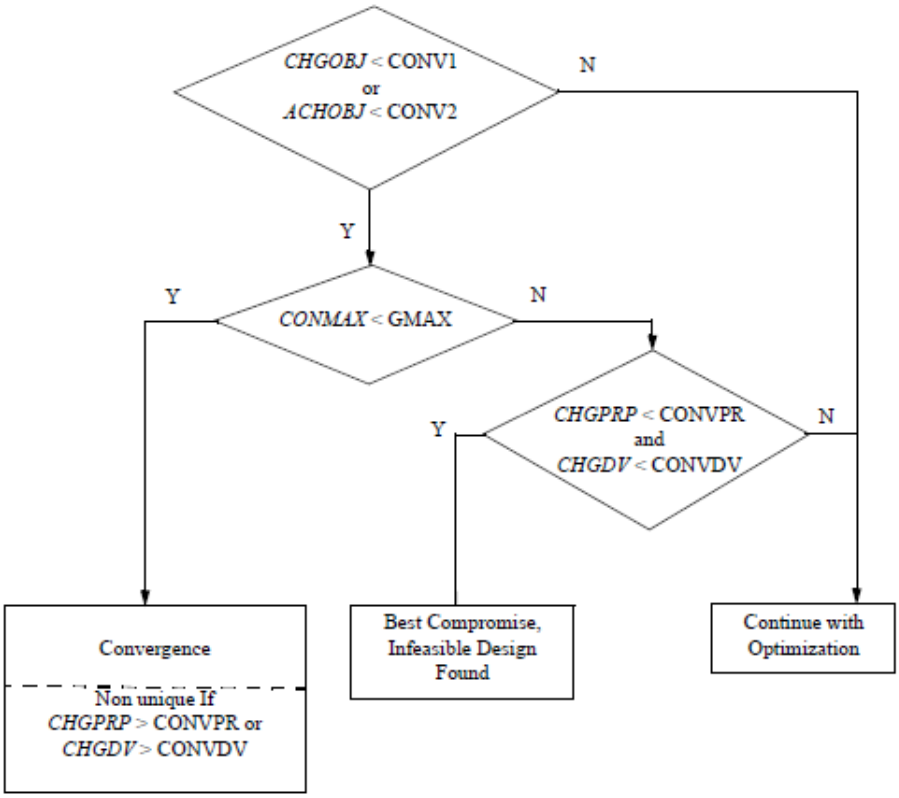

Figure 2-5 Logic for the Hard Convergence Decision [12]

As with the soft convergence, the first process of the hard convergence check is performed with respect to the relative and absolute changes in the objective function. The reason for using “or” which can be seen at the left bottom box in Figure 2-5 is based on the magnitude of the objective function. For instance, if the value of the objective function is large, then forcing convergence according to the fractional change of the values of the objective function may be meaningless. On the other hand, if the magnitude of the objective function is very small, then the absolute change may be more meaningful. After the objective function is satisfied, there is another check to terminate the design process related with constraints. If the value of the maximum constraint is under its maximum value then the optimization stops with the hard convergence.

Table 2-1 Convergence Criteria Parameters [12]

Internal Variable	Definition	Parameters	Default
CHGPRP	$\max_{1 \le i \le NPROP} \left(\left\| \frac{P_i^{(P)} - P_i^{(P-1)}}{P_i^{(P-1)}} \right| \right)$	CONVPR	0.001
CHGDV	$\max_{1 \le i \le NDV} \left(\left\| \frac{x_i^{(P)} - x_i^{(P-1)}}{x_i^{(P-1)}} \right| \right)$	CONVDV	0.001 (1.0E-4 for topology optimization)
CHGOBJ	$\left\| \frac{OBJ^{(P)} - OBJ^{(P-1)}}{OBJ^{(P-1)}} \right\|$	CONV1	0.001 (1.0E-5 for topology optimization)
ACHOBJ	$OBJ^{(P)} - OBJ^{(P-1)}$	CONV2	1.00E-20
CONMAX	$\max_k \{g_k(\mathbf{x})\}$	GMAX	0.005

2.4 Multidisciplinary Structural Optimization of Wing Structures

Aerospace industry has always the leading technology and most of the innovations are firstly used in this industry. Day by day, to go further, aircraft structures are becoming more and more complex, therefore more than one discipline is being obliged to work together. Especially in aircraft structures, there are lots of strength criteria to accomplish the required missions securely. All analysis groups such as static, fatigue and structural dynamics are responsible for creation of optimum structure using their strength criteria. Due to limitations such as time and resources, the manual iterative process is usually stopped after achieving a design which is feasible, from a static strength viewpoint; however, that particular design is not necessarily "a minimum weight design" without integrating other disciplines such as fatigue and aeroelasticity. Because of the size and the complexity of the work, it is required to use advanced tools integrating and accelerating the design process and this need results in emerging of the multidisciplinary optimization methods (MDO).

MDO is a field of engineering that uses optimization methods to solve design problems incorporating various number of disciplines and allows designers to incorporate all relevant disciplines simultaneously. The optimum solution of a simultaneous problem is superior to the design found by optimizing each discipline sequentially, since it can exploit the interaction between these disciplines.

A considerable number of studies about multidisciplinary wing optimization with different approaches are available in the literature.

Guo [14] performed multidisciplinary study to optimize the composite commercial aircraft wing under gust response by using MSC NASTRAN Sol 200. In this study, both strength and aeroelastic constraints are taken into consideration. To investigate the effect of strength and aeroelastic constraints discretely in the weight of the wing, the optimization process was taken in two stages. In the first stage, multiple stress constraints including failure index and damage tolerance from the strain point of view were considered. Whereas in the second stage, in addition to stress constraints,

aeroelastic tailoring was also considered. For all optimization studies in this particular research, the thickness of the composite laminates and the fiber directions were selected as design variables. As a conclusion, it is seen that, the weight is reduced by 44.6% in the first stage; however, by also including the aeroelastic constraints, weight saving is dropped to 34.5%.

In order to show the advantage of the MDO in terms of evaluating the different wing structures in a short time, Chen and his collogues [15] prepared automized process for the development of conceptual supersonic aircraft which is also sponsored by NASA as shown in Figure 2-6. Both static strength and aeroelastic constraints were included. In this study, first, a meshable parametric geometry was created with CATIA, after generating structural and aerodynamic FEMs using MSC PATRAN interface, external loads were calculated with trim analysis in MSC FLDS. Input files including design variables and constraints were created with the aid of python scripts. As inferred from the obtained results that when the aeroelastic constraint was included on top of the static one, it provided the aircraft flutter-free up to 1.15 dive speed but resulted in weight increase of 18.5%.

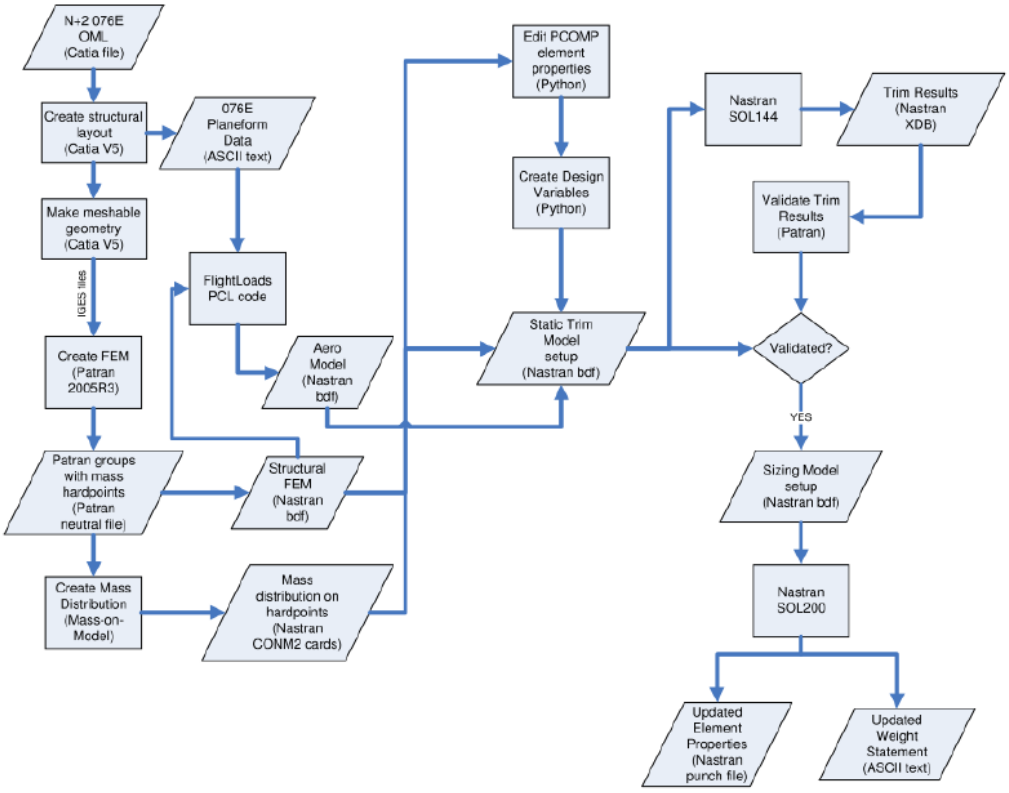

Figure 2-6 Flowchart Used for Structural Optimization Study of [15]

In another study in the field of interest [16], the minimum weight optimization of the composite aircraft wing was performed with constraints including the flutter speed. As different from others, in order to decrease the number of the design variables, Li tried a method that stacks all uni-directional plies in one and simulated them with a one design variable in the optimization problem. Since the ply thickness cannot be changed continuously, in the post-process section, thicknesses increased to the standard values. According to the results of the study, including the post-process of the thicknesses of the plies to make them manufacturable, the weight is decreased by 16.3%.

2.5 Aeroelastic Stability Analyses

As a most general meaning, aeroelasticity deals with elastic structures situated in the air flow in which aerodynamic, inertial and structural loads interact with each other. Most known figure visualizing the interdisciplinary relations in aeroelasticity is Collar's triangle and can be seen in Figure 2-7.

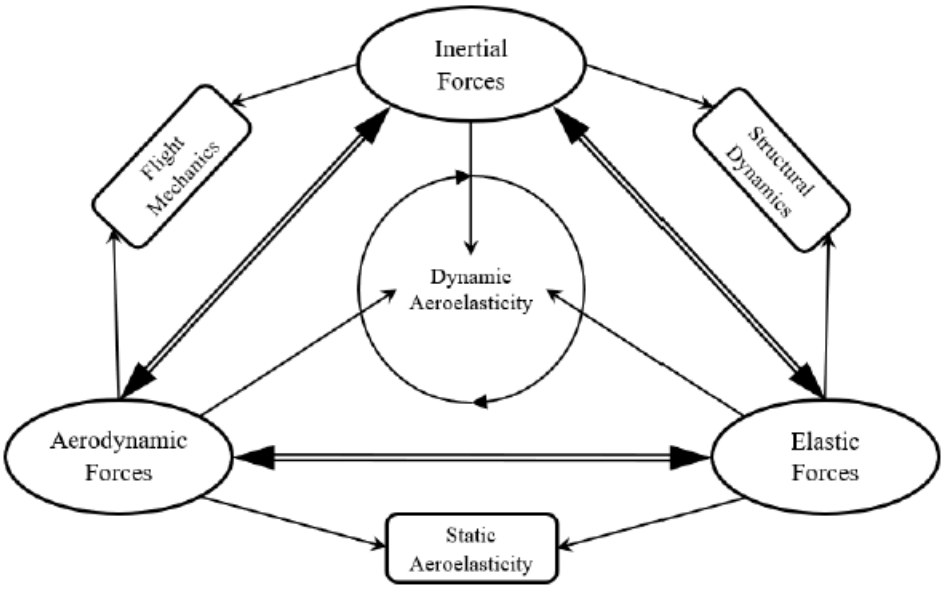

Figure 2-7 Collar's Aeroelasticity Triangle [17]

As inferred from Figure 2-7, aeroelasticity can be investigated in two main titles, static and dynamic aeroelasticity. Whereas static aeroelasticity is interested with conditions in which only aerodynamic and elastic forces interact such as divergence, load redistribution and control surface reversal, dynamic aeroelasticity stays on the center of the triangle, interacts with all disciplines. Flutter and buffeting are said to be the main subjects of the dynamic aeroelasticity.

Flutter is one of the most important aeroelastic problem to be dealt with in the aerospace industry. At the low speeds, vibration modes of the aircrafts are stable, in other words, if the aircraft is perturbed externally then it becomes stable again by itself. On the other hand, at the high-speed conditions, with the effect of air flow, two or more vibration modes are coupled and consequently, the vibratory structure

starts to take energy from the air flow. If the energy taken is spent through a structural damping internally; the modes become stable; however, if the energy increases continuously and aircraft comes to speed in which the taken energy is not spent any more internally, dangerous phenomena called flutter occurs [18]. Simply, flutter can be defined as dynamic instability of a structure in the air flow and the flutter speed is the minimum speed that exposes the structure to a simple harmonic motion.

The term of flutter is first encountered in the documents of Hundley – Page bomber aircraft seen in Figure 2-8, during World War I in 1916. There were no remarkable progress related with flutter until the accident involving death in JU90 aircraft in 1938. From that date, theoretical studies and wind tunnel tests are increasingly a subject for flutter studies [19].

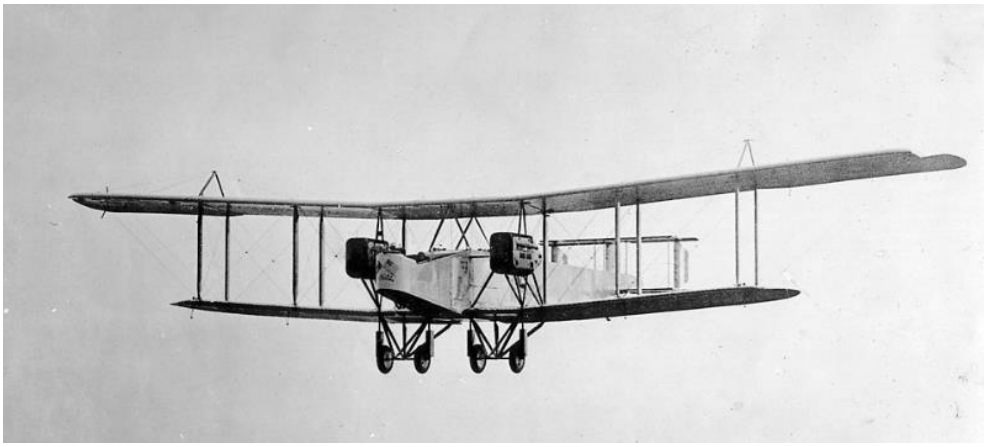

Figure 2-8 Handley – Page O-400 [19]

The general equilibrium condition of the forces in time domain for the multi-degree of freedom systems is known as [20],

$$[M]\{\ddot{x}(t)\} + [C]\{\dot{x}(t)\} + [K]\{x(t)\} = \{F(x,t)\} \qquad (2.2)$$

where,

$[M]$, $[K]$ and $[C]$ represents the mass, damping and stiffness matrices, respectively.

$x(t)$ is the structural deformation vector.

$F(x,t)$ is the applied aerodynamic force vector.

Applied aerodynamic term is also defined as sum of the forces due to structural deformation and external forces such as gust effect.

$$\{F(x,t)\} = \{F_e(t)\} + \{F_a(x(t))\} \tag{2.3}$$

$\{F_e(t)\}$ is the force due to external effects and $\{F_a(x)\}$ denotes the forces due to deformation in the structure. Therefore, substituting Equation 2.3 into Equation 2.2 yields to following equation,

$$[M]\{\ddot{x}(t)\} + [C]\{\dot{x}(t)\} + [K]\{x(t)\} - \{F_a(x(t))\} = \{F_e(t)\} \tag{2.4}$$

However, generally the forces coming from external effects are ignored and final equation is acquired as follows,

$$[M]\{\ddot{x}(t)\} + [C]\{\dot{x}(t)\} + [K]\{x(t)\} - \{F_a(x(t))\} = 0 \tag{2.5}$$

The aerodynamic force term $\{F_a(x(t))\}$ shows non-linear behavior according to structural deformation. Besides, according to the FEM used for the aeroelastic analysis, dimension of the stiffness and mass matrices may be so large and therefore the solution of the eigenvalue problem will be compelling. To overcome these difficulties, after mathematical processes such as linearization, Laplace transforms and modal superposition, Equation 2.5 takes the following form,

$$\left[\left[s^2[\bar{M}]\right] + s[\bar{C}] + [\bar{K}] - q_\infty[\bar{Q}(p)]\right]\{q(s)\} = 0 \tag{2.6}$$

where, $[\bar{M}]$, $[\bar{C}]$, $[\bar{K}]$ and $[\bar{Q}(p)]$ represent the generalized mass, damping, stiffness and aerodynamic force matrices, respectively. q_∞ is the dynamic pressure and it should be noted that, the matrices in Equation 2.6 are in the Laplace domain, therefore p and s are special Laplace parameters.

Equation 2.6 is said to be the most general aeroelastic stability equation and there are many methods to solve this eigenvalue problem to define aeroelastic stability phenomena such as flutter.

In this study, capabilities of MSC NASTRAN solver is used to determine flutter speed of the model wing structures. MSC NASTRAN has three different method to solve Equation 2.6 which are all in frequency domain. These methods are,

- K method
- K-E method
- P-K method

Having advantages such as obtaining solution for only specified velocities and more realistic estimations for damping value than other methods, it is decided to use P-K method as a solution method for further flutter analysis.

With the assumption of simple harmonic motion for aerodynamic matrix and replacing Laplace variable (s) with (iw), flutter solution is performed with based on following equation for the P-K method [17],

$$\left[\left(\frac{V_\infty}{L}\right)^2 [\bar{M}]p^2 + \left(\frac{V_\infty}{L}\right)[\bar{C}]p + [\bar{K}] - \frac{\rho {V_\infty}^2}{2}\left[\frac{p}{k}\bar{Q}(ik)^I + \bar{Q}(ik)^R\right]\right]\{\bar{q}\} = 0 \qquad (2.7)$$

where,

V_∞, selected air speed

L, reference semi chord

p, eigenvalue $(\gamma + i)$

k, reduced frequency

γ, transient decay rate coefficient

$\bar{Q}(ik)^I$, imaginary part of aerodynamic matrix (aerodynamic damping matrix)

$\bar{Q}(ik)^R$, real part of aerodynamic matrix (aerodynamic stiffness matrix)

$\bar{q}$, modal amplitude vector.

The eigenvalues of Equation 2.7 are complex and solution process for this equation needs iterative procedure such that pre-specified reduced frequency list which is supplied by the user and imaginary part of p is matched for every mode. This iterative process continues until the predefined tolerance is obtained. The crossing value on the velocity line for the damping versus velocity graph that goes from negative to

positive is used to specify the flutter speed in any of the modes as shown in Figure 2-9.

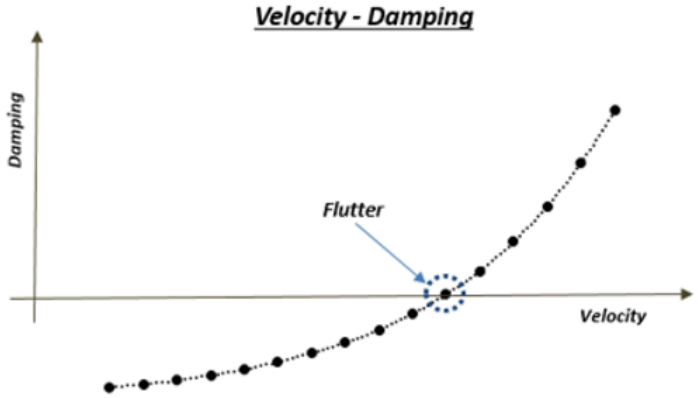

Figure 2-9 Representation of Velocity – Damping Graph

2.6 Mode Separation Method for Postponing Flutter Speed

In addition to the constraint given on the damping value, increasing the gap between the modes which are also critical from the aeroelastic aspects is another method used to postpone the flutter speed. According to the studies performed on this subject, mode separation is very effective as compared with directly applied flutter constraint to the optimization routine.

As mentioned before, ASTROS is one of the powerful optimization tool which integrates all necessary disciplines affecting aircrafts in the preliminary design stage and is also used to increase the flutter speed of the composite wing structure [21]. Both flutter constraint and mode separation method are tried in this particular study and it is observed that flutter speed can be shifted with less increase in the weight by separating the critical frequencies rather than imposing a flutter constraint.

Another study that attends to delay flutter speed of the tip stored wing by separating the modes was presented by Janardhan [22]. In this study, four different constraint sets are implemented and they individually comprise;

1. Mode 1 (bending) and stress constraint applied
2. Mode 2 (torsion) and stress constraint applied
3. Stress and frequency (Mode 1 and Mode 2) constraints applied
4. Stress, frequency (Mode 1 and Mode 2) and flutter constraint applied

The increase of the flutter speed is succeeded with separation of the first two natural frequencies using multidisciplinary optimization study. According to results of the analyses tried for four different constraint sets, it is deduced that the second (i.e. torsion) mode is more effective in increasing flutter speed compared to the first bending mode. Interestingly, when both the first and the second constraint sets were applied concurrently, the almost same increase was obtained with the second constraint set only. Optimization with mode separation constraints and the one with flutter constraint led to similar increase in the weight. However, mode separation approach is found to be much more effective from the computational effort point of view.

2.7 Conclusion

In this chapter, the wing types of the jet fighters were briefly introduced. Then, optimization types which are extensively used in aircraft structures were presented. Each method was also investigated with their advantages and disadvantages and the decision was made upon which optimization type would be used in this research study. The multidisciplinary method combining at least two different disciplines was familiarized with the published studies from the past to present especially in relation with the aeroelastic issues. Finally, an aeroelastic stability equation was expressed briefly and a method used to increase flutter speed of the aircrafts known as mode separation was also presented.

CHAPTER 3

DESIGN OF A TRAINER JET WING STRUCTURE

3.1 Introduction

A design of the wing may be investigated under three consecutive phases as the same in whole aircraft. These namely are conceptual, preliminary and detail phases. Conceptual design phase is the starting point for design projects in which all possible designs that can provide requirements are determined and sketched. After proceeding the conceptual phase, the next step is the preliminary design. In this phase, the selected concept is investigated by the engineers using various analysis tools. Optimization studies are generally performed by considering disciplines such as structural and/or aerodynamics. Wind tunnel tests are also performed in this phase. The final step is the detailed design phase in which all created designs are analyzed in details and preparation are made for manufacturing stage.

In this thesis study, conceptual and preliminary design stages are included for the trainer jet wing. At first, all possible wing layouts that are applicable to swept and tapered wing geometry are created by investigating the tried concepts in other aircrafts and after creating possible wing layouts, all candidate geometries are sized by considering both strength and stiffness aspects in the following chapters.

3.2 Outer Boundary of the Designed Wing

In Figure 3-1, the most general sketch of the wing geometry that will be used in this study is shown with its dimensions. The outmost border shows the external aerodynamic surface and it will be used in load calculations as a reference. While

the boundary in span-wise direction of the wing box starts from root rib (i.e. Rib 0 as wing root), the starting locations of the leading and the trailing edge control surfaces are used in the determination of the outer boundaries of wing box in chord-wise direction.

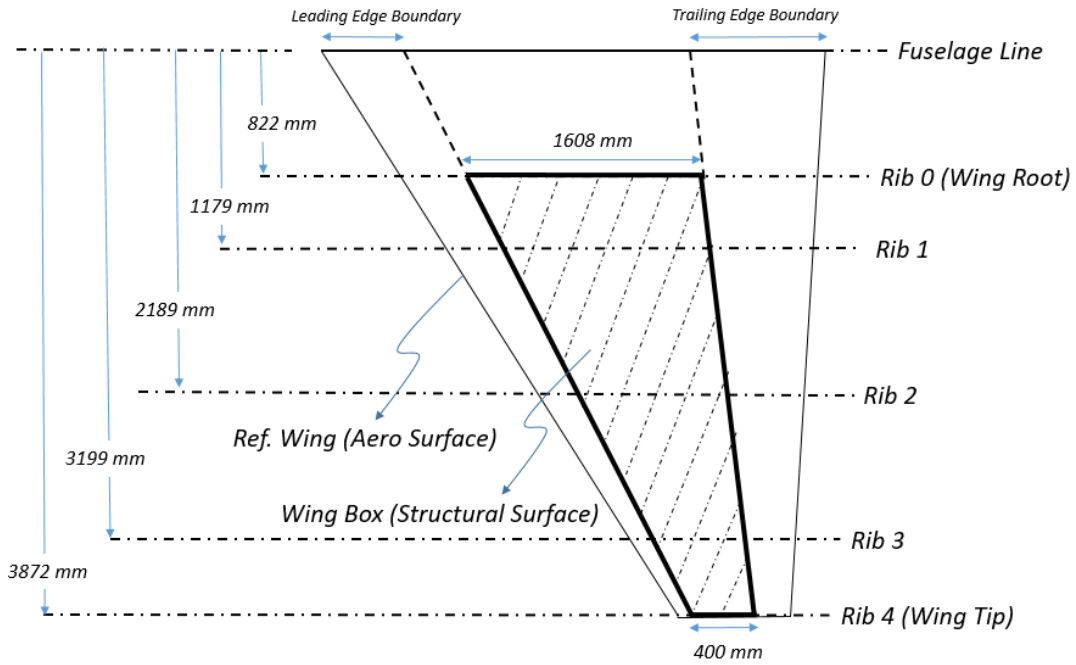

Figure 3-1 General Structural an Aerodynamic Borders of Wing Geometry

After determining the border of the wing box, the next important step is to decide the number and the locations of the interior load carrying components such as ribs and spars. In following subsections, possible concepts for rib/spar locations (i.e. the layout) will be presented.

3.2.1 Load Carrying Components

The main load carrying components of wing structures are the skin and the stiffeners along the span-wise and chord-wise directions.

Ribs are mainly used to maintain the airfoil shape of the wing. Local loads created by control surfaces, external stores such as missiles, gun, reserve fuel tank are

transferred to the box structure via ribs. Besides decreasing the buckling span, panel buckling stability may also be increased with sufficient number of ribs. The ribs are also used to divide the span-wise stiffeners, thus the load carrying capacities of the stiffeners can be increased. They also carry inertia loads resulted from equipment's, fuel, external stores, etc.

The spars are main load carrying components of the wing structures. The dominant load used in the structural sizing of the wing structures, which can also be considered as a cantilever beam in simple, is the bending load and most of the bending load is carried by the spars. Spars are generally located on the wing in span-wise direction. They consist of two pieces; flanges and webs. While flanges carry mainly axial and bending loads, shear loads are supported by the webs of the spars.

And finally, skin covers all of the wing geometry. All aerodynamic loads are transferred to the structure by the skin. In the first built aircrafts, skin was the main load carrying component and these types of structures are known as monocoque and they are no longer in use. Indeed, semi-monocoque structures are adopted for the modern aircrafts. Some of the loads mainly bending, which are taken by the skin, and most of the loads are carried by underlying stiffeners. The most critical load case for the wing structures is generally symmetric pull-up case in which the g limits of the aircraft are forced by the pilots. In these cases, wing deflects in upward direction and due to high bending loads, while the lower skin is in tension; the upper skin is exposed to high compressive loads which may affect the structure seriously. Therefore, particular importance must be given to the upper skin related with static load issues while the lower skin should be investigated from the fatigue load related issues.

3.2.2 Multi Rib / Multi Spar Comparison

When the layout of the wing is fixed, in order to optimize the structure by aiming to decrease the weight, a lot fewer parameters could be changed with the control of the

engineers. Therefore, the final decision on the layout is crucial. Most widely used approach on the selection of wing layout in preliminary design stage is to compare the number of spars and ribs used in other similar aircrafts. A precious study has been carried out in [23] by comparing 65 combat aircrafts and results are presented in Figure 3-2.

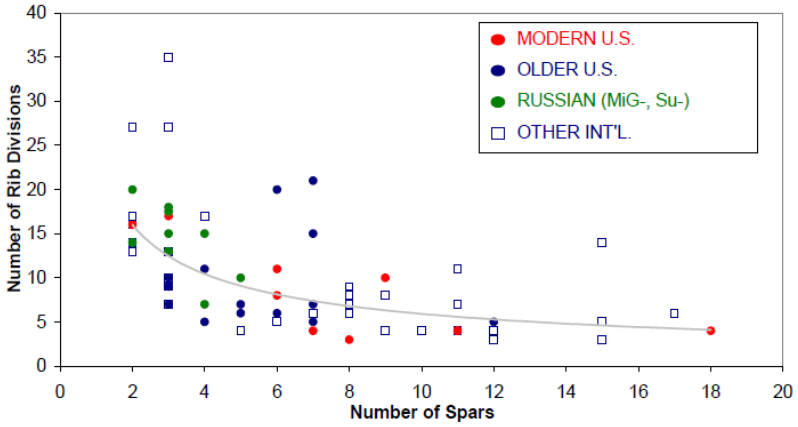

Figure 3-2 Investigations for the Number of Rib and Spars [23]

It can be observed from the above figure that by exclusion of some of the aircrafts, all designs can be investigated in two different categories. In the first one, the aircrafts use many ribs and a few spars (< 5). Many of the Russian aircrafts and early American fighters fall into this category. Mig-31 Foxhound and F-15 Strike Eagle are the most distinctive examples of multi – rib design. While 18 chord-wise division is found in Mig-31, on the other hand, it has only three spars at the root section and has two at the tip as shown in Figure 3-3.

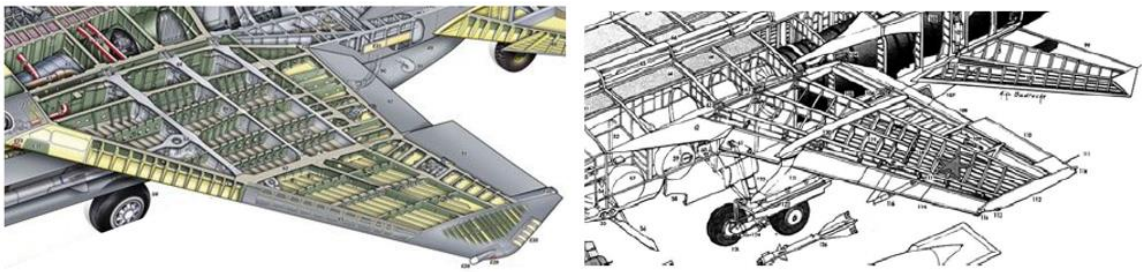

Figure 3-3 Representation for Aircrafts with Multi-Rib Configuration [24]

The second category involves wing with multi-sparred and less-ribbed. As seen from the Figure 3-4, this trend is more demonstrative on post 1960's American fighters. The first aircrafts coming to mind for multi-sparred configurations are F-16 Fighting Falcon and F-22 Raptor as shown in Figure 3-4. The internal layout of the F-22 wing is nearly contrary to Mig-31, it comprises 16 stiffeners in span-wise direction and four stiffeners in chord-wise direction.

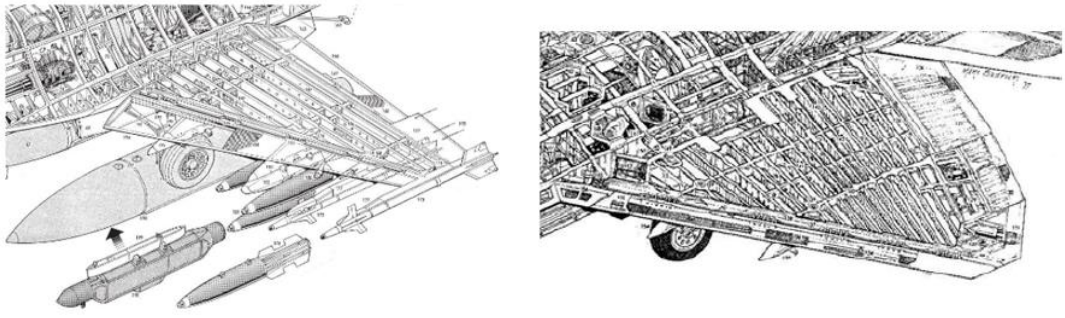

F – 16 Fighting Falcon F -22 Raptor

Figure 3-4 Representation for Multi-Spar Configuration [25], [26]

In addition to these, buckling strength of the plates (i.e. rib/spar webs and skin) plays a significant role in determining the multi-rib/spar concept since it is the most dominant constraint while sizing the components, especially for the upper skin. Plate buckling strength equation for isotropic plates are given in Equation 3.1. For the orthotropic and anisotropic plates, equation is almost the same except the stiffness parameters.

$$\sigma_{buckling} = \frac{k.\pi^2.E}{12.(1-\nu^2)}.\left(\frac{t}{b}\right)^2 \quad (3.1)$$

As inferred from Equation 3.1, buckling strength depends on width (b) which is illustrated in Figure 3-5, elastic modulus of the panel material (E), Poisson's ratio (ν), thickness (t) and buckling coefficient which is known as (k).

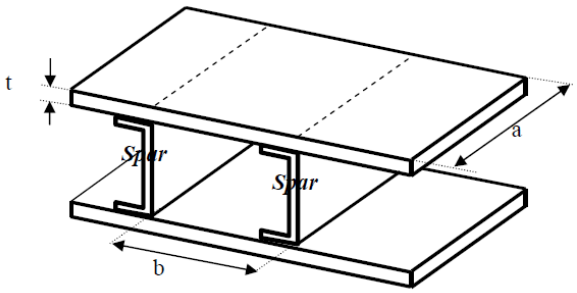

Figure 3-5 Dimensions for Buckling Analyses [27]

Besides the buckling strength, buckling coefficient also depends on panel dimensions which are shown in Figure 3-5. The alteration of buckling coefficient for compressive loading for simply supported is seen in Figure 3-6.

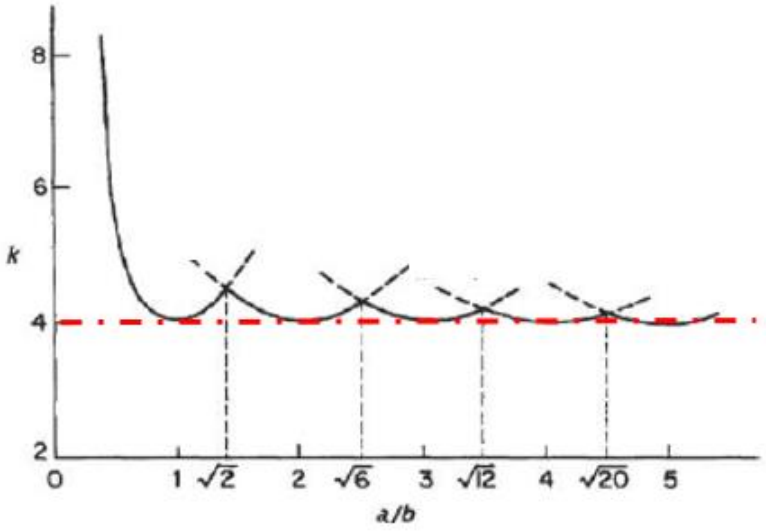

Figure 3-6 The Distribution of Buckling Coefficient for Simply Supported Conditions [28]

As it can be seen in Figure 3-6, the buckling coefficient (k_c) curves converge to a value of 4.0 for the panels having aspect ratio (a/b) greater than 1.5. Thus, it is not meaningful to increase buckling strength by changing the number of the ribs.

On the other hand, as can be seen from Equation 3.2, decreasing the buckling span (b), enhances the buckling strength quadratically while buckling coefficient converges to a value of 4.0. Therefore, it is obvious that using multi-sparred

configurations are much more meaningful from the viewpoint of increasing buckling strength of the panels.

$$\sigma_{buckling} \propto \left(1/b\right)^2 \tag{3.2}$$

As studied in [23], new combat aircraft designs are in the tendency of using more number of spars and less number of ribs. Multi-spar designs require a narrow spar spacing and wider rib spacing. As described in [29], in addition to ease of decreasing the weight, multi-spar configurations have the advantage of such as easiness of producing the panels, simple design and ease of ribs sealing.

As a consequence of all abovementioned specifications, in this study, multi-sparred design approach for the wing layout is preferred to generate various structural layouts.

3.3 Design Candidates

Several geometric candidates having different layouts are created while the outer geometry of the wing is kept constant. Design candidates are separated from each other with respect to number of spars, orientation and discontinuity. In general, design candidates can be investigated in three different families.

- The first family comprises spars parallel to each other with two different number of spars (i.e. parallel to rear spar). The most known fighter that uses this configuration is F-16 Fighting Falcon (Figure 3-7 and Figure 3-8).
- Second family comprises of converging spars with three different number of spars which are known as fanning type such as F-18 Super Hornet and F-104 Starfighter (Figure 3-9, Figure 3-10 and Figure 3-11).
- Final family consists of discontinuous spars which are known as runout. Examples for this family are Eurofighter Typhoon and F-22 Raptor (Figure 3-12 and Figure 3-13).

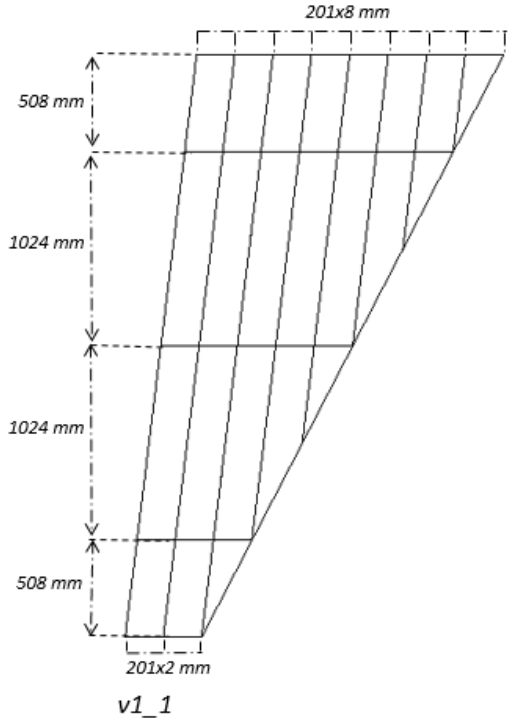

Figure 3-7 The First Candidate of Family 1 (v1_1)

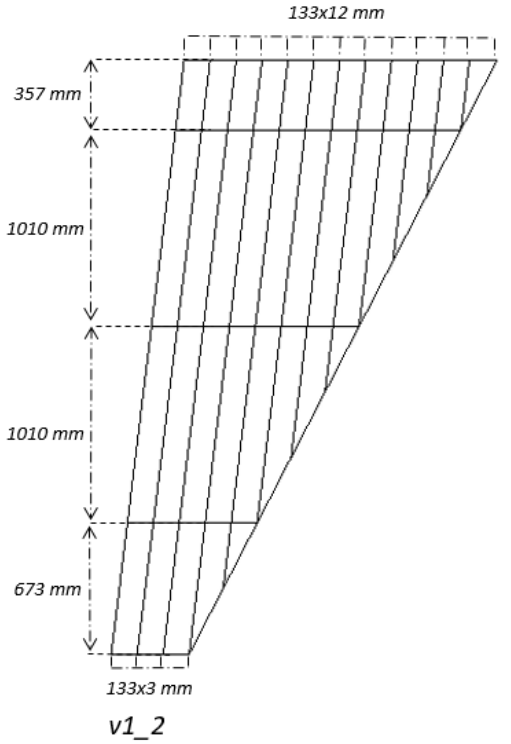

Figure 3-8 The Second Candidate of Family 1 (v1_2)

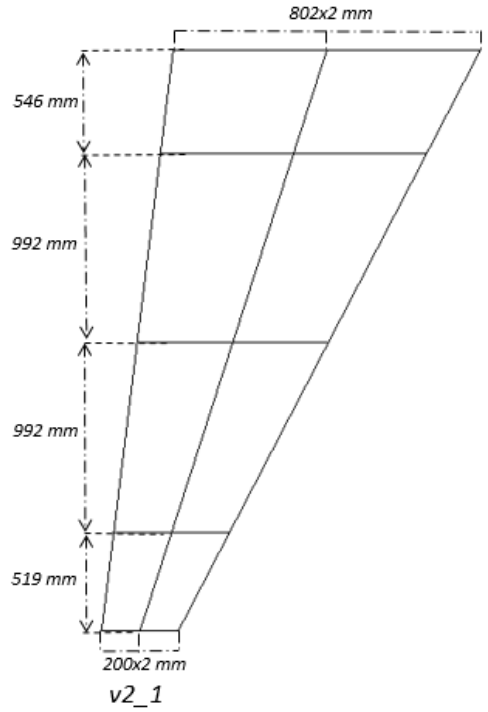

Figure 3-9 The First Candidate of Family 2 (v2_1)

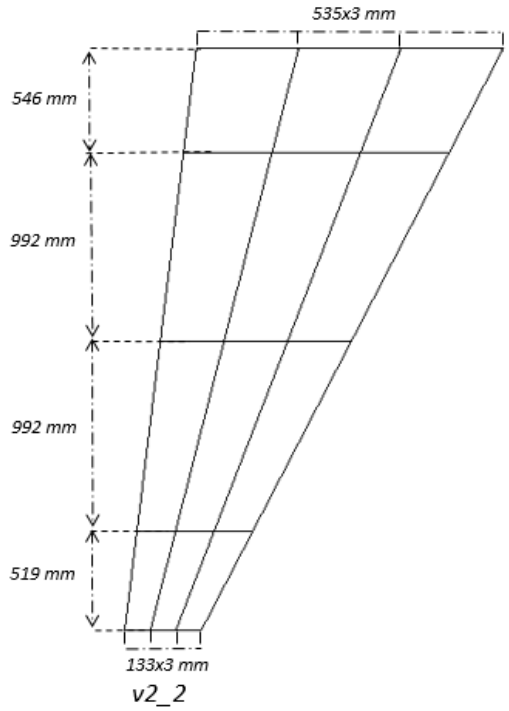

Figure 3-10 The Second Candidate of Family 2 (v2_2)

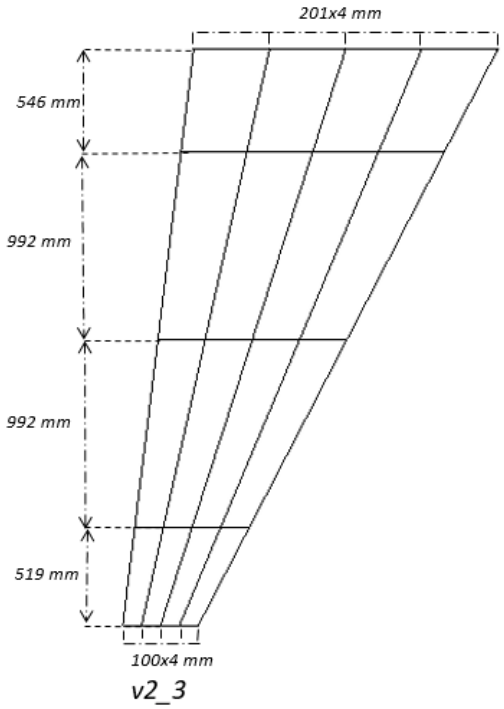

Figure 3-11 The Third Candidate of Family 2 (v2_3)

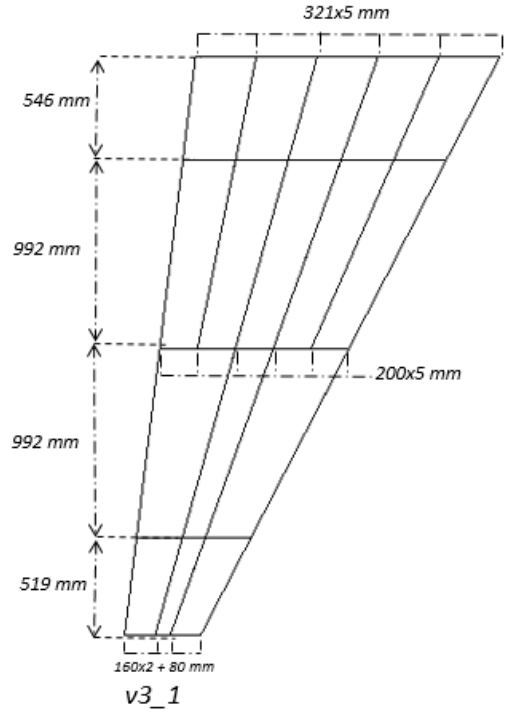

Figure 3-12 The First Candidate of Family 3 (v3_1)

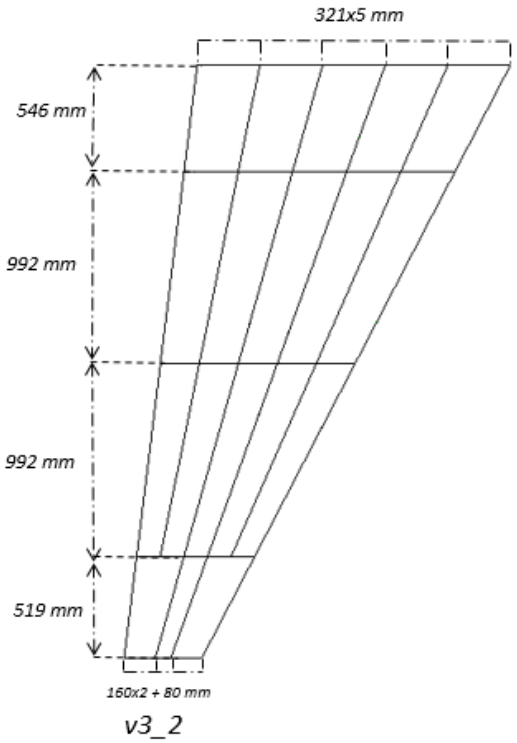

Figure 3-13 The Second Candidate of Family 3 (v3_2)

Finally, all of the candidate designs are listed in below Table 3-1 with their number of the ribs and the spars.

Table 3-1 Summary of the Candidate Designs

	Candidate	Number of Ribs	Number of Spars
Family 1	**v1_1**	5	9
	v1_2	5	13
Family 2	**v2_1**	5	3
	v2_2	5	4
	v2_3	5	5
Family 3	**v3_1**	5	6[1]
	v3_2	5	6[2]

[1] Two of the spars are until third rib
[2] Two of the spars are until fourth rib

3.4 Conclusion

In this section, first of all, the boundaries for both structural and aerodynamic surfaces are determined. After a brief explanation related with structural components, the theoretical background for concept layout selection is also presented. Finally, having decided on multi-spar concept, all possible configurations are created for predefined wing outer geometry and shown with their dimensions.

CHAPTER 4

STRUCTURAL FINITE ELEMENT MODELLING AND ANALYSIS

4.1 Introduction

Most of the airframe structures are generally designed as redundant which means that there is always backup when one of the structural elements fails to bear to the applied loads and in this type of structures, in order to calculate the internal forces occurred in the elements, the equilibrium conditions are not adequate. Extra equations such as compatibility equations are also needed. Therefore, analyzing aircraft structures become impracticable without using finite element models and in this study, all analyses are performed with the aid of finite element modelling and analysis tool.

4.2 Structural Modelling of the Wing

Finite element models have important role in the cost of the analyses, especially in optimization studies in which multiple analyses must be converged and they should be trustable by the engineers to be used for the sizing of their structures.

After designing the outer surfaces of the wing with the aid of CATIA, shown in Figure 4-1, all meshable geomeries are imported to the MSC PATRAN interface which is one of the most widespread pre-processor used in the aircraft industries.

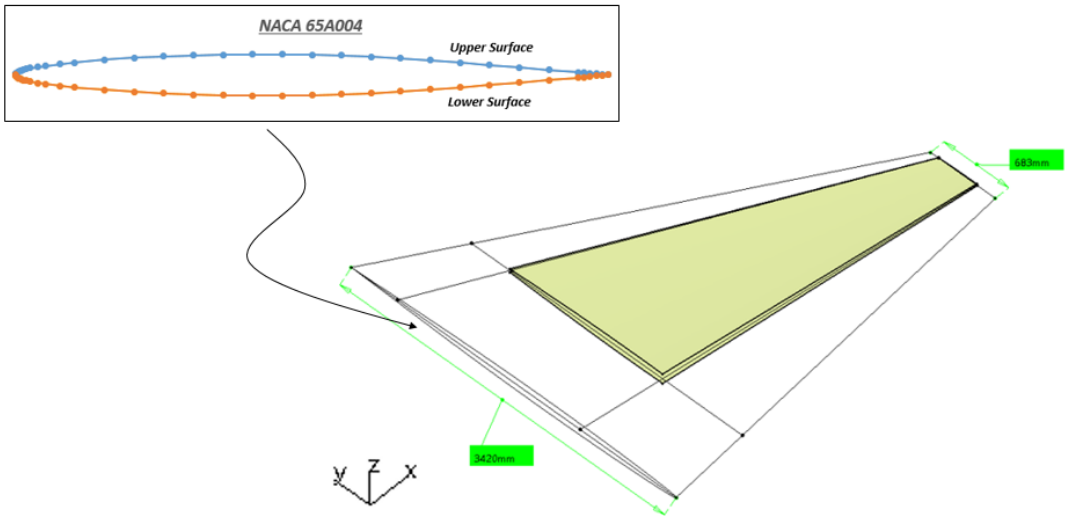

Figure 4-1 Airfoil Profile and the Outer Geometry of the Wing

In finite element modelling theory, at first, there are three different element types to model structures. While membrane elements carry only in-plane loads, plate elements carry out-off plane loads and the shear elements are used for only shear loads. Then, with the emerge of shell elements having the capability of carrying all of the three loading types, FEMs can be constructed by using less number of elements. Actually, FEMs can also be performed by using 3-D elements, however, advantages of solution time and easiness of evaluating results lead engineers to use 2-D elements more widely.

In the aircraft industry, global finite element models (GFEMs) are used to perform the initial sizing of the componenets in the preliminary design stage as shown in Figure 4-2. In the GFEMs, all design zones consisting of intersection of the rib and spars are generally modelled with only one element. However, nowadays, with the increase of the performance of the computers and the capability of solving complex models in a short time, finer meshes are started to be used widely in prelimanary stage as well.

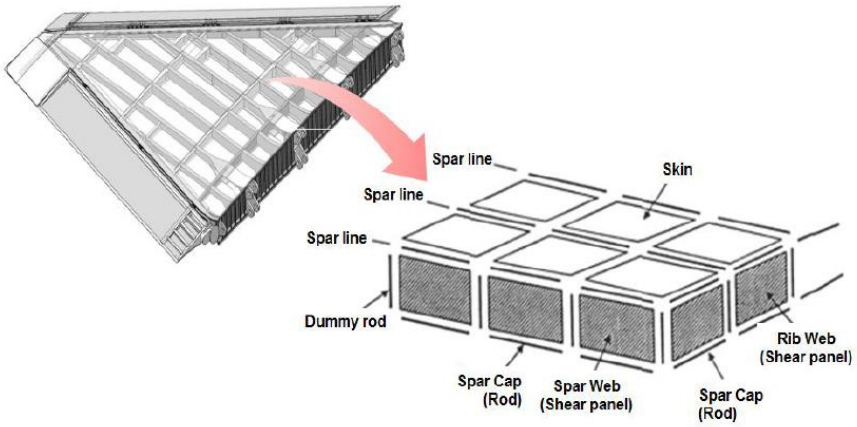

Figure 4-2 Representation of the GFEMs for the wings [30]

Depending upon the geometry mentioned in the previous section, all FEMs are created with the aid of pre- and post- processor program MSC PATRAN.

To determine the adequate mesh size, for each candidate, four different models in different sizes are created and mesh convergence studies are performed. All obtained mesh convergence results for each candidate can be found in Appendix A. According to the outcome of the mesh convergence studies, finer model in which the size of the elements are 55 mm is found to be sufficient to determine the load path effectively as it can be seen from the Figure 4-3.

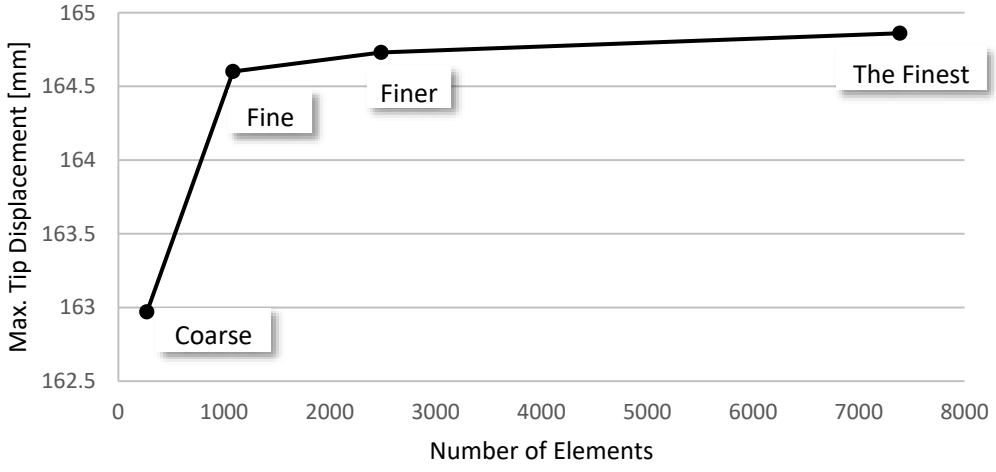

Figure 4-3 Mesh Convergence Results for Wing v1_1

While creating the FEMs, the attention is paid to use CQUAD4[3] element since CTRIA[4] elements are stiffer [31] and when they are excessively used instead of CQUAD4 elements, they are undertaken much more stress, and therefore, the load path may not be simulated properly. 2485 elements and 2157 nodes are used to create the FEM of the wing v1_1 which is shown below in Figure 4-4. The main load carrying components in the wing structure is presented in Figure 4-5.

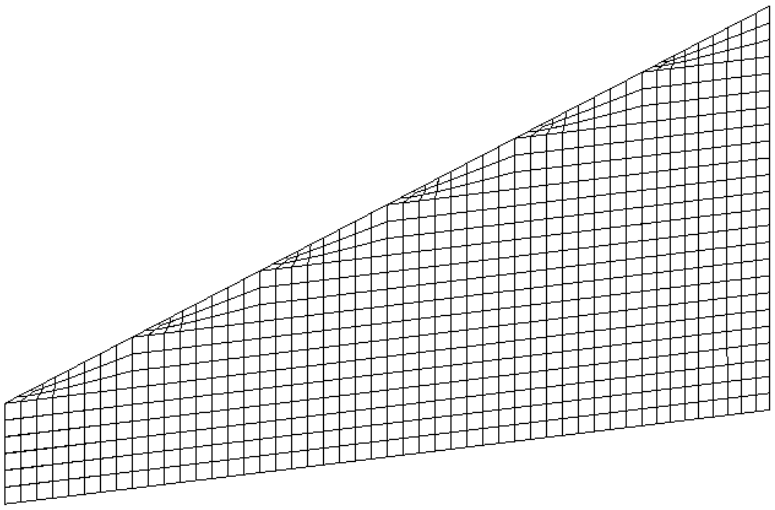

Figure 4-4 Finite Element Model of the Wing v1_1 (Top view)

[3] CQUAD4 represents 4-node bilinear quadrilateral element
[4] CTRIA represents 3-node linear triangular element

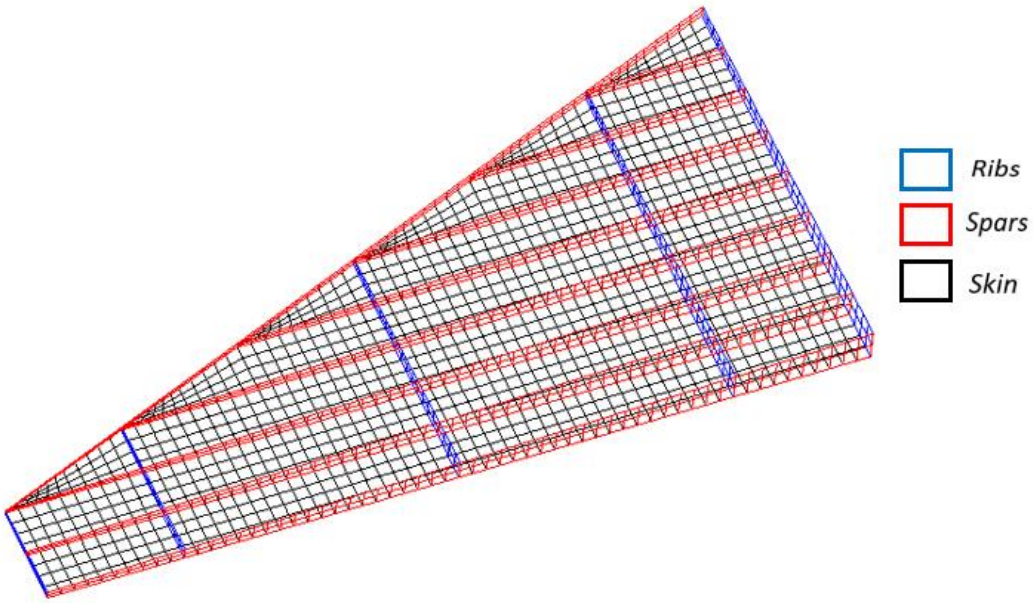

Figure 4-5 Main Structural Components of the Wing v1_1

Finally, the boundary condition for the wing is applied by using rigid body elements. The independent node of rigid body element (here is RBE2) is fixed in three translational directions (i.e. along x, y, z) and only one rotational (i.e. about x) direction according to given coordinate system. The representation of boundary conditions applied for the wing v1_1 is presented below in Figure 4-6. As it can be seen from Figure 4-6, the model is not fixed from all rotational directions to avoid bringing of extra stiffness and the boundary condition along the rotational directions of y and z are intended to be provided with coupling of other fixations.

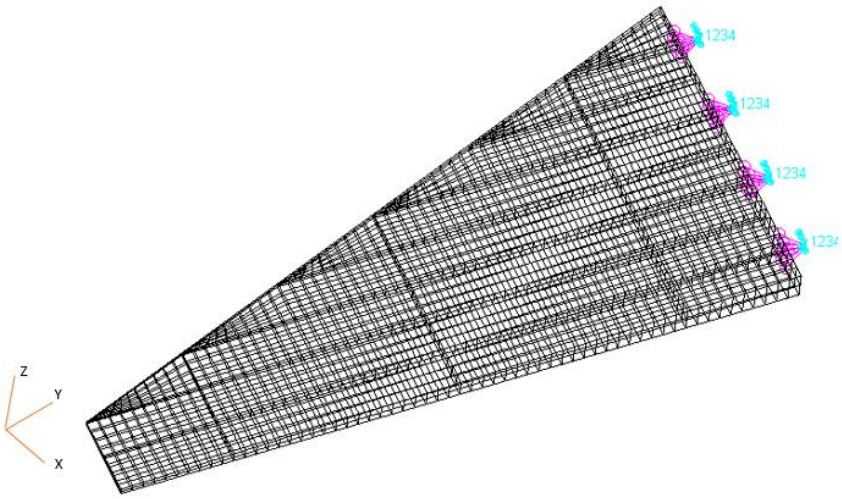

Figure 4-6 Boundary Conditions of the Wing v1_1

4.3 Material Properties

For this study, both metallic and composite materials are used for modelling the structural components. With a general approach for modern fighters, skin is considered to be formed of composite materials and both ribs and spars are modelled as metallic. As for the composite material, Hexply AS4/8552/RC34/AW134 is selected which consists of unidirectional carbon fibers and are widely used by aircraft companies. The material properties of the Hexply AS4/8552/RC34/AW134 is presented below in Table 4-1.

Table 4-1 The Properties of Hexply AS4/8552/RC34/AW134 [32]

Elastic Modulus 11	E_{11}	130000 N/mm^2
Elastic Modulus 22	E_{22}	8700 N/mm^2
Poisson's Ratio 12	ν_{12}	0.36
Shear Modulus 12	G_{12}	2900 N/mm^2
Limit Tensile Strength 11	X_T	2280 N/mm^2
Limit Tensile Strength 22	Y_T	35 N/mm^2
Limit Compressive Strength 11	X_C	1360 N/mm^2
Limit Compressive Strength 22	Y_C	223 N/mm^2
Limit Shear Strength	S	107 N/mm^2
Cured thickness of ply	t	0.13 mm

It should be noted that, “1” and “2” in Table 4-1 represents the longitudinal and transverse direction of the fibers, respectively. As mentioned before, all of the skin elements of the wings are modelled with this material.

For the metallic components (i.e. ribs and spars) used in this study Al 7050 T7451 material is used. The thicknesses of the ribs and spars are sized by using continuous design variables so that the thickness transition will be smooth between the adjacent zones. Sheet materials have only discrete values and in order to apply a continuous approach, machinable materials should be used. For this reason, Al 7050 T7451 is selected and the material properties of it can be seen in Table 4-2.

Table 4-2 The Material Properties of Al 7050 T7451 [33]

Elastic Modulus	E	72000 N/mm^2
Poisson’s Ratio	ν	0.33
Tensile Ultimate Strength	F_{tu}	524 N/mm^2
Tensile Yield Strength	F_{ty}	469 N/mm^2
Compressive Yield Strength	F_{cu}	441 N/mm^2
Ultimate Shear Strength	S	310 N/mm^2
Density	ρ	2.83 g/mm^2

4.4 Modal Analysis of the Wing Structure

To investigate the dynamic attitudes of the wing structure, modal analysis is performed. Understanding of the natural frequencies or eigenmodes is very important especially from the view of aeroelasticity since structural problems such as resonance and flutter which are totally based on the frequency values of the wing may result in fatal accidents [34]. Therefore, modal analyses of the wing structures should be performed at the beginning of the preliminary design stages by the engineers.

The geometric properties of the wing such as taper ratio and swept angle are very important parameters affecting the natural frequencies and in order to have an idea about the levels of the natural frequencies of the wing and as the optimizations starts

with the random variables and while beginning to this thesis study, there are no referable thickness values for any of the wings, a dummy model is created. Therefore, the thicknesses of all elements used in this model are defined as 1 mm before starting the optimization as an initial value with the material of Aluminum 7050 T7451.

Flutter phenomena generally arises from the coupling of the 1st bending and 1st torsion modes of the wing structures [34]. The first three mode shapes of the wing which are used in this study show the first out-of-plane bending, the bending-torsion coupling and the first torsion characteristics, respectively. Values of the natural frequencies are listed in Table 4-3 and associated mode shapes are demonstrated in Figure 4-7, Figure 4-8 and Figure 4-9 respectively for the initial design of configuration wing v1_1.

Table 4-3 The First Three Natural Frequencies of the Wing v1_1

Mode ID	Natural Frequency [Hz]	Description of the Mode
1	12.89	The First Out-of-Plane Bending
2	44.36	Bending-Torsion Coupling
3	69.16	The First Torsion

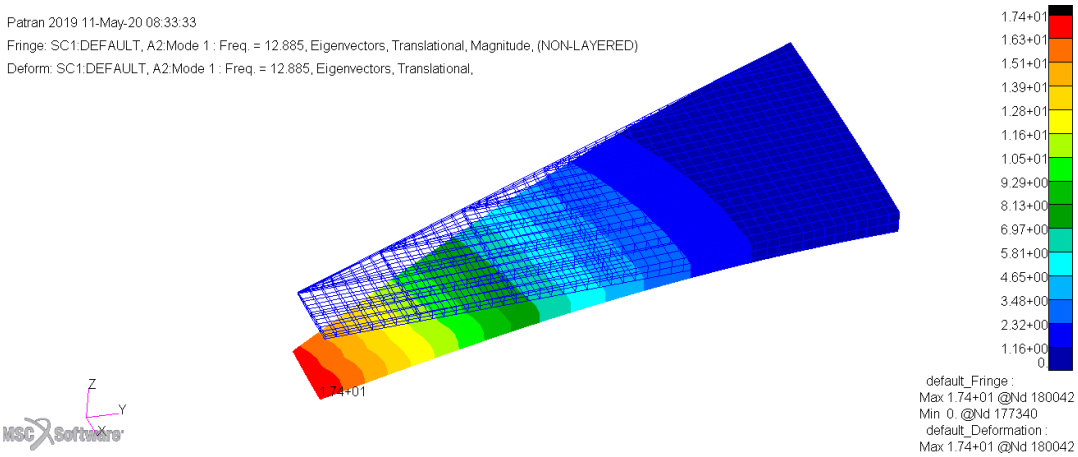

Figure 4-7 The First Out-of-Plane Bending Mode Shape of the Wing v1_1

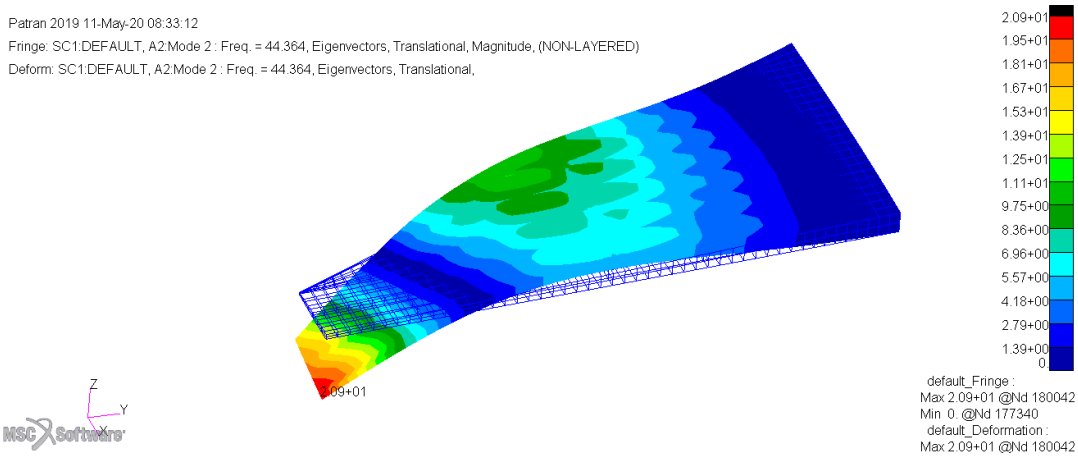

Figure 4-8 Bending-Torsion Coupling Mode Shape of the Wing v1_1

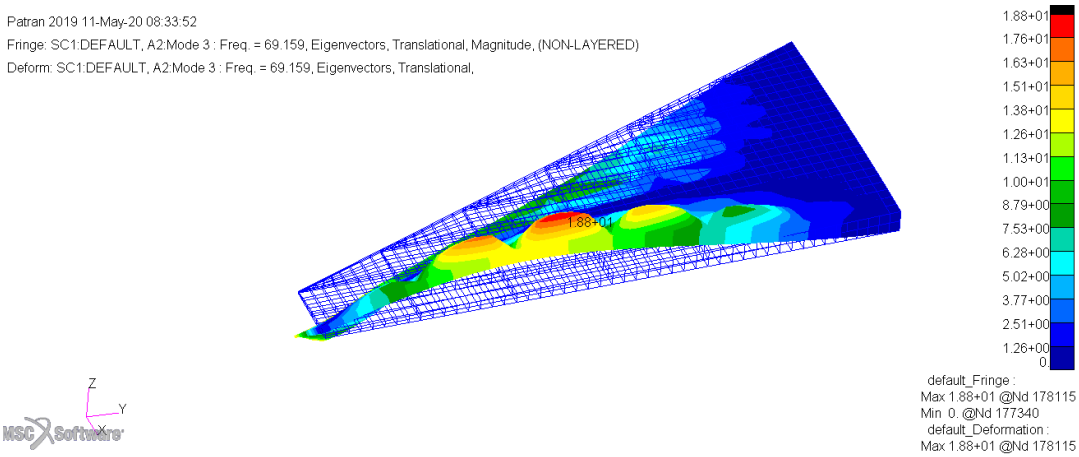

Figure 4-9 The First Torsion Mode Shape of the Wing v1_1

4.5 Conclusion

In this part, structural FEMs are created by using generated surfaces in CATIA. Mesh size to be used in the models is determined according to the mesh convergence study and finally is defined as 55 mm. Only the model belongs to wing v1_1 is shown as an example. Material properties used for the modelling of the structural components are also presented. Besides, in order to investigate the dynamic characteristics of the wing structure, modal analyses are performed with dummy properties using MSC NASTRAN. The first three modes which contain the first out-of-plane bending and

first torsion modes are especially investigated since these modes are the critical ones for further aeroelastic analyses.

CHAPTER 5

AERODYNAMIC MODELLING AND TRIM ANALYSIS FOR DETERMINATION OF LOADS

5.1 Introduction

The thickness distribution of the structures represents the internal load distribution and the internal loads depend on the external loads within the applied boundary conditions. The load cases are generally designated according to the certification specifications such as MIL-A-8861B for the military aircrafts [35]. In addition to certification specifications, there are also additional maneuvers requested by air forces of the countries. Control surfaces movements, weapons and landing may lead to critical loads for the wing structures, however for the preliminary design stage in which the candidate structures are compared, pull-up maneuver with maximum g limits will be sufficient [36].

5.2 Aerodynamic Modelling Methodology

In this study, determination of the loads is on the basis of FEM as the same in structural analysis and optimization studies. Processes in the analysis and the optimization sections for this study are performed by using the loads which are obtained via the capabilities of MSC FLDS and MSC NASTRAN. The aerodynamic models are created on interface of MSC FLDS and the results related with loads are produced by MSC NASTRAN using the linearized panel methods such as Doublet-Lattice and ZONA 51 which are used for subsonic and supersonic conditions, respectively [37]. Basically, the aerodynamic loads are developed when the flow is

disturbed by a deflection of flexible structure in which deflections include both rigid body motions of the structure and structural deformations due to maneuvers. The main elements in aerodynamic modelling are box or strips (Figure 5-1) on which aero loads are calculated. Both Doublet-Lattice Method and ZONA 51 require these panels as long as their edges are parallel to free-stream velocity.

The Doublet-Lattice method is published by Rodden and Albano in 1969 [38] and the other method used for supersonic conditions, ZONA 51, is revealed by Chen and Liu in 1985 [39]. They are both very practical and time saving methods which could be used especially for the aircrafts at the preliminary design stage. Supplying the inputs related with flight regime such as Mach number and dynamic pressure, loads acting on the structures can be found in short time using MSC FLDS and the solver MSC NASTRAN, compared to other computational fluid dynamic (CFD) methods.

To benefit from these methods, first, the wing planform is divided into trapezoidal elements and all surfaces, in which the aerodynamic elements are located on, are aligned with the free-stream velocity. All of the calculations related with these methods are fulfilled in control points which are located on aero elements (i.e. strips) and location of these points changes according to the method. While for the Doublet-Lattice Method, the location of a control point (or a collocation point) is assigned at ¾ of the chord as shown in Figure 5-1 and this location is situated at 95% chord-wise station for each aero element in ZONA 51 [40].

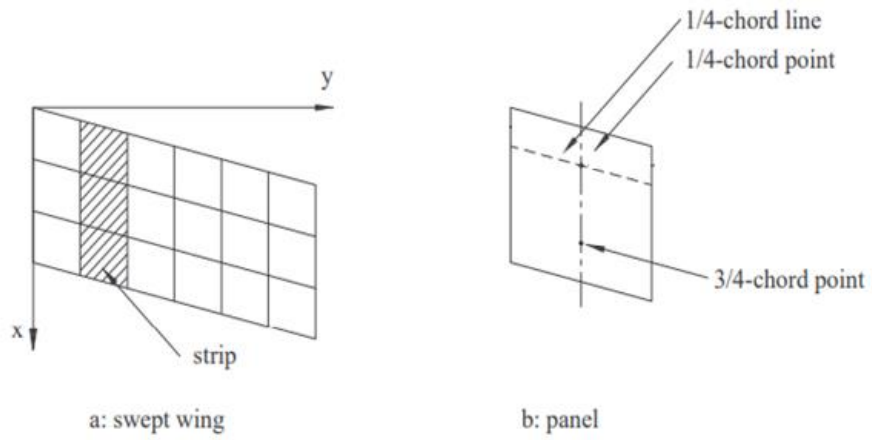

Figure 5-1 Surface Representation by Quadrilateral Elements [41]

Although the locations of the control points are different, relationship between the pressures occurred in each aerodynamic elements and local angle of attack according to the freestream velocity which is generally known as downwash could be calculated by the same matrix equations for both methods. This relationship is also known as aerodynamic influence coefficient (AIC). The basic equation for relation of pressure and downwash can be summarized as below [42];

$$w_j = \left({}^{1}/_{q}\right)\left[AIC_{jj}\right]\{p_j\} \tag{5.1}$$

where,

w_j, downwash

p_j, pressure on aerodynamic element

AIC_{jj}, aerodynamic influence coefficient matrix

q, dynamic pressure.

Two different type of displacement sets are calculated in MSC FLDS for any type of aeroelastic analysis. The first of these is the displacement of grids on the aerodynamic elements which is known as dependent displacement (u_k) and the second one is the structural displacement and generally known as independent displacement set (u_g) which includes the structural grid displacements. In order to

couple the aerodynamic and structural element, spline method is used. The structural and aerodynamic model have no connection until the splines are used to build an interpolation matrix. This matrix is used to determine the motion of the aerodynamic grids based upon the motion of the structural grids since the MSC NASTRAN aeroelastic analyses are fulfilled by using motion of the structural grids. Spline method constitutes the interpolation matrix $[G_{kg}]$ that relates the aerodynamic (u_k) and structural grid point deflections (u_g) [43].

$$\{u_k\} = [G_{kg}]\{u_g\} \tag{5.2}$$

In order to obtain the interpolation matrix, five different methods are provided in MSC FLDS. These are [17] namely;

- Infinite plate spline
- Thin plate spline
- Finite plate spline
- Linear (Beam) spline
- Point to point spline

In this study, surface spline method is used to provide an aero-structure coupling of the wing and the beam spline for the horizontal stabilizer. It should be noted and can be inferred from the below Figure 5-2 that although each structural node can be used for more than one for the spline and each aero node must be used for only one spline in aero-structure coupled models as a rule for surface splining in MSC FLDS [44].

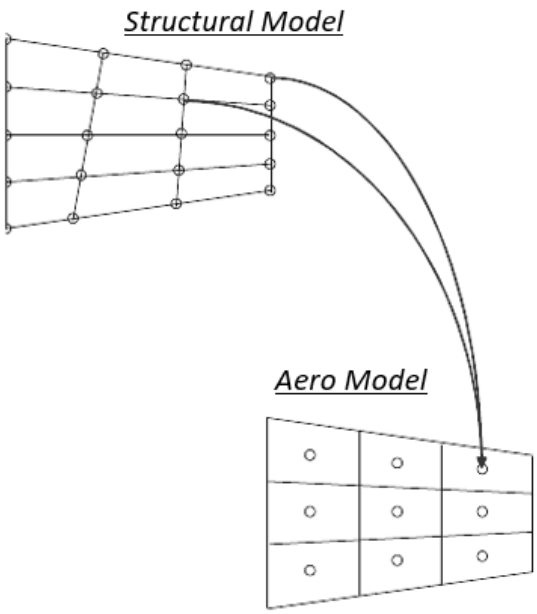

Figure 5-2 Surface Spline [44]

5.3 MSC FLDS for Trim Analysis and Load Calculation

In the flight mechanics, trim means that aircraft is in the equilibrium condition with constant speed. To trim the aircrafts longitudinally, all movable surfaces should be adjusted to provide the equilibrium conditions in three directions. The general forces acting on the aircraft is shown in Figure 5-3. For the aircraft at the symmetric maneuver condition, total forces (F) about x and z directions are [45],

$$\sum F_x = L\sin(\alpha_e) + \tau_e \cos(K) - D\cos(\alpha_e) - mg\sin(\alpha_e + \gamma_e) = 0 \qquad (5.3)$$

$$\sum F_z = mg\cos(\alpha_e + \gamma_e) - L\cos(\alpha_e) - D\sin(\alpha_e) - \tau_e \sin(K) = 0 \qquad (5.4)$$

where, α_e, body incidence angle, γ_e angle of steady flight path and K is leaning angle of thrust line according to body x axis.

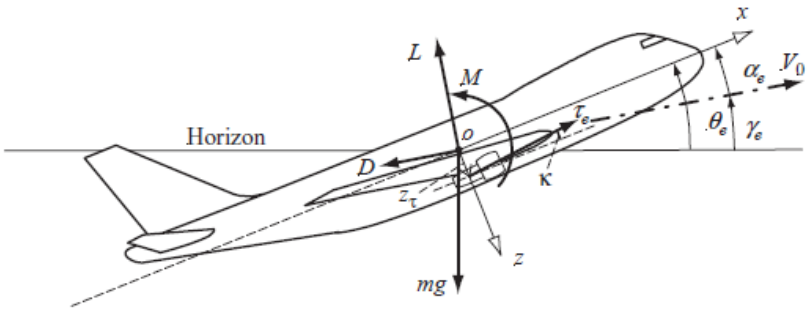

Figure 5-3 Longitudinal Forces Acting on the Aircraft [45]

The external load calculation of the aircrafts is generally performed with using 3-D CFD methods. However, in the beginning design phases of the aircrafts in which the outer geometries are changing frequently and design flexibility is needed, updating 3-D meshes and running CFD analyses are very time consuming. MSC Software Corporation realized the requirement for the trustable and rapid load calculations and developed a tool to support companies in the field of aeroelasticity and loads called as MSC FLDS (FlightLoads). The MSC FLDS uses MSC PATRAN as a pre- and post- processor and MSC NASTRAN as a solver [37] and the most general procedure for MSC FLDS is given below in Figure 5-4.

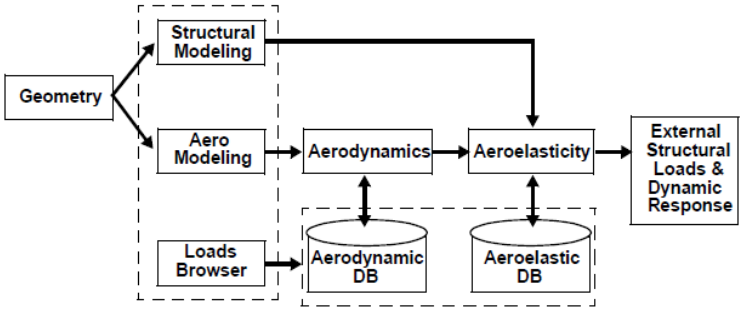

Figure 5-4 FLDS Architecture Overview [37]

Based on the inputs provided by the user such as reference chord, span, area and density, the outputs of the MSC FLDS are the balanced external loads which can be obtained as a nodal value whether on the aero nodes or on the structural nodes.

Besides, MSC FLDS has the capability of collecting the loads on the predefined monitor stations at certain intervals.

In this study, aerodynamic properties of the aircraft simulated at the trim analysis is the one similar to T-38 Talon which is named as “ARI” in Turkish Air Force and the aero model of which is created for the trim analysis and it is shown in Figure 5-5.

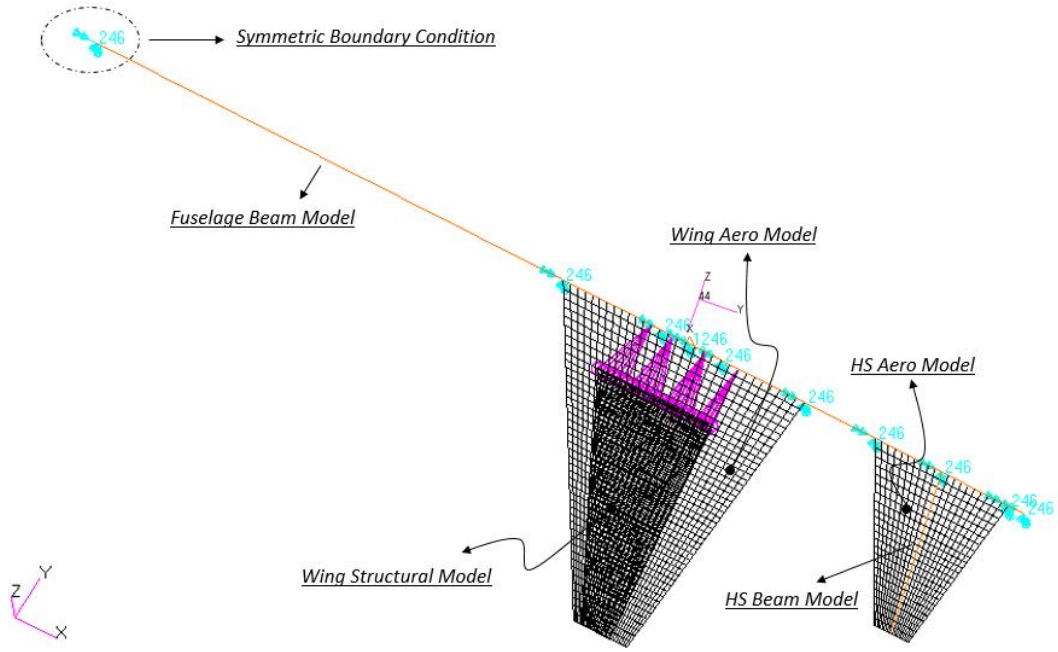

Figure 5-5 Representation of the Created Trim Model

As it can be concluded from Figure 5-5 that the half model is used in this study. The wing has an aspect ratio of 3.75 and there is no dihedral nor any incidence angle according to fuselage. At the quarter chord station, sweepback angle is 25 degrees. Reference wing span (i.e. full span) is 7700 mm while the reference chord is used as 3260 mm and reference wing area for the full aircraft is 1.62×10^7 mm^2.

For the trim analysis, fuselage and horizontal stabilizer should be included in the aerodynamic model. Actually, vertical stabilizer should also be modelled, however in this study, as no rolling maneuvers will be considered, there is no need to model the vertical stabilizer. The horizontal stabilizer, on the other hand, is modelled with aspect ratio of 2.85 and a reference area of 2.9×10^6 mm^2. The FEM of the horizontal

stabilizer is idealized with aluminum bar elements. The cross-sectional area of the bar elements is modelled as 4000 mm^2 and moment of inertia values I_{xx} and I_{yy} (where x and y are the mutually perpendicular axes to the centroid axis of the bar cross-section) are assumed as $1.2x10^8$ mm^4. Similarly, the fuselage is modelled with aluminum bar element which has 13190 mm in length. The cross-sectional area of the fuselage beam is taken as 10000 mm^2 and considered as the same at every station. The moment of inertia value for the fuselage beams is taken as $2x10^9$ mm^4 [43]. Finally, to simulate the weight of the aircraft, conm2 element [46] is located approximately at the center of gravity and the value of this mass element is considered as 3.26 ton.

In general, customers want aircraft to fly at its maximum g limit both in subsonic and supersonic regimes. However, in supersonic regime, sizing the aircraft structure according to maximum g limit that is sustained at subsonic regime, results in heavier structure and decreases the payload capacity of the aircraft. In [47], designing the aircraft to fly at 0.8 times of its maximum g limit for subsonic conditions is stated as an overall approach for determining maximum limits of the aircraft in supersonic flights. Therefore, while determining the supersonic flight condition, this approach is adopted.

As indicated in Table 5-1 the aircraft is assumed as flying at two different flight regimes, first one is the subsonic pull-up case with +7g at sea level and the other case is the supersonic flight regime with +5.6g at10000 ft (3048 m).

Table 5-1 Load Case Definition

Load Case	**Type**	**Mach**	**Altitude [ft]**	**n_z [g]**	**q [Pa]**
1	Pull-Up (subsonic)	0.6	Sea Level	+7.0	$0.0255 x10^6$
2	Pull-Up (supersonic)	1.3	10000	+5.6	$0.0827 x10^6$

n_z represents the load factor in the z direction sustained by the aircraft and q is the dynamic pressure.

Using NASTRAN Static Aeroelastic Solver (Sol 144), the trim results are obtained. It should be noted that using both predefined two load cases in the optimization process concurrently, increases the computational effort. Therefore, total loads which are collected in the predefined monitor stations [Appendix B] are compared with each other and the subsonic +7g subsonic pull-up condition is found to be more critical for the structure and it is used for all optimizations which are performed in this study. When the elevator is in 5.1 degrees and the angle of attack is 23.2 degrees, the aircraft is found to be at the trim condition for the +7g subsonic pull up condition. It should be noted that, an increase in the angle of attack after around 15-20 degrees become dangerous related with the stall issues. Besides, it is also known that with the design improvements such as including high lift devices, aircrafts can fly safely with very high angle of attacks. Therefore, as it is beyond the scope of the this thesis study, the trim analysis is not checked whether the aircraft stably fly or not at 23.2 degrees of angle of attack, however, in further detailed studies, this should also be checked. The force and the bending moments are summed at the predefined monitor stations as shown in Figure 5-6 to distribute them to the structural model via rigid body elements (RBE3).

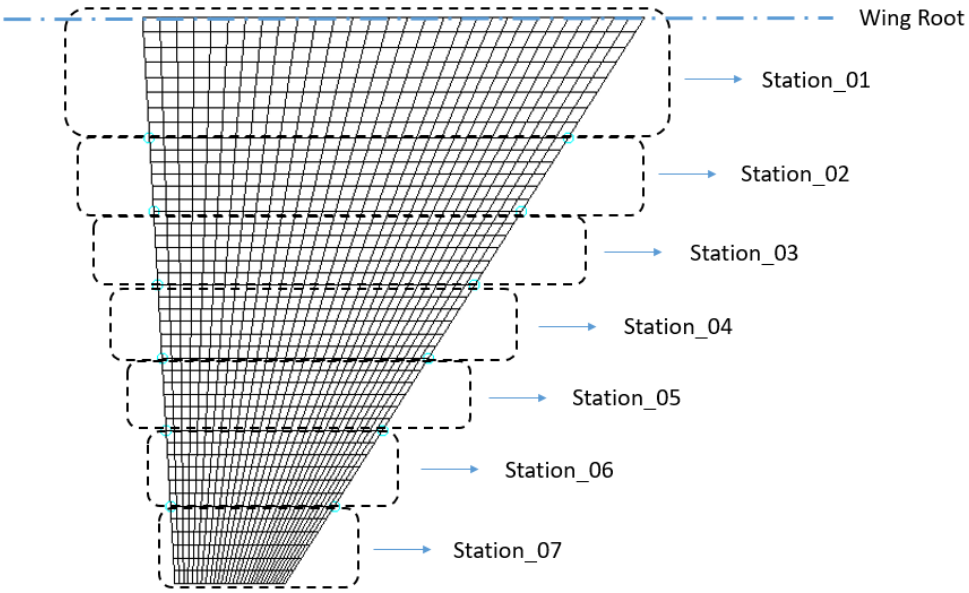

Figure 5-6 Monitor Stations

The shear and the bending moment distributions along the span direction are graphed by using MSC FLDS and shown in Figure 5-7 and Figure 5-8. For the purpose of investigating the effect of aero mesh density to the loads, another trim analysis is performed with fine aero mesh and no significant difference between obtained loads is observed and the results are presented in [Appendix A] as well.

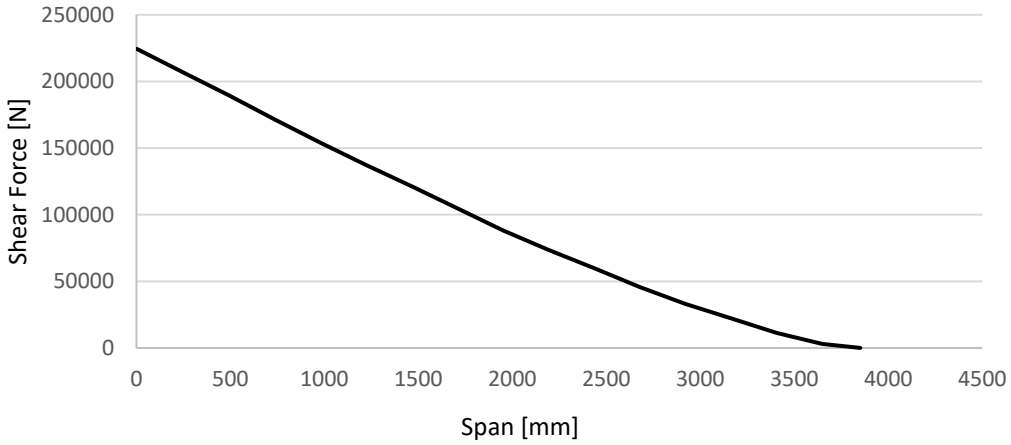

Figure 5-7 Shear Force Distribution using MSC FLDS

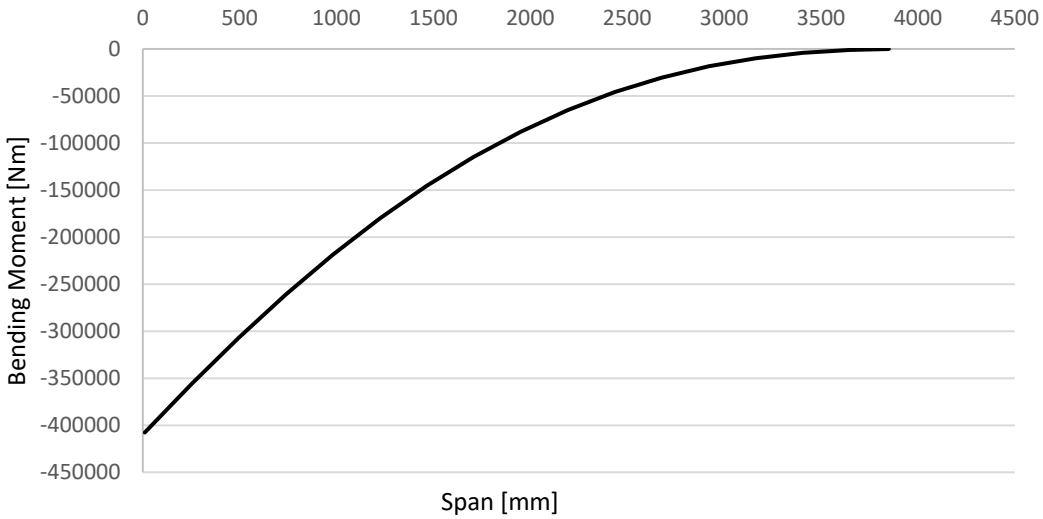

Figure 5-8 Bending Moment Distribution using MSC FLDS

As it can be seen from Figure 5-7 that, at the root section, the shear force is almost the half of the aircraft weight with +7g pull up maneuver and equal to 224544 N.

$$^{nW}/_{2} = 223978.8\ N$$

The difference is approximately 0.25% between the half weight of the aircraft with +7g inertia and then shear force obtained from MSC FLDS trim analysis and this result indicates that it can be used reliably for preliminary design stage prior to the CFD analyses.

5.4 Schrenk's Approximation

After obtaining loads on the wing by using MSC FLDS, in order to correlate and be able to claim that load distribution along the span direction is meaningful, another method known as Schrenk's approximation founded by Oscar Schrenk in 1940 [48] is used.

The method states that the resultant load distribution is an arithmetic mean of:

1. A load distribution representing actual planform shape,
2. An elliptic distribution of the same span and the area.

The formula for the elliptical lift distribution is given by:

$$w(y) = \frac{4nW}{\pi b}\sqrt{1 - \left(\frac{2y}{b}\right)^2} \tag{5.16}$$

and the formula for the trapezoidal distribution is derived as:

$$w(y) = \frac{4nW}{(1+\lambda)b^2}(\lambda - 1)y + \frac{2nW}{(1+\lambda)b} \tag{5.17}$$

where,

n, load factor

W, weight of the aircraft

b, full span of the wing

y, span-wise position

λ, taper ratio.

To sum up, distributed forces with unit span for the whole wing is,

$$w(y) = \frac{w(y)|_{elliptical} + w(y)|_{trapezoidal}}{2} \tag{5.18}$$

and graph that shows the lift distribution can be seen below in Figure 5-9.

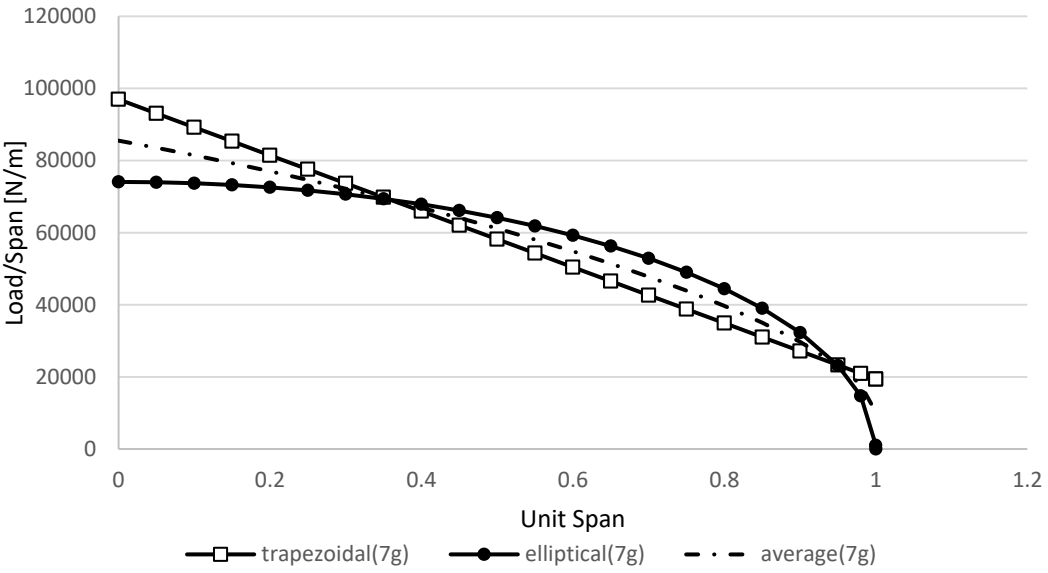

Figure 5-9 List Distribution along Unit Span with Schrenk's Approximation

The relation between the distributed force, shear force and the bending moment is simply given as;

$$\frac{dV}{dx} = -w, \qquad \frac{dM}{dx} = V$$

Using above relations, the shear force and the bending moment distribution on the wing with Schrenk's Approximation can be found. It should be noted that, in Schrenk's Approximation, loads are calculated for the center of pressure the location where the resultant force on the airfoil acts. For the subsonic wings, the center of pressure is generally assumed to be located on 25% of chord length. The obtained distributions for the shear force and the bending moment along the wing span are shown below in Figure 5-10 and Figure 5-11, respectively.

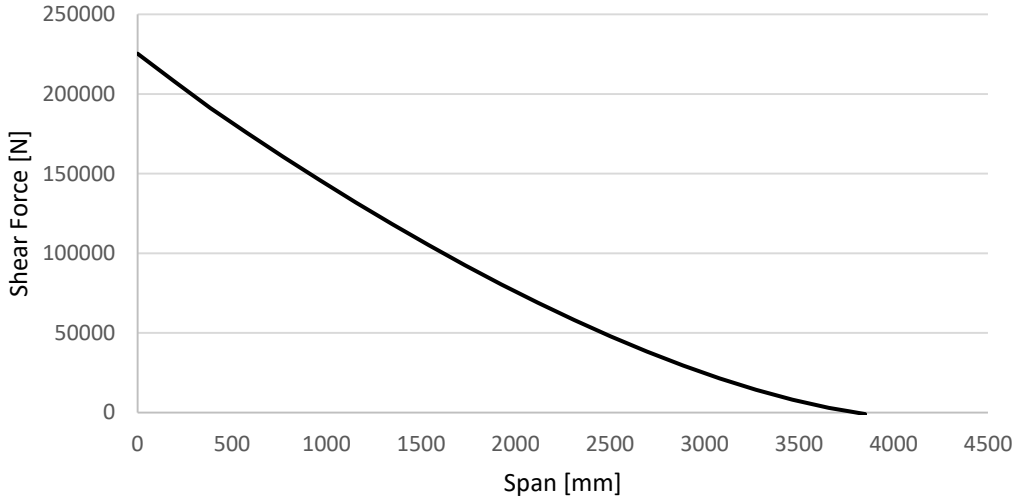

Figure 5-10 Shear Force Distribution along Wing Span using Schrenk's Approximation

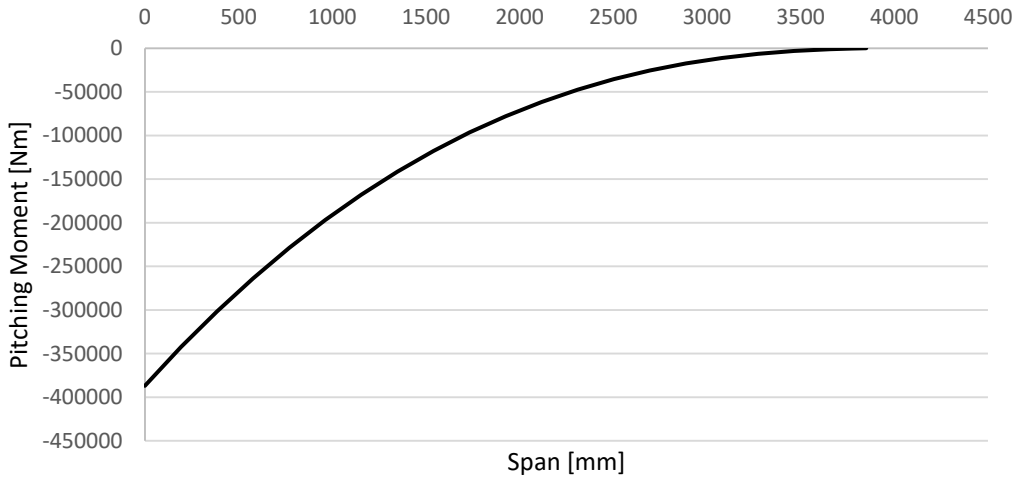

Figure 5-11 Bending Moment Distribution along Wing Span using Schrenk's Approximation

5.5 Comparison of the Methods for Shear and Bending Moment Distributions

In this section, shear force and bending moment distributions obtained by using two different methods are compared. The first method used is doublet lattice method with

the aid of MSC FLDS which requires both aero and structural FEMs. On the other hand, the second method is Schrenk's Approximation which is solely based on the mentioned analytical equations. Comparisons of the results for the +7g pull-up maneuver condition can be seen in Figure 5-12 and Figure 5-13.

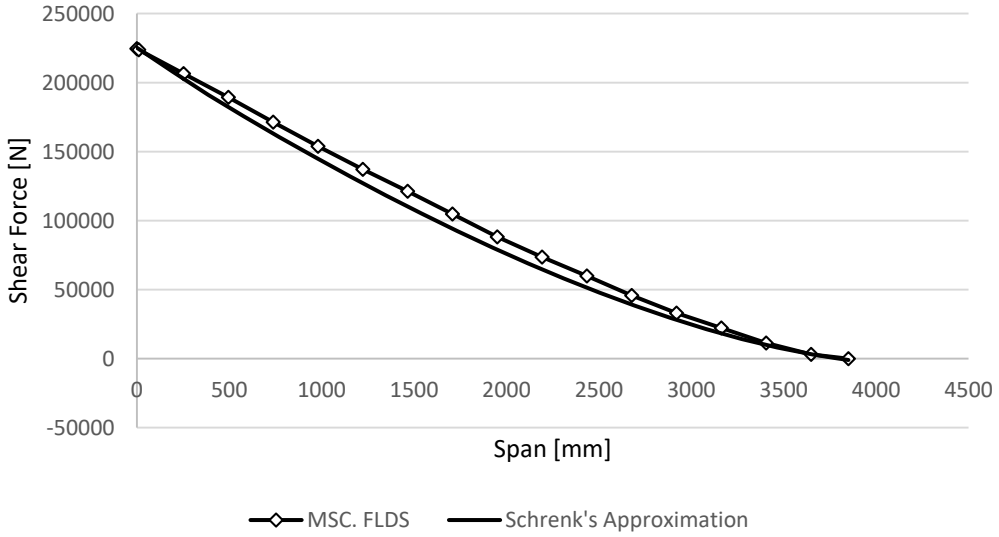

Figure 5-12 Comparison of Two Method for the Shear Force Distribution

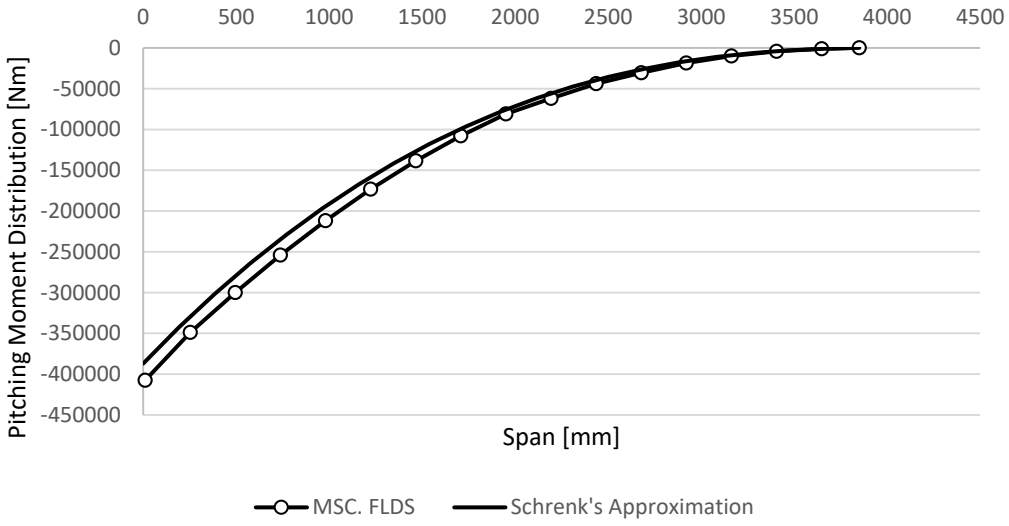

Figure 5-13 Comparison of two Method for the Bending Moment Distribution

5.6 Conclusion

In this section, steps related with the determination of the loads are explained. For this purpose, two different methods are used which are namely; MSC FLDS and Schrenk's Approximation. First, the background for aerodynamic load calculation methods which is based on Doublet-Lattice Method for subsonic conditions and ZONA 51 for supersonic conditions are introduced with general assumptions. The created aerodynamic model coupled with structural model through splines is presented and the specifications of model are described elaborately. As mentioned before, in addition to linearized panel methods via MSC NASTRAN, the loads are also calculated by using Schrenk's Approximation to be sure that the obtained loads are meaningful. After acquiring the loads via two different methods, shear force and bending moment distributions are compared with each other. As a result, it can be seen that the distributions are too close to each other, however the loads are a little bit higher for the MSC FLDS with a modest difference of around 10%. In this study, the loads which are summed at the predefined monitor stations are then used for the purpose of the optimization of the candidate wing structures.

CHAPTER 6

OPTIMIZATION METHODOLOGY ON WING STRUCTURE

6.1 Introduction

As beforementioned in Section 2.3.1, for the structural optimization of the wings, the number of design variables may be over the range of thousands which directly depend on the design zones. In addition to the number of design variables, the selection of the requested design responses such as stress, displacement and frequency, the dimension of the sensitivity matrix may also reach to enormous values. MSC NASTRAN is an ideally suited solver for this issue and can be used effectively by the engineers in the optimization studies. Besides, in this study, using the capability of the design variable linking of MSC NASTRAN, number of design variables are decreased significantly and especially for the metallic structures, smooth thickness distribution along the span-wise and chord-wise directions are obtained. Optimization studies comprise of three main subtitles which are namely; design variables, constraints and an objective function. All of them will be discussed elaborately in following sections.

6.2 Isoparametric Elements: Global to Natural Coordinate Transformation

Finite element analysis (FEA) is known as a simulation of any physical engineering problem by dividing whole component into the simpler parts based on the FEM. First appearance of the FEM goes back to the 1940s [49] and from that time, capabilities of FEMs evolved continuously. However, in 1968, significant progress in the method was encountered with the advent of isoparametric elements. Before 1968,

capabilities of the FEM is limited to linear variation of boundary [50] and therefore to model the curved geometries, it is inevitable to use great number of elements to obtain accurate results. Simply, the isoparametric elements are defined as the elements whose geometric and field variables are described by the same shape functions. With the foundation of the isoparametric elements, curved boundaries are modelled with polynomial shape functions on the simpler shapes for the complex elements and all calculations are performed over these simpler regions. Consequently, the large number of elements required to idealize the curved boundaries is prevented by using isoparametric elements [51].

The shape functions represent the behavior of the solution such as displacement, stress etc. Therefore, it is significant to choose the shape functions within each element to be defined. The shape functions can be defined in the order of constant, linear or quadratic. While in some of the solutions, constant or linear shapes are sufficient, high order polynomial shape functions may be required to simulate the cases in which the gradient of the variables change frequently [52] as shown in Figure 6-1. Therefore, it is a significant issue for the isoparametric elements to decide which shape function will be used during the analysis.

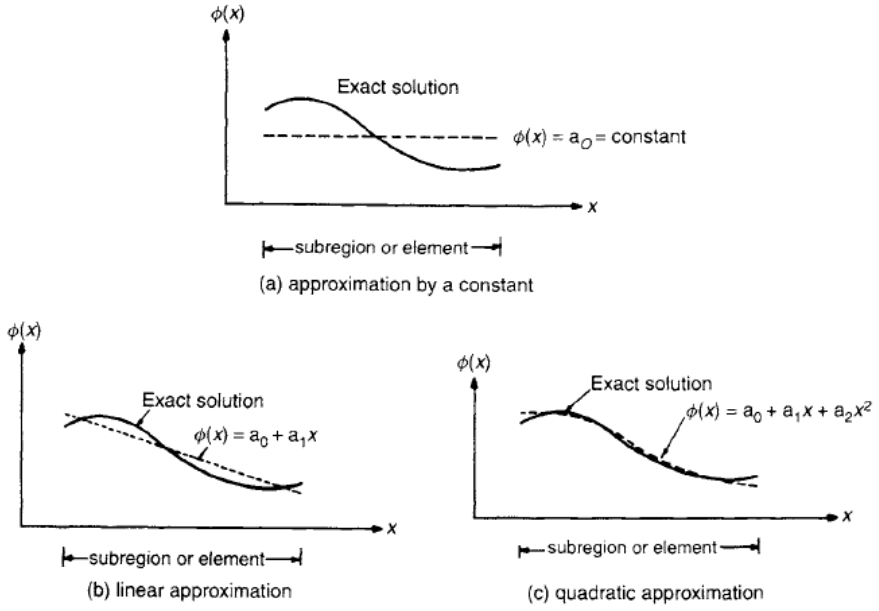

Figure 6-1 Approximations of the Shapes for the Solution [52]

There are two types of coordinate systems for the isoparametric elements; a global coordinate system (x, y) and natural coordinate system (ζ, η). A general representation of quadrilateral isoparametric element in both global and natural coordinate system is shown in Figure 6-2.

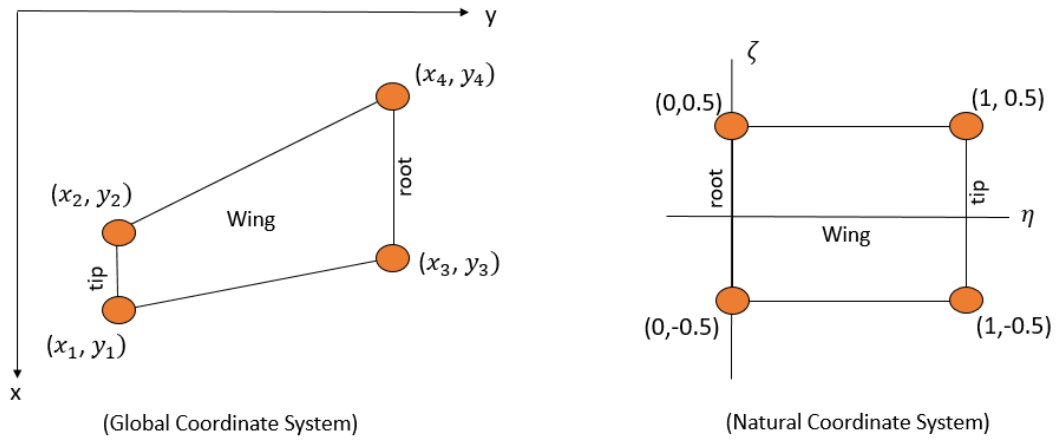

Figure 6-2 An Isoparametric Element in two Different Coordinate Systems

A natural coordinate system is a special type in which all coordinates are dimension free and lie between ±1. Then, for easiness of interpreting the locations of the elements, the span locations are shifted as starting from 0 and finishing at 1. On the other hand, as it is intended to obtain the thickness as higher as possible at the mid chord length and as lower as possible at the leading and the trailing edges of the wing, the outer border of the wing is changed as located between ±0.5 to obtain the thickness distribution as mentioned before. The most important advantage of using the natural coordinate system is the easiness of integration between the elements and relate them to each other in thickness values via their locations.

$$-0.5 \leq \zeta \leq 0.5$$

$$0 \leq \eta \leq 1$$

In this study, to simulate the thickness distribution along the wing span and chord-wise direction with respect to location of the elements, isoparametric elements in natural coordinate system are used and by means of this, the number of design

variables in the optimization problem are aimed to be decreased significantly and meaningful results are obtained from the manufacturing point of view.

Although the finite element solvers are using natural coordinate systems in their background, in the interface of the FEA programs, the location of the elements and the nodes of all the created FEMs are generally in global coordinate (i.e. Cartesian coordinate) system and in order to use the design variable linking method, those coordinates must be transformed back into the natural coordinate system via the transformation process performed with the method proposed by Hua [53].

The transformation process from global to natural coordinate system for quadrilateral isoparametric elements is performed by following the steps shown below as;

$$\begin{bmatrix} b_1 & c_1 \\ b_2 & c_2 \end{bmatrix} \begin{Bmatrix} \zeta \\ \eta \end{Bmatrix} = \begin{Bmatrix} d_1 - a_1\zeta\eta \\ d_2 - a_2\zeta\eta \end{Bmatrix} \tag{6.1}$$

where,

$$d_1 = 4x - (x_1 + x_2 + x_3 + x_4) \tag{6.2}$$

$$d_2 = 4y - (y_1 + y_2 + y_3 + y_4) \tag{6.3}$$

The coefficients of a, b and c's in Equation (6.1-6.3) are functions of global coordinates of grids which depend on the choice of the local numbering sketch which is shown in Figure 6-3 for the quadrangle isoparametric element.

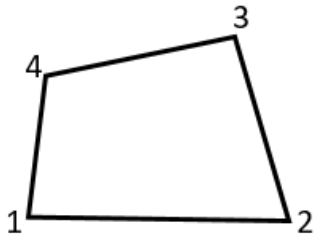

Figure 6-3 Numbering Sketch for Quadrangle Isoparametric Element

According to selected numbering scheme, following transformation matrix is offered in [53].

$$\begin{bmatrix} a_1 & a_2 \\ b_1 & b_2 \\ c_1 & c_2 \end{bmatrix} = \begin{bmatrix} 1 & -1 & 1 & -1 \\ -1 & 1 & 1 & -1 \\ -1 & -1 & 1 & 1 \end{bmatrix} \begin{bmatrix} x_1 & y_1 \\ x_2 & y_2 \\ x_3 & y_3 \\ x_4 & y_4 \end{bmatrix} \tag{6.4}$$

After performing this stage, the remaining steps are the solution of algebraic equations to accomplish the transformation from the global coordinate system to the natural coordinate system as it is proposed by Hua [53].

It should be noted that, Equation 6.4 cannot be performed without an additional geometric property constraint of quadrangle of the isoparametric elements. Lemma is designated as the name of this condition. According to Lemma, the following two inequality must also be satisfied.

$$a_1 \neq b_1 \tag{6.5}$$

$$a_2 \neq c_2 \tag{6.6}$$

In the situation of $a_1 \neq 0$, if $a_2 = 0$, then $c_2 \neq 0$ by the Lemma and Equation 6.1 takes the form of,

$$\begin{bmatrix} b_1 & c_1 \\ b_2 & c_2 \end{bmatrix} \begin{Bmatrix} \zeta \\ \eta \end{Bmatrix} = \begin{Bmatrix} d_1 - a_1\zeta\eta \\ d_2 \end{Bmatrix} \tag{6.7}$$

I. If $b_2 = 0$, then

$$\zeta = \frac{d_1c_2 - c_1d_2}{a_1d_2 + b_1c_2} = \frac{d_c}{a_1d_2 + b_1c_2} \quad , \eta = \frac{d_2}{c_2} \tag{6.8}$$

II. If $b_2 \neq 0$, solving Equation 6.9 gives the following for η:

$$a_1b_2\,\zeta^2 + (c_1b_2 - a_1d_2 - b_1c_2)\zeta + (d_1c_2 - c_1d_2) = 0 \tag{6.9}$$

where, $\zeta \in [-1.0 \quad 1.0]$ and η is found as,

$$\eta = \frac{d_2 - b_2\zeta}{c_2} \tag{6.10}$$

By implementing the above relations into a script, the coordinate transformation process is performed in a shorter time and the preparations are finalized prior to the usage of the design variable linking method.

6.3 Design Variables: Design Variable Linking Method

In this thesis study, rib and spar web thicknesses for the metallic structures and ply thicknesses in predefined directions for the composite structures are used as design variables. The optimizer sets the value of the design variables within the predefined interval according to the constraint values. To provide all of the identified constraints, the optimizer changes the variables and try to find an optimum distribution of the variables. Being different from the general optimization studies, in this particular approach, the design variable linking method is used to define the design variables.

An important issue in structural optimization studies is the interpretation of the obtained results. The engineers are responsible from the results as to whether feasible or not. A well-designed wing layout is supposed to have minimum skin thickness since it has a maximum weight portion compared to the ribs and spars it is having and to obtain feasible results, the interval of design variables should be determined attentively. As mentioned in [12], MSC NASTRAN Sol 200 optimizer which is based on the gradient-based methods starts to the sizing from internal structure before the skin and if the rib or the spar buckles due to the inadequate interval of design variables, the optimizer may stop with excessive thick skin and this leads to an infeasible design. To overcome this problem, the maximum limit for the thicknesses used in internal structures is increased sensibly in the DESVAR cards which are used in the MSC NASTRAN Sol 200 in order to define the minimum, the maximum and the starting thickness values for the design variables. By this means, the optimizer continues to reduce the skin thickness and end up with a lighter design.

In this method, design variables can be defined at two different levels, namely; local and global variables. All properties of the FEM can be defined as local variables, on the other hand, global variables are directly involved in the optimization process. Local and global design variables can be connected to each other with various methods. Benefits related with manufacturing considerations and being suitable for

the decrease in the number of variables significantly, linking with shape function is adopted in this research study so as to link the global and local variables.

The wing structures are generally fixed from their root section to the fuselage and it is expected that the maximum stress values decrease from root to the tip section and the thicknesses are expected to decrease in a similar way. However, there might be components located on the wing such as control surfaces, external fuel store, etc. and local high stress values can be observed in anywhere of the wing due to these components. Therefore, as a result of the optimization, a large thickness variation may be encountered between the predefined adjacent design zones. On the other hand, in the optimization of the wing structures, design variables are generally defined according to the rib/spar intersections. It is known that the thickness value of the composite plies or metallic structures are allowed to change independently in the design zones and the number of design zones strictly depend on the number of ribs and spars. Simply, the more ribs/spars the wing has, the higher the number of the design variables are reached in the problem.

Besides, the usage of the composite materials also increases the design variables significantly if the plies in each direction are allowed to change. Consequently, the cost of the optimization problem might increase unfavorably.

To overcome all of the abovementioned drawbacks, the design variable linking is asserted as an efficient method. By applying design variable linking method with shape functions, a practicable thickness distribution which is very important from the manufacturing point of view and a significantly reduced number of design variables can be achieved.

The implementation of the design variable method in this study of the optimization of a wing structure starts with the coordinate transformation process as mentioned in Section 6.2. By using Python based script, all of the center location coordinates are first transformed to the natural coordinate system to parametrize the coordinates between 0 and 1 in the span direction and -0.5 and 0.5 in the chord direction in order to simulate the thickness distribution along the wing. In this method, local variables

are the weighted sum of global variables such that the size of the shape function is controlled by the selected global variables [7].

The shape functions are used to smoothly vary the element thicknesses along both chord-wise and span-wise directions. Each design zone can have different shape functions which are defined by the optimizer and the order of the shape functions can separately be set as constant, linear or quadratic polynomial by the designer as it is shown in Table 6-1.

Table 6-1 Coefficients for Determination of Order of Shape Functions

	a_{00}	a_{10}	a_{01}	a_{11}	a_{20}	a_{02}
Constant	+	N/A	N/A	N/A	N/A	N/A
Linear	+	N/A /+	N/A /+	N/A	N/A	N/A
Quadratic 1D	+	N/A	+	N/A	N/A	+
Quadratic 2D	+	+	+	+	+	+

Using the shape functions described above, the thickness of the components can be determined in the intended direction and the order of the shape functions are shown in the below equations.

$$t_{constant} = a_{00} \tag{6.11}$$

$$t_{linear}(\eta) = a_{00} + a_{01}\eta \tag{6.12}$$

$$t_{linear}(\zeta) = a_{00} + a_{10}\zeta \tag{6.13}$$

$$t_{quadratic\_1D}(\eta) = a_{00} + a_{01}\eta + a_{02}\eta^2 \tag{6.14}$$

$$t_{quadratic\_2D}(\zeta, \eta) = a_{00} + a_{10}\zeta + a_{01}\eta + a_{11}\zeta\eta + a_{20}\zeta^2 + a_{02}\eta^2 \tag{6.15}$$

If Equation 6.11 is used for any component, the thickness will be taken as constant for all design zones. On the other hand, Equation 6.12 – 6.13 imply that the thickness can be tailored linearly in span-wise and chord-wise directions. Similarly, the thickness can also be tailored quadratically for only span-wise direction (Equation 6.14) or both span-wise and chord-wise directions (Equation 6.15).

As mentioned before, by using design variable linking method in the structural optimization studies of the wings, total number of design variables can be decreased

significantly and by also comparing classical approach and the implemented method on one of the candidate wing geometry, the decrease in the design variables are also shown.

In this study, the thickness distribution of the components is intended to be smoothly changed and therefore in addition to rib/spar intersections, the design zones consist of subdivided sections as it is shown in Figure 6-4 for the configuration of wing v1_2.

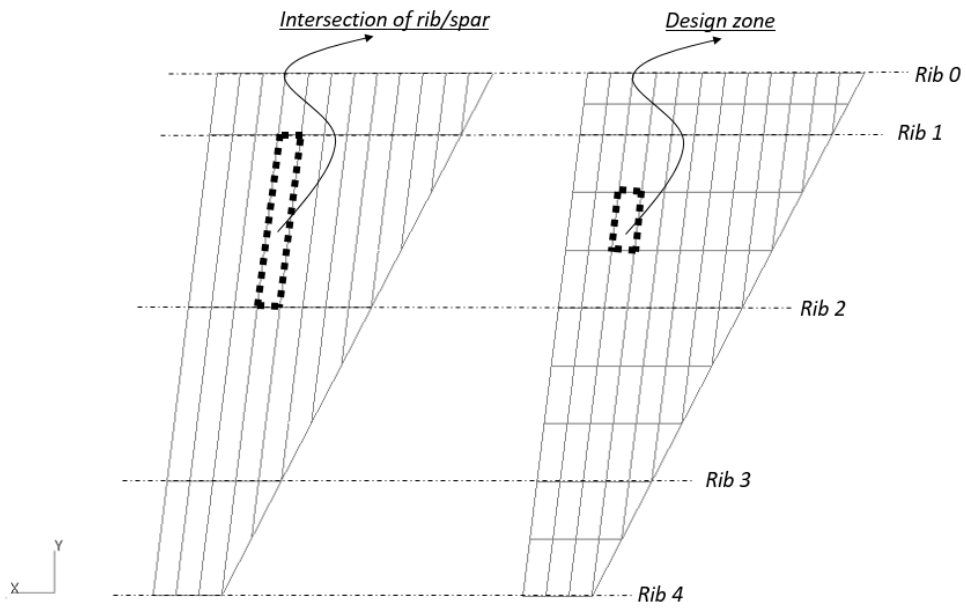

Figure 6-4 Representation of the Design Zones for v1_2

The wing configuration shown in Figure 6-4 comprises of thirteen spars and seven ribs in addition to the lower and the upper skin. It is assumed that the ribs and spars are produced from metallic materials and the skin is from composite materials which comprise of plies in four different directions (0°/+45°/-45°/90°). The thickness of the plies and the thickness of the metallic components are designated as design variables. Finally, the total number for the design variables in the general optimization approach are calculated as follows;

13 Spar & 5 Rib $\Longrightarrow$ 63 Section $\Longrightarrow$ 84 Design Zones for one skin

- For skin: 84 x 3 x 2 = 504 DV
- For spars: 94 DV
- For ribs: 39 DV

} Total = 637 DV

where, DV represents the design variables.

As it is seen from the above example that, using the general optimization approach in which all design variables in the design zones varies freely regardless of the adjacent design zones results in 637 design variables which are enormous for a wing in the preliminary design stage.

On the other hand, by using design variable linking method, it is provided that structural optimization can be performed by using much smaller numbers of design variables effectively. In the wing structures, especially with the common use of composite materials in the aviation industry, the thicknesses might be different in any location of the wing. However, in order to be reasonable from manufacturing point of view, while the skin thickness changes in both chord-wise and span-wise directions, the thickness of the spars and the ribs are free to change in only along their own lied directions. With this approach, to see the effectivity of the linking method, for the configuration of v1_2, complex polynomial thickness distribution for the skin in which the thickness varies both in chord-wise and span-wise directions quadratically (Equation 6.18) and linear distribution for the ribs (Equation 6.16) and spars (Equation 6.17) in which thicknesses are tapered linearly in only one direction are applied and therefore the total design variable number can finally be calculated as follows;

$$t_{rib}(\zeta) = a_{00} + a_{10}\zeta \tag{6.16}$$

$$t_{spar}(\eta) = a_{00} + a_{01}\eta \tag{6.17}$$

$$t_{skin}(\zeta,\eta) = a_{00} + a_{10}\zeta + a_{01}\eta + a_{11}\zeta\eta + a_{20}\zeta^2 + a_{02}\eta^2 \tag{6.18}$$

where, $a_{00}, a_{01}, a_{10}, a_{11}, a_{02}$ and a_{20} are the design variables which constitute the thickness values for the components, and ζ, η are the natural coordinates where they define the location of the design zones on the wing.

- For skin: 6 x 3 x 2 = 36 DV
- For spars: 2 x 13 = 26 DV
- For ribs: 2 x 5 = 10 DV

} Total = 72 DV

In the above calculation for the skin, "6" represents the number of design variables, "3" for the plies in the direction of (0°/±45/90°) and "2" for the lower and upper skin. Similarly, in the next and the following calculations, "2" represents the design variables and "13" and "5" are the number of the spars and ribs for the selected configuration of wing, respectively. It is worth noting that, only symmetric and balanced composite laminates are used in this study and knowing that balanced laminates have the same number of the plies in the direction of $+\theta$ and $-\theta$, thicknesses of the $-45°$ and $+45°$ plies are forced to be equal in the optimization.

Consequently, as seen from the comparison of two different approaches, the total number of the design variables are decreased significantly from 637 to 72 by implementing the design variable linking method and the number of the total design variables are independent from the created design zones. Thereby, the requested computer capacity and the elapsed time in solution process are decreased advantageously.

6.4 Constraints

The main task in this thesis study is to design an optimum wing structure while satisfying the requirements which are forced by multi-disciplines and these disciplines might be categorized in the two main sections; related with the strength and the stiffness of the structures.

6.4.1 Strength Related Constraints

The strength-only constraints will be von Mises yield criteria for metallic structures and Tsai-Wu failure criteria for composite structures which completely depend on material compressive and tension allowable. It is expected to provide that the maximum calculated von Mises stress on the elements is under the allowable stress for metallic structures and similarly minimum failure index for the composite structures is lower than 1.0.

The von Mises stress constraint for metallic elements can be defined as,

$$\sigma_{\text{von Mises}} = \sqrt{\sigma_{11}^2 - \sigma_{11}\sigma_{22} + \sigma_{22}^2 + 3\sigma_{12}^2} < \sigma_{\text{allowable}} \tag{6.19}$$

where, σ is the stress and the indices "11" and "22" represent the longitudinal and the transverse directions, respectively and "12" is used for the shear stress.

The Tsai-Wu failure criteria for symmetric condition for two-dimension can be summarized as below,

$$F_{11}\sigma_1^2 + 2F_{12}\sigma_1\sigma_2 + F_{22}\sigma_2^2 + F_1\sigma_1 + F_2\sigma_2 + F_{66}\tau_{12}^2 \leq 1.0 \tag{6.20}$$

where,

$$F_{11} = {}^{1}/_{X_t X_c} \tag{6.21}$$

$$F_{22} = {}^{1}/_{Y_t Y_c} \tag{6.22}$$

$$F_1 = {}^{1}/_{X_t} - {}^{1}/_{X_c} \tag{6.23}$$

$$F_{22} = {}^{1}/_{Y_t Y_c} \tag{6.24}$$

$$F_2 = {}^{1}/_{Y_t} - {}^{1}/_{Y_c} \tag{6.25}$$

$$F_{66} = {}^{1}/_{S^2} \tag{6.26}$$

where, σ_1 and σ_2 represent the principal stresses in the longitudinal and the transverse directions, respectively. X and Y represent the allowable for the fibers in the longitudinal and the transverse directions, respectively and s is the in-plane shear

strength where the indices t and c stand for the tension and compression. As it is seen, there is no equation for the interaction term of F_{12} since it cannot be calculated analytically and depends on the material which can be obtained with tests. MSC NASTRAN uses zero for F_{12} term as a default unless otherwise specified [46].

As already mentioned before, weight minimization is crucial in aircrafts and to obtain the lightweight structure as much as possible, the components are generally allowed either to buckle in the limit loads or in the certain percentages of the limit loads. However, the buckled structures are deformed in the out-off plane direction and especially for the skin elements, this kind of deformation breaks the smooth aerodynamic surface. The wing used here for the optimization study is considered as it belongs to a supersonic aircraft and protecting this particularly important aerodynamic surface is a significant issue for the flight performance in high speeds. Therefore, buckling of the any components are not allowed up until the ultimate loads. In other words, the minimum buckling eigenvalue must be greater than 1.0.

It should also be mentioned about the safety factor and material allowables used in this thesis study. The limit load is known as the maximum load encountered by the aircraft during its service life and the ultimate loads are obtained as multiplying the limit loads with safety factor of 1.5. Any part of the aircrafts must be able to resist to the limit loads without plastic or permanent deformation. Although the aircraft is not expected to experience even limit loads, they are sized with respect to ultimate loads and under the ultimate loads the aircraft must be able to endure at least three seconds according to CS 23.305 (b) [54].

The safety factor for ultimate loads must be used as 1.5 unless otherwise specified in the aviation industry [55]. This safety factor is mainly used for possible variations in material properties, possible errors in production or assumptions made in aerodynamic and structural analysis processes.

In this study, the wing structures are sized according to the ultimate loads. Since the loads obtained from trim analyses are limit loads, all of them are multiplied by 1.5 safety factor before applying to the structure. Therefore ultimate allowable values of

the materials are used while defining constraints in the optimization. For the allowable of the composite materials, there is no difference of limit or ultimate allowable since the plasticity effect does not exist for the composite materials, therefore all allowables given in Table 4-1 are directly used in this study. However for the metallic materials, there are both limit and ultimate allowables and for some of the metallic materials, 1.5 time of the limit allowables are known as lower than ultimate allowables [56], therefore in this study, while defining the constraints for the metallic components, allowable stress value is defined as minimum of the 1.5 x limit strength (yield) and ultimate strength values.

For instance for the Al 7050 T7451;

$$1.5 \text{ x Tensile Yield Strength} = 1.5 \text{ x } 469 \text{ MPa} = 703 \text{ MPa}$$

$$\text{Tensile Ultimate Strength} = 524 \text{ MPa}$$

Since 1.5 x Tensile Yield Strength is much higher than the tensile ultimate strength, tensile ultimate strength value is directly used for the constraint of the metallic structures according to von Mises failure criteria in this study.

6.4.2 Stiffness Related Constraints

The main constraint related with the stiffness of the wing is a flutter speed. The alteration of the flutter speed indicates a non-linear attitude for the structures. Therefore, bringing the flutter speed to the intended level which depends on the certification requirements such as MIL-HDBK-516C and CFR 14 Part 23 is a computationally expensive process. Besides, it is not possible to constrain the flutter speed directly in the MSC NASTRAN Sol 200 optimizer. To eliminate the flutter problem from the flight regime of the aircraft, a very efficient method is proposed by Hajela [57] in 1983. According to [57], the constraint is directly given to the damping value such that at specified velocities, the damping values will not cross the $g = 0$ line and this procedure is also adopted by the ASTROS [22] and MSC

NASTRAN [17]. The method used to constraint the damping value is specified as follows,

$$g = \frac{\gamma_{ij} - \gamma_{ireq}}{GFACT} \leq 0 \tag{6.27}$$

where, γ_{ij} is the damping value for the j^{th} mode at i^{th} velocity. γ_{jreq} is the required damping value at i^{th} velocity and generally defined by the users as 0.3. GFACT is the scale factor that transforms the damping values to be consistent with other constraints used in the optimization study, typically set to a value of 0.1.

In brief, using common values for the γ_{ireq} and GFACT which are 0.3 and 0.1 respectively, the damping value is aimed to be lower than -0.3 by the optimizer. Using this method, there is no need to calculate the flutter speed of the structures at each iteration.

As specified in MIL-A-8870C [58], the aircraft must not be encountered with the flutter phenomena under 1.15 times its dive speed. Therefore, if the dive speed of the aircraft is assumed as 1.3 Mach, the whole wing structure should be designed as the flutter speed is higher than approximately 510 m/s.

Finally, for the frequency related constraints, two different approaches are adopted. First of all, the constraint is directly given to the first natural frequency of the sized wing with respect to strength-only constraints and secondly given to the gap between the first bending and the first torsion modes of the wing, by this means the two natural frequencies at these modes are tried to be separated from each other.

6.5 Objective Function

The main objective in this study is to obtain the minimum weight for the created wing structures while satisfying all of the aforementioned constraints.

6.6 Flowchart for the Optimization Studies

In this study, two staged optimization approach is adopted. In the first step, all of the created design candidate geometries having different layouts but same outer geometry as shown in Figure 4-1 are sized with strength-only constraints including von Mises, failure index and global buckling. After optimization results are obtained for all of the candidates, the total weights are then compared with each other and the flutter speeds are calculated manually by using NASTRAN Sol 145. The candidate wings with sized properties with flutter speeds which are below the predefined value depending solely on the certification requirements are subjected to the second step of the optimization study. In the second step, stiffness related constraints are also included in addition to the strength-only constraints and it is expected to obtain a lightweight wing while satisfying required flutter speed along with the strength-only constraints. It should be noted that, the stiffness related constraints are investigated in the two different parts. In the first one, the constraint is directly given to the flutter speed through the damping value and in the second one, the first bending natural frequency and the spacing between the first bending and the first torsion modes of the wing are adopted as the stiffness related constraints. Finally the performance of the two different stiffness related constraints are compared with each other. The flowchart that is followed through this study can be seen in Figure 6-5.

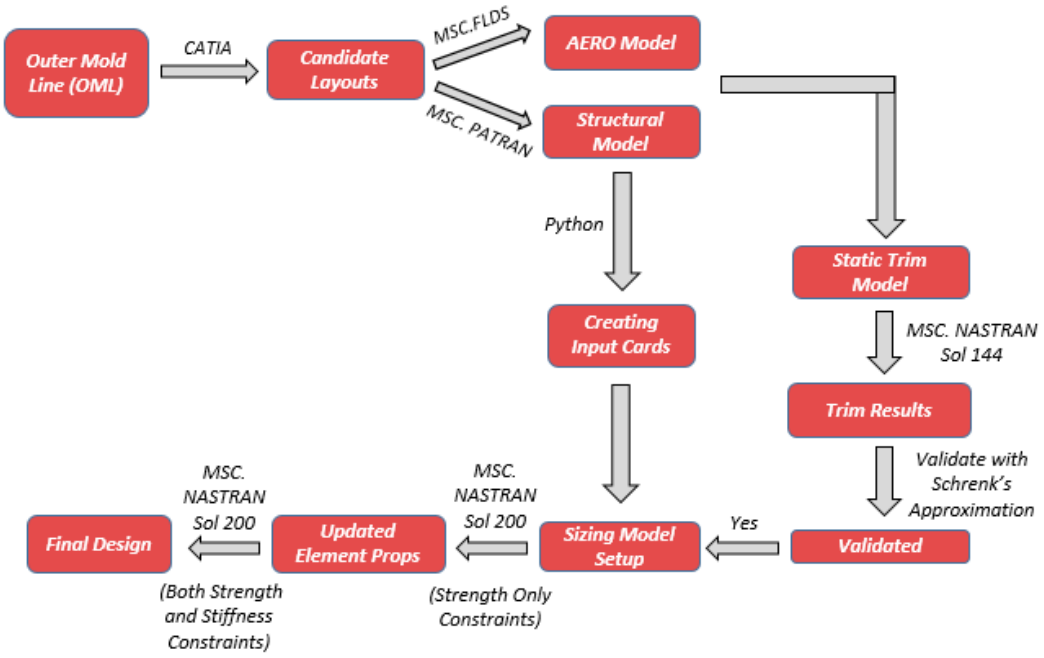

Figure 6-5 Analysis Process Applied to Each Wing

First of all, the Outer Mold Line (OML) is created in CATIA according to the defined airfoil and dimensions which are presented in Section 3.2, then sketches of the possible different layouts which are also used in the produced real aircrafts are prepared. Following this, FEMs are created for each of them in the MSC PATRAN interface. In MSC FLDS, the aerodynamic model is then created and after performing the related processes such as splining the aero- and structural- models, static trim model is created to obtain the aerodynamic loads on the wing and the acquired loads are then compared with analytical load determination method named as Schrenk's Approximation using the obtained shear and bending moment distributions along the span-wise direction. The necessary input cards for the optimizer are created automatically for each candidate layout by using the script developed in Python. Finally, all of the layouts are sized with adopted variable linking method in two steps to achieve minimum weight wing layout via MSC NASTRAN Sol 200.

6.7 Conclusion

First of all, the isoparametric elements are introduced briefly and then, the methodology for the transformation of the global coordinates to the natural coordinates is performed. Through the transformation process, the locations of the elements are nondimensionalized. After that, the design variable linking method which is used mainly for obtaining smooth thickness transitions between adjacent design zones and decreasing the total number of the variables is introduced. The available shape functions which are used for linking process are also introduced. As an example, by using the variable linking method with shape functions, how the number of the design variables can be decreased effectively is proved for one of the candidate wing layouts. Additionally, the constraints and the objective function used in the optimization study are mentioned and finally, by presenting a flowchart, all the processes followed through this study are summarized briefly.

CHAPTER 7

CASE STUDIES

7.1 Introduction

In this chapter, developed multidisciplinary optimization methodology is experienced on the created design candidates introduced in Section 3.3. Before starting to analyze the design candidates, the performance of the different shape functions is compared with each other for one of the candidate layout. After constructing the optimization problem including the design variables, constraints and the objective function, two-staged optimization approach is applied on to the different wing design candidates. At the first stage, all of the design candidates are sized through only using strength constraints. The obtained results are then compared with each other from the weight point of view. After that, the investigation of the aeroelastic stability is done by calculating the flutter speeds of the wings which are sized according to the strength-only constraints and the wings of which the flutter speeds are not satisfied according to the certification requirements are subjected to the second stage of the optimization. At this second stage, the flutter constraint is also included in addition to the strength constraints for the same objective which is weight minimization. In addition to the flutter constraint, another method for postponing the flutter speed is performed by adding frequency constraint to the optimization. Finally, the performances of two methods are compared with each other.

7.2 Shape Function Comparison

In this study, the design variable linking method is used as mentioned in Section 6.3, and the variables can be connected to each other via different shape functions as the thickness distribution will be either constant, linear or polynomial. Type of the shape functions depend on including of the terms such as ζ, η, ζ^2 and η^2 into the thickness equations as given in Section 6.3.

To compare the performance of the shape functions, four different analyses are performed. To be reasonable from the manufacturing point of view, for the ribs and the spars, constant and linear functions and for the skin, all of the functions are used. The combinations of the shape functions which are used for the comparison study are listed as below;

1. The thickness of all of the components varies with constant function;

$$t_{ribs,spars,skin} = a_{00} \tag{7.1}$$

2. The thickness varies linearly for the skin and the spars in the span-wise direction and in the chord-wise direction for the ribs;

$$t_{ribs}(\zeta) = a_{00} + a_{10}\zeta \tag{7.2}$$

$$t_{spars,skin}(\eta) = a_{00} + a_{01}\eta \tag{7.3}$$

3. The thickness of the skin varies quadratically in the span-wise direction and the thickness of the ribs and the spars varies linearly in the chord-wise and in the span-wise directions, respectively;

$$t_{ribs}(\zeta) = a_{00} + a_{10}\zeta \tag{7.4}$$

$$t_{spars}(\eta) = a_{00} + a_{01}\eta \tag{7.5}$$

$$t_{skin}(\eta) = a_{00} + a_{01}\eta + a_{02}\eta^2 \tag{7.6}$$

4. Thickness of the skin varies quadratically in both the span-wise and the chord-wise directions and the thickness of the ribs and the spars varies linearly in the chord-wise and in the span-wise direction, respectively;

$$t_{ribs}(\zeta) = a_{00} + a_{10}\zeta \tag{7.7}$$

$$t_{spars}(\eta) = a_{00} + a_{01}\eta \tag{7.8}$$

$$t_{skin}(\zeta,\eta) = a_{00} + a_{10}\zeta + a_{01}\eta + a_{11}\zeta\eta + a_{20}\zeta^2 + a_{02}\eta^2 \qquad (7.9)$$

The shape function comparison study is performed on only the wing v1_2. Four different optimization models are created that are consisting of the composite skin and metallic ribs/spars with different shape functions as specified above and all of the models are subjected to the same constraints (i.e. including strength-only constraints) under the same loading conditions [59].

After starting with the same initial values to the optimization, four different weights for each model are obtained as expected. The weight results and solution time for each shape functions can be seen in Table 7-1 below.

Table 7-1 Weight Comparison for Different Shape Functions

Type of Shape Function	**Number of Iterations**	**CPU Time [s][5]**	**Weight [kg]**
Constant	24	118	361.1
Linear	26	144	133.1
Quadratic 1D	18	172	121.3
Quadratic 2D	34	224	114.7

The Figure 7-1 represents the convergence of the optimization models with different shape functions including number of the iterations and weights for the wing v1_2

[5] Intel(R) Xeon ® CPU @ 3.5 GHz 16GB Ram 64 Bit Operating System

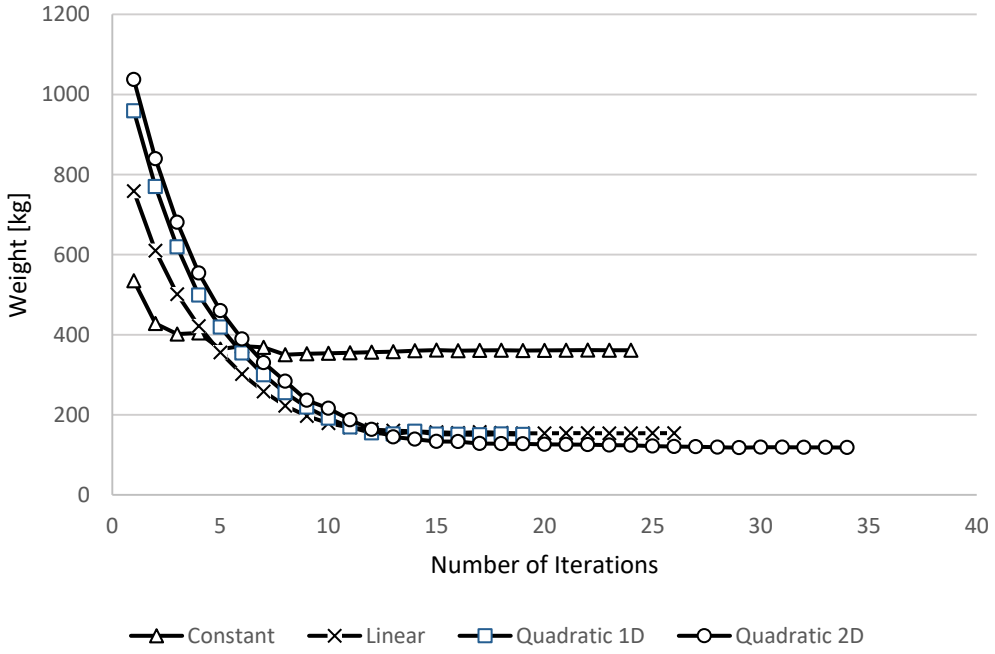

Figure 7-1 Iterations till Converged Results

As can be inferred from Figure 7-1, model with the constant shape function provides the heaviest case. Since all of the structural components including the skin, the ribs and the spars must have only one thickness value after the optimization and all of the constraints must be satisfied for the successful optimization, the thickness values are sized according to the maximum stress values by the optimizer. Therefore, the weight obtained from the optimization is worse than the other models having linear or polynomial shape functions.

As compared with the constant shape function, the linear and the quadratic shape functions where the thickness values change linearly or quadratically in only the chord-wise or the span-wise directions result is similar and much lower weights. However, as expected, the performance of the quadratic 2D shape function comes out to be the best. By using quadratic 2D shape function for the skin in design variable linking method, the thickness of the upper and the lower skin are optimized in both the chord-wise and the span-wise directions. Therefore, each design zones

starting from root to tip have different thickness values which satisfy the predefined constraints in the optimization problem.

The thickness distribution of the wing v1_2 is given in Figure 7-2. The thicknesses for the lower skin, the upper skin, the spars and the ribs are presented separately. As inferred from Figure 7-2, for each component, there is only one thickness value as an output of the optimization.

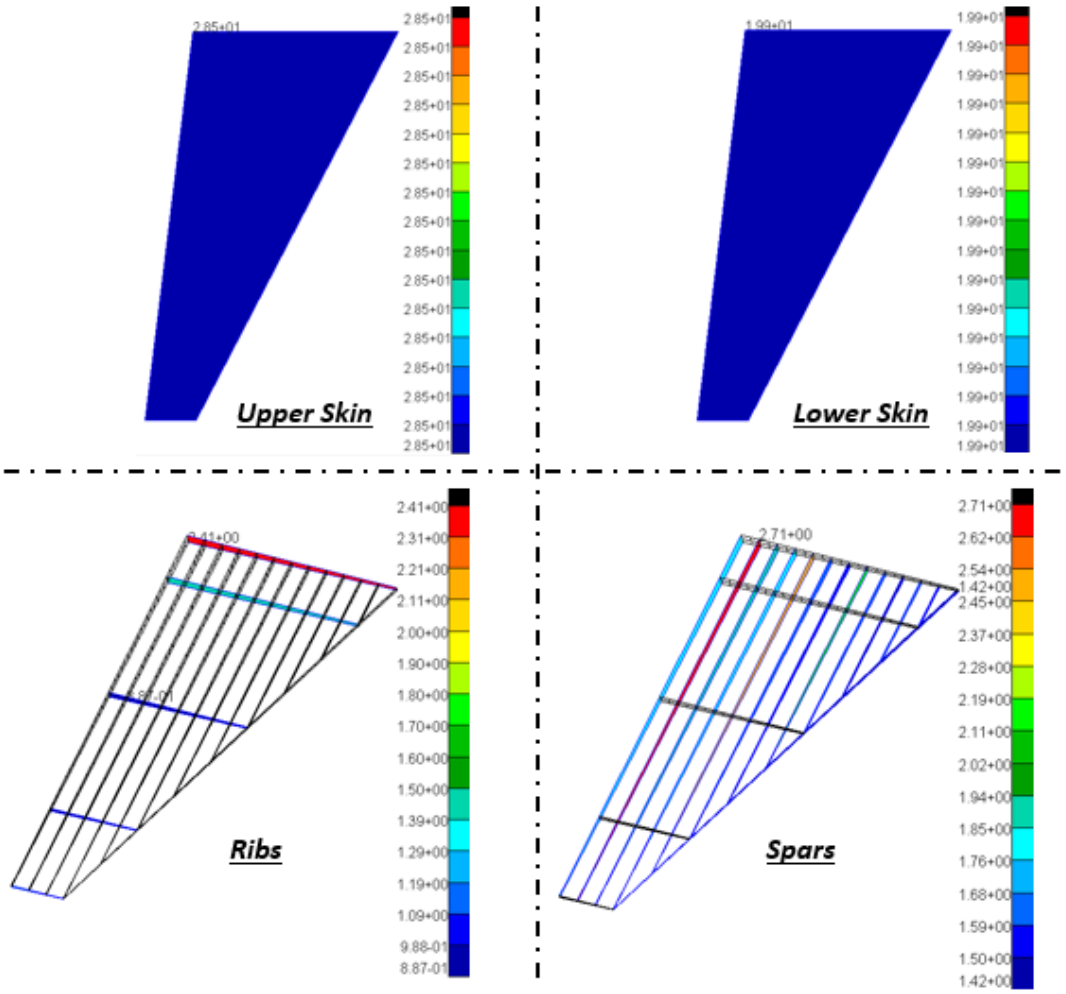

Figure 7-2 Thickness Plots of the Wing v1_2 using Constant Shape Function

The thickness plots of the optimization with the linear shape functions in only one direction for each component can be seen in Figure 7-3.

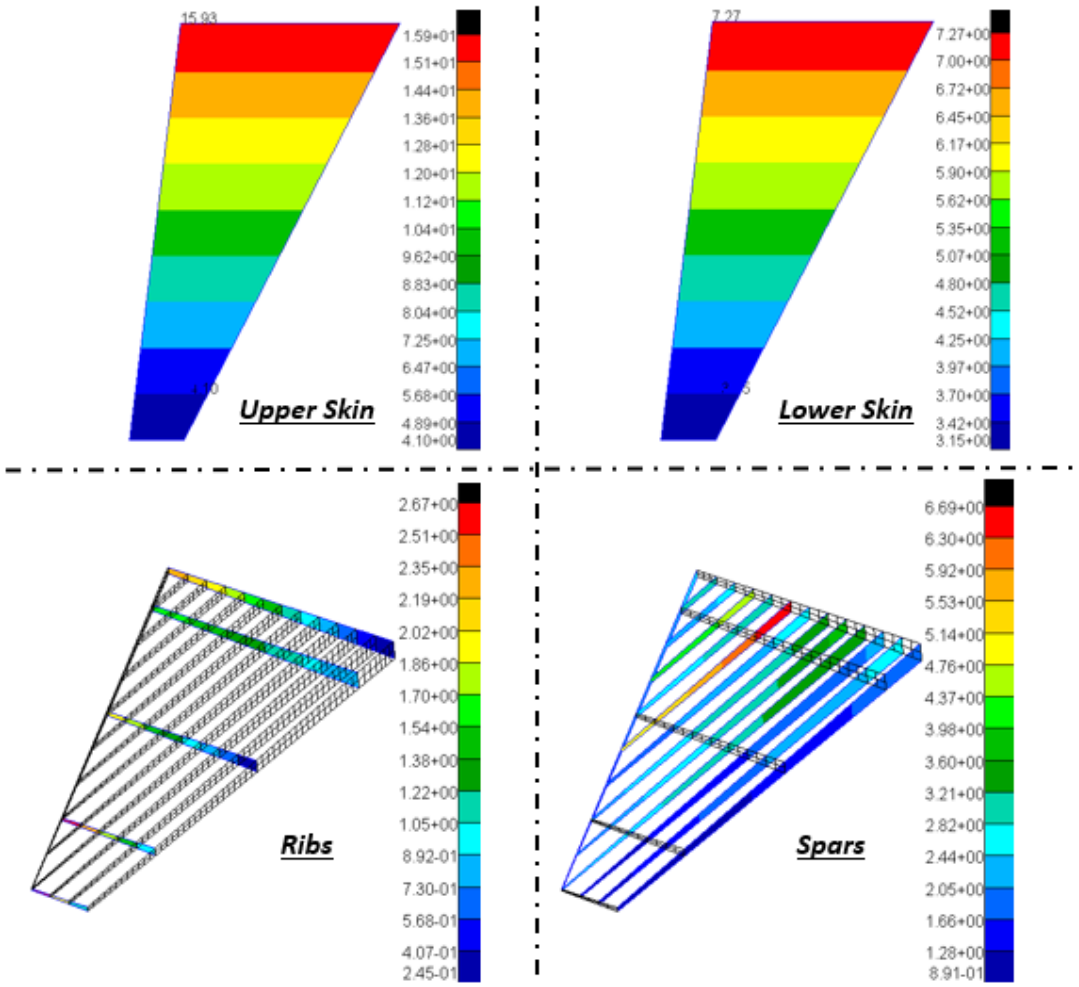

Figure 7-3 Thickness Plots of the Wing v1_2 using Linear Shape Function

Similarly, the thickness plots of the optimization with quadratic 1D shape function can be seen in Figure 7-4. The thickness change is the same with linear one for the ribs and the spars, however the thickness varies quadratically in the span-wise direction for the skin.

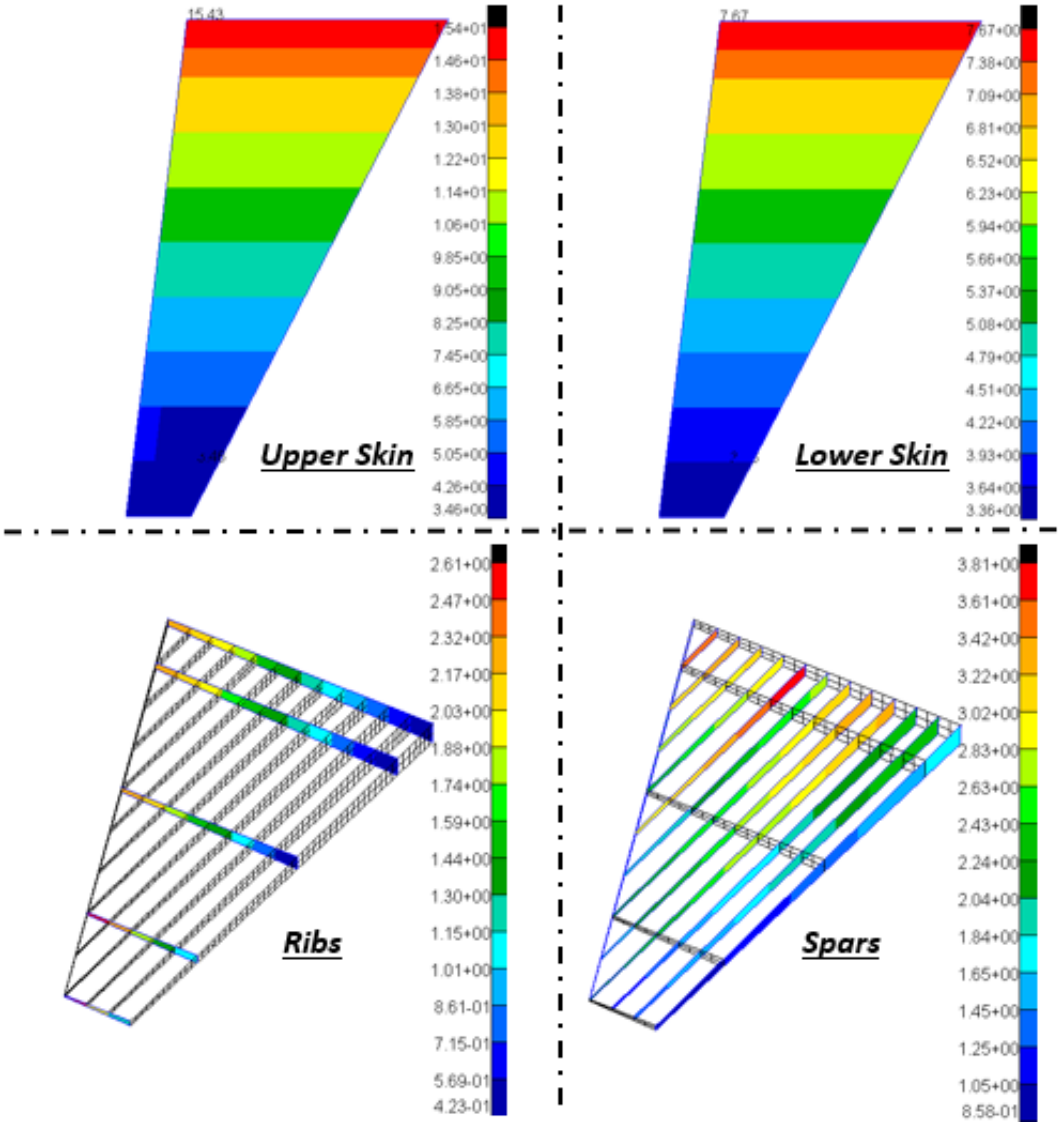

Figure 7-4 Thickness Plots of the Wing v1_2 using Quadratic 1D Shape Function

Finally, the optimization results with quadratic 2D shape functions in which the thicknesses are sized in both the chord-wise and the span-wise directions for the skin and linearly for the ribs and the spars is given in Figure 7-5.

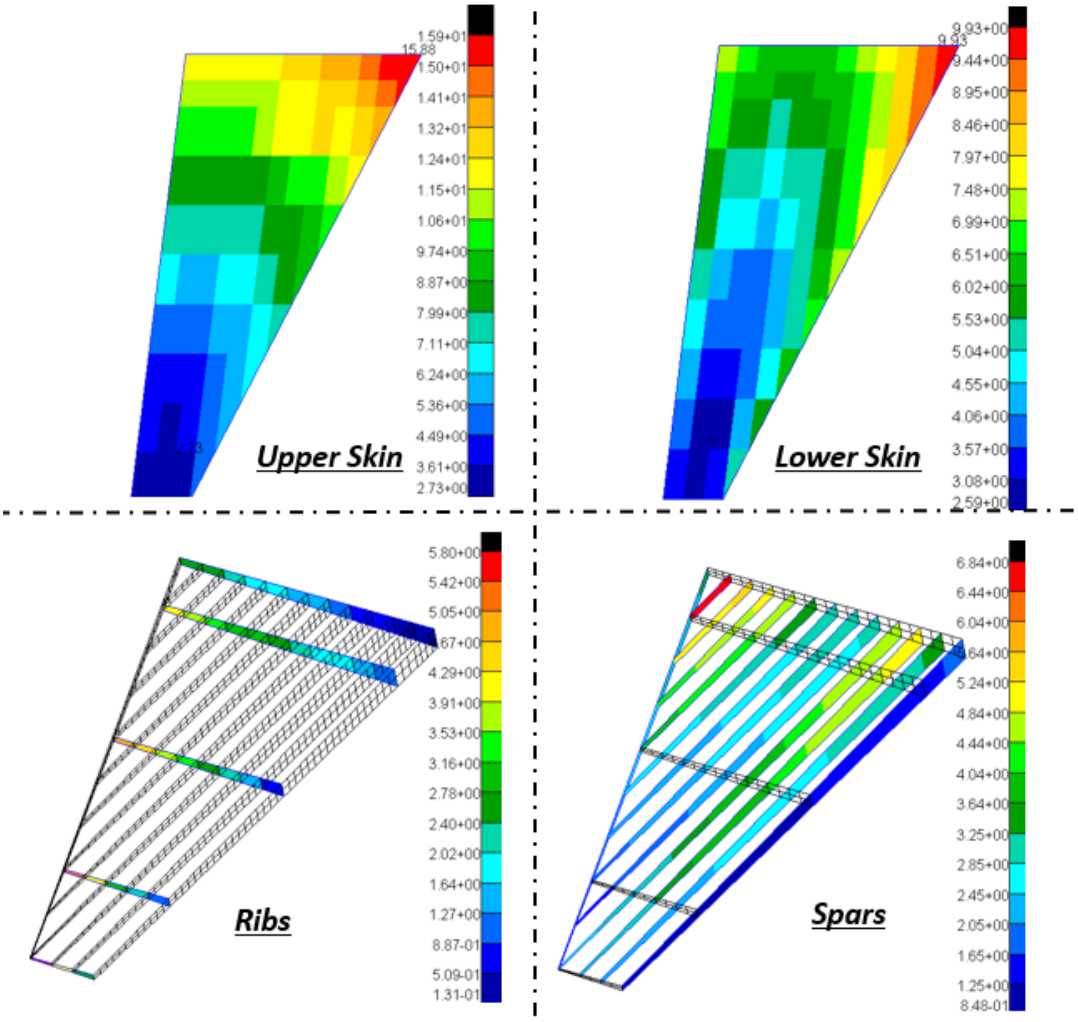

Figure 7-5 Thickness Plots of the Wing v1_2 using Quadratic 2D Shape Function

It can be concluded that, the optimization with the design variable linking method using quadratic 2D shape functions for the skin provides the minimum weight. Since the portion of the skin to the wing is the maximum, the minimization of the skin thickness plays a significant role in reducing the total weight of the wing. Therefore, for all the optimizations in the following sections in this study, quadratic 2D shape

functions are used for the skin, on the other hand, the linear shape functions are adopted for the spars and the ribs.

7.3 Optimization with Strength-Only Constraints

As mentioned before, the optimization of the wing layouts is two-staged. First, the sizing is performed with the strength-only constraints including von Mises yield criteria for metallic structures and Tsai-Wu failure criteria for composite structures. Besides, the global buckling of the structure is also of the interest of the study at this particular stage. This optimization step aims the comparison of the weights of the candidates under the same loading conditions. After sizing them with the strength-only constraints, the wings with the flutter speeds under 510 m/s are subjected to the second stage of the optimization which consists of stiffness related constraints in addition to strength related ones.

7.3.1 Design Zones

The design zone means that the variables are free to change in the defined area. Normally, the intersection of the ribs and the spars are used for this purpose. The finer design zones are better in terms of the minimization of the weight, on the other hand, this results in higher number of design variables and the optimization problem ultimately becomes highly complex in the general optimization approach where there are different design variables for each design zone. However, increasing the number of design zones is not an important issue if one uses the design variable linking method during the optimization as the thicknesses on each design zone are represented by a few shape function coefficients as mentioned in Section 6.3. By using this property of the method, the design zones are increased by dividing the intersection of the ribs and the spars into an equal part in order to obtain a smooth thickness transition. Created design zones for the skin (both upper and the lower

one), spars and the ribs of the wing v1_2 can be seen from Figure 7-6 to Figure 7-9, respectively.

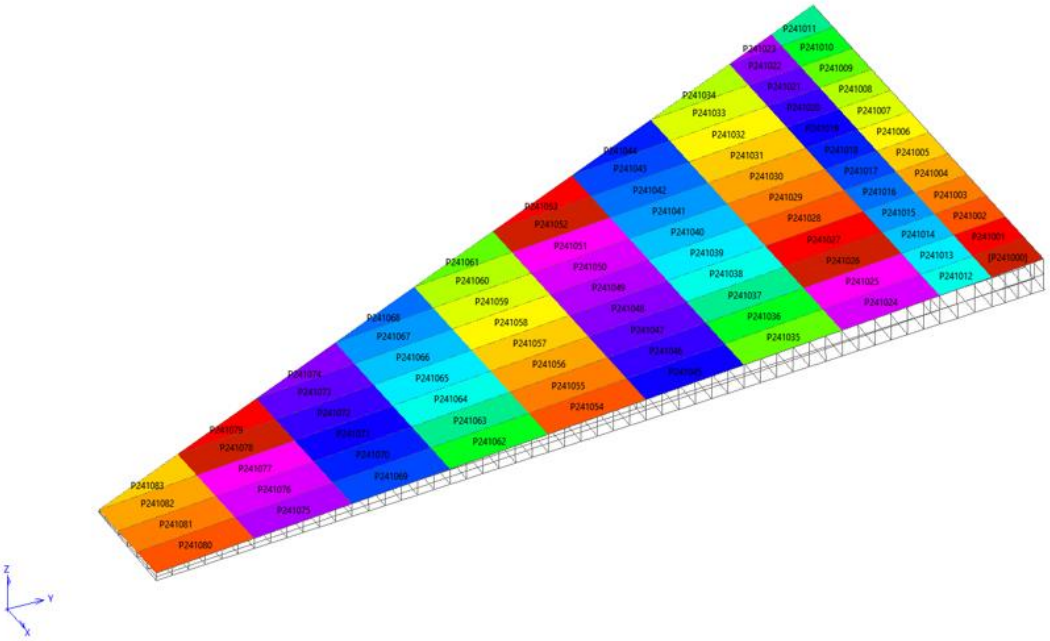

Figure 7-6 Design Zones for Upper Skin of the Wing v1_2

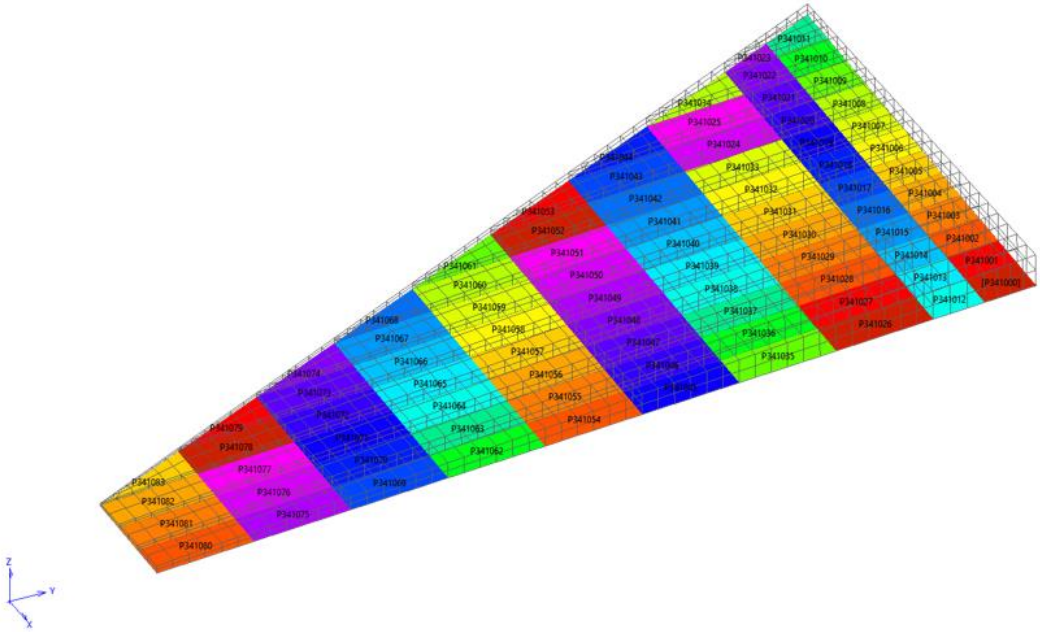

Figure 7-7 Design Zones for Lower Skin of the Wing v1_2

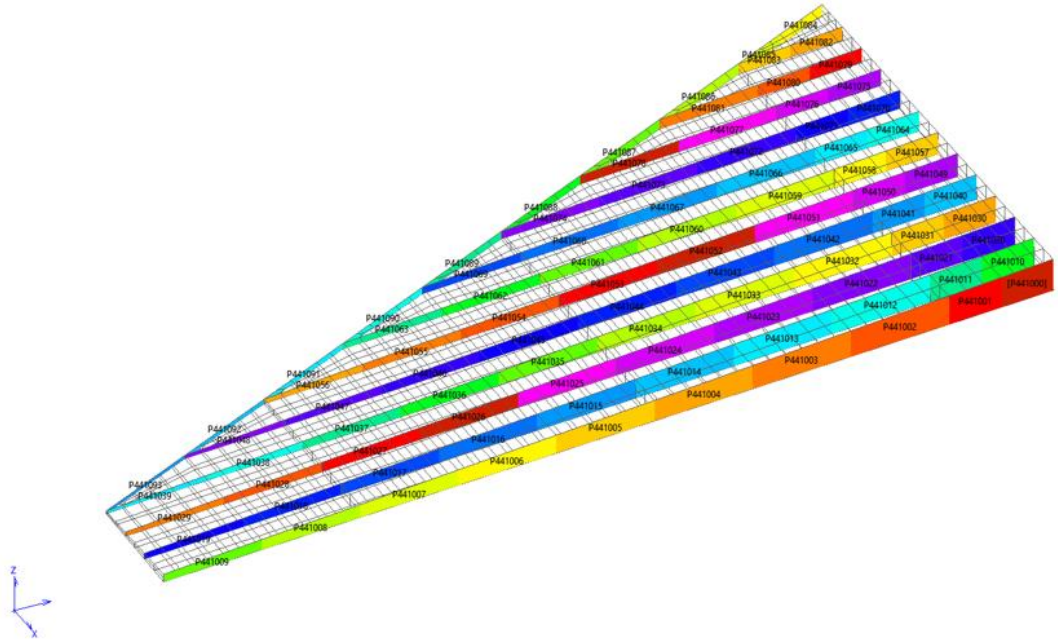

Figure 7-8 Design Zones for Spars of the Wing v1_2

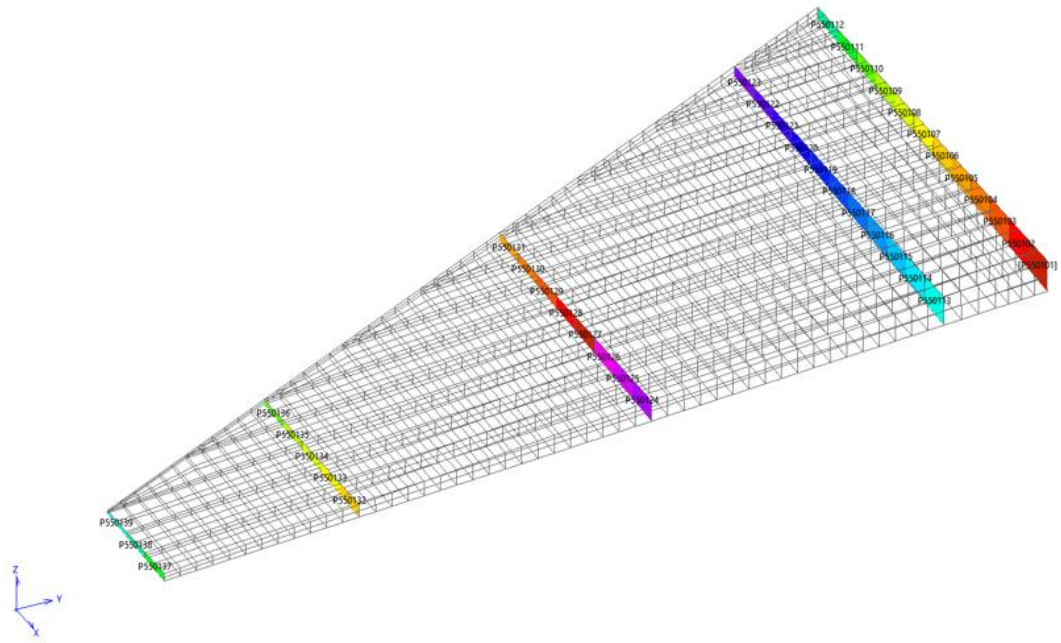

Figure 7-9 Design Zones for Ribs of the Wing v1_2

7.3.2 Design Variables

The shape functions which are used to represent the thickness values in the design zones are determined by using the comparison study and it can be found in Section 7.2. All of the thicknesses for the structural components are represented by the below predefined equations.

$$t_{ribs}(\zeta) = a_{00} + a_{10}\zeta \tag{7.10}$$

$$t_{spars}(\eta) = a_{00} + a_{01}\eta \tag{7.11}$$

$$t_{skin}(\zeta, \eta) = a_{00} + a_{10}\zeta + a_{01}\eta + a_{11}\zeta\eta + a_{20}\zeta^2 + a_{02}\eta^2 \tag{7.12}$$

The coefficients of $a_{00}, a_{10}, a_{01}, a_{11}, a_{20}$ and a_{20} are the design variables for the optimization problem. For each rib and spar which are metallic structures, all thickness distributions which are in the chord-wise or in the span-wise directions are represented by Equation 7.10 and Equation 7.11. Briefly, there are two design variables for each rib and spar.

On the other hand, for the composite skin, the total thickness of each design zone comprises the sum of the thicknesses of all the plies in the direction of 0°, ±45° and 90°. Therefore, there are six design variables for each ply in the principal directions. As it can be seen, the number of the design variables are free from the number of design zones and they only depend on the number of the ribs and the spars. Total number of the design variables which are used for the optimization studies of each candidate are presented in Table 7-2.

Table 7-2 Number of Design Variables of Candidates

Candidate (Wing ID)	Number of Design Variable per			Number of			Total number of Design Variables
	Skin	Spar	Rib	Skin	Spar	Rib	
v1_1	18	2	2	2	9	5	64
v1_2	18	2	2	2	13	5	72
v2_1	18	2	2	2	3	5	52
v2_2	18	2	2	2	4	5	54
v2_3	18	2	2	2	5	5	56
v3_1	18	2	2	2	5	5	56
v3_2	18	2	2	2	5	5	56

Each optimizer needs upper and lower limits for the predefined design variables and the starting values for the optimization must be between those lower and upper limits.

The minimum and the maximum values for the design variables which are determined for each structural component are seen in below Table 7-3.

Table 7-3 Minimum and Maximum Limits for Design Variables

	For Ribs		For Spars		For Skin	
	Min [mm]	Max [mm]	Min [mm]	Max [mm]	Min [mm]	Max [mm]
a_{00}	0.6	15	0.8	15	0.13	10
a_{01}	N/A	N/A	0.8	15	0.13	10
a_{10}	0.6	15	N/A	N/A	0.13	10
a_{11}	N/A	N/A	N/A	N/A	0.13	10
a_{20}	N/A	N/A	N/A	N/A	0.13	10
a_{02}	N/A	N/A	N/A	N/A	0.13	10

One of the most important subjects for the structural optimization problems when gradient-based optimization methods are used is from the fact that they use continuous design variables. Therefore, after the optimization is performed, the output thickness values cannot be directly used for the manufacturing especially for composite materials since the thickness for composite structures directly depend on the number of the plies which can only be found at discrete values. MSC NASTRAN has various capabilities providing the continuous optimization results which are

suitable for the production. By using DDVAL card, which is used in the MSC NASTRAN Sol 200 for storing all of the possible discrete values for the materials, the output thickness values can be obtained as discrete ones. There are various methods adopted by NASTRAN including round up and round down to the nearest discrete value or the method of the design of experiment which uses orthogonal arrays. As mentioned before, the main objective is to compare the candidates and find the minimum weight layout under symmetric pull-up loading condition. Therefore, in this study, optimizations are performed with continuous design variables. It is worth noting that, the results obtained after optimizations are generally not ready for the production phase and it is known that although the weights obtained by using continuous variables increase the weight for each candidate when discrete variables are used, this increment do not affect the weight order of the candidates.

Another important issue for the gradient-based optimization methods is that the sensitivity of the results depends on the initial values of the design variables. The optimization might not be converged to the optimum results when the optimization starts with poor design variables. Besides, in the gradient-based methods, after optimization is converged to the optimum value, it is not guaranteed that the optimum point is the global optimum. This issue is one of the drawbacks of the gradient-based optimization methods. Therefore, to minimize this particular risk, the comparison study is performed by also starting from different initial values for the each candidate.

For that purpose, three different optimization models having the same inputs are prepared, except the initial values for design variables are different. For the design variables, the initial values are set according to the minimum (min), middle (mid) and the maximum (max) of the values are shown in Table 7-3.

By using the strength-only constraints under the ultimate loading condition, the weights of the sized wing v1_2 which are obtained with different design variables are summarized in Table 7-4 and the convergence history of the objective function

for these three different optimization studies can be seen in Figure 7-10. The results for the all other candidates can be seen in Appendix C.

Table 7-4 Optimization Result with Different Initial Design Variables

Starting from	Number of Iterations	Weight [kg]	Difference from Mid [%]
Min	31	115.2	0.44
Mid	34	114.7	N/A
Max	28	121.8	6.19

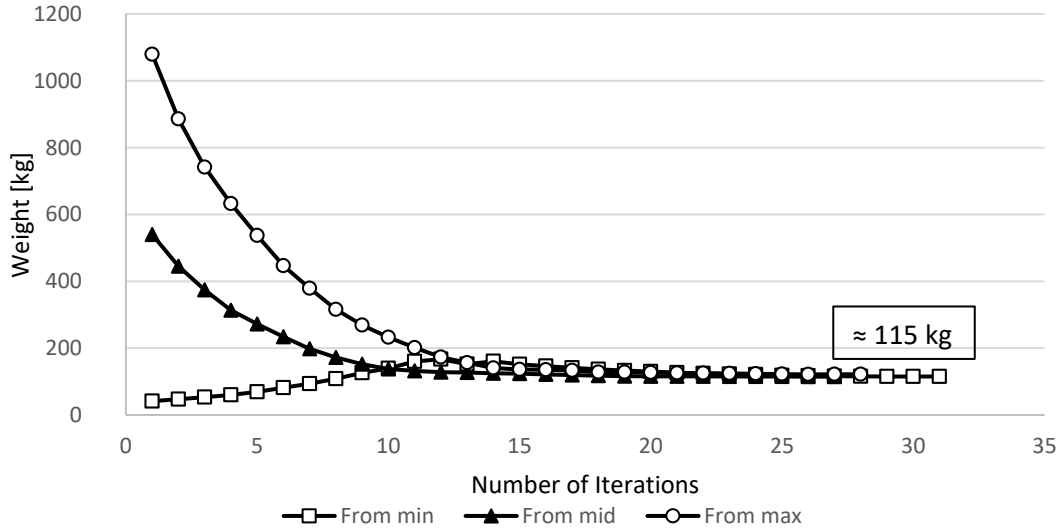

Figure 7-10 Convergence History for Wing v1_2 with Strength-Only Constraints

As it can be deduced from Table 7-4 and Figure 7-10, all of the three optimizations provide similar results. However, the minimum weight is obtained when the optimization starts with the middle values of the design variables consisting of the average values of the minimum and the maximum values of the design variables defined in Table 7-3. It may be attributed to the optimum results which are obtained after the optimization with strength-only constraints. Since the optimum results are closer to the middle values of the design variables, the optimizer converges easily to the optimum one when it starts with the middle design variables and the percentage difference between the minimum and the maximum obtained weight results comes out as 6.19%.

7.3.3 Comparison of the Weight of the Candidates

After the methodology for optimization is decided including the shape functions used for variable linking and the starting values for the design variables defined, in this section, all of the created wing design candidates which have the same outer boundary and different layouts are then compared according to their weight under the same loading condition. The results for the weight of the candidates which are subjected to strength-only constraints are presented in a block diagram and can be seen in Figure 7-11.

Table 7-5 Comparison of the Weight of the Candidates

Candidate	Number of the Spars	Number of Iterations	Weight [kg]
v1_1	9	21	182.2
v1_2	13	27	114.7
v2_1	3	45	188.0
v2_2	4	60	149.7
v2_3	5	21	164.6
v3_1	6[6]	31	156.8
v3_3	6[7]	27	138.2

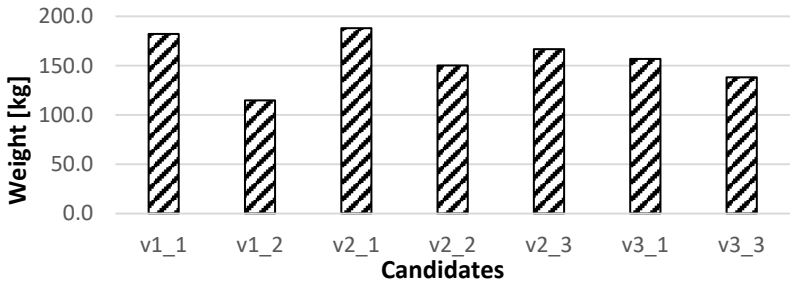

Figure 7-11 Total Weights of the Candidates according to Strength-only Constraints

[6] 2 spar is discontinuous from the 3rd to the tip rib
[7] 2 spar is discontinuous from the 4th to the tip rib

Figure 7-11 reveals that the wing v1_2 takes the attention at the first glance in terms of lightness whereas the worst candidate as being the heaviest turns out to be as v2_1.

It is known that all of the created layouts have the same number of ribs but different number of spars. Therefore, the comparison in this study is based on the multi-spar concepts. In general terms, increasing the number of spars results in more efficient design in terms of the weight except the second family which is shown in Section 3.3. As it is seen in Figure 3-9, in this family, all of the spars are converging to each other which is known as fanning type and increasing the number of spars in this type results in less spacing between the spars in the tip of the wings especially for the wings which are highly swept and having high aspect ratios. For the wing geometry which is used in this study, the spar spacing at the tip section decreases under 100 mm when the number of spars is increased above five and this spacing value becomes unreasonable for both panel breaker and manufacturing constraints point of view. As it can be seen that, the minimum weight for fanning type family obtained in the second candidate wing (v2_2) in which the spar spacing at the tip section is 133 mm which is also the same in the lightest candidate wing (v1_2) in this study. It can be concluded that for the wings which are highly swept and the length in the tip section is not high, runout family in which some of the spars are not going until the tip section might be more efficient compared to the fanning type. On the other hand, the most efficient wing layout for this type of wing geometries is seen as the first family in which all spars lie according to the rear spar.

As beforementioned in the section 2.3.3 and in order to satisfy the hard convergence check, in addition to the comparison of the objective function of the last two finite element analyses, the maximum value of constraints must also be under the predefined values provided by the user. The history of the maximum value of constraint values for the wing v1_2 both for optimizations starting from the minimum, middle and the maximum design variables under strength-only constraints can be seen in Figure 7-12, Figure 7-13 and Figure 7-14 respectively.

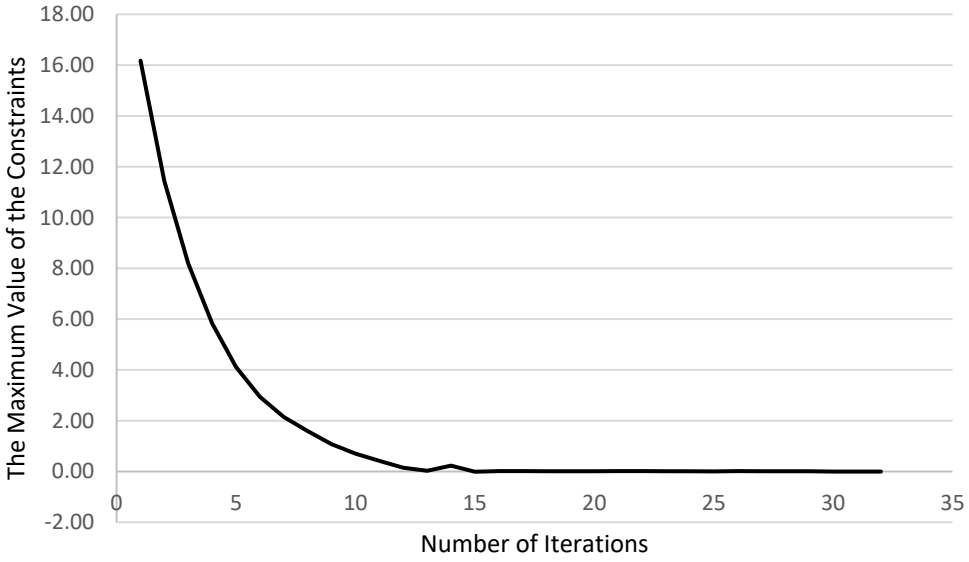

Figure 7-12 The Maximum Value of the Constraints vs Number of Iterations with Starting from the Minimum Design Variables

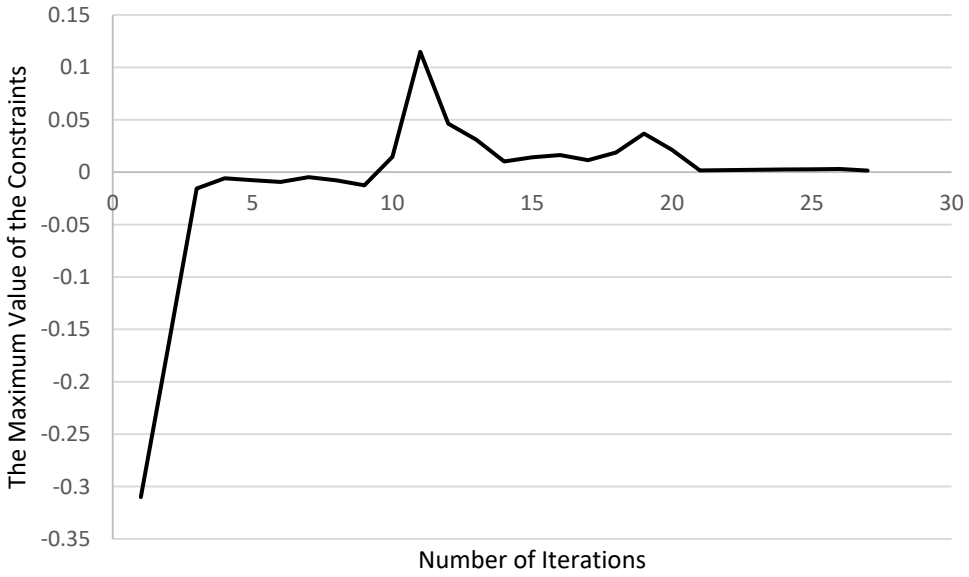

Figure 7-13 The Maximum Value of the Constraints vs Number of Iterations with Starting from Middle Design Variables

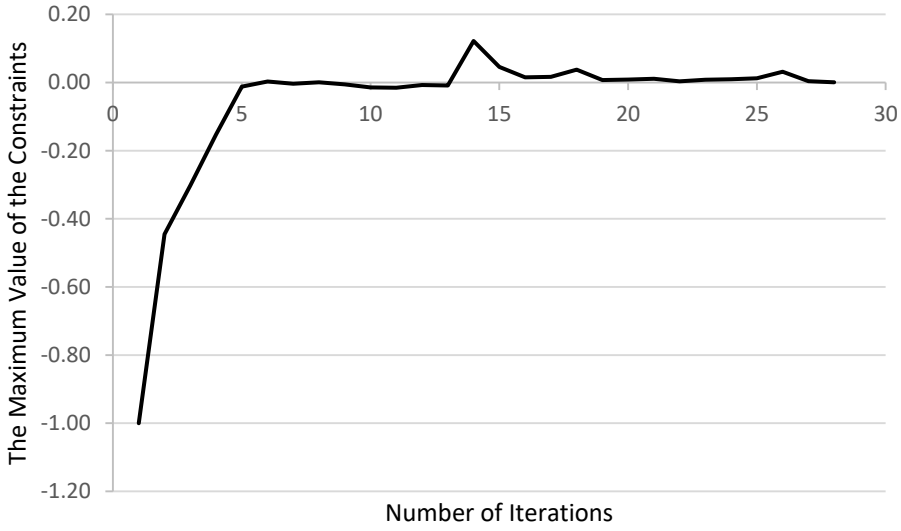

Figure 7-14 The Maximum Value of the Constraints vs Number of Iterations with Starting from the Maximum Design Variables

These maximum value of constraints represent the normalized constraints which are available in the output file of the MSC NASTRAN Sol 200. According to these values, it can be clearly said whether the final design satisfies the defined constraint values or not. As can be seen from the above Figure 7-12, while starting to the optimization with the minimum design variables, the maximum value of constraint values starts from high values, decreases smoothly and finally converges to approximately zero. In other words, in the initial design, the constraint values are violated and when the optimizer starts to improving the design, maximum constraint values converges to approximately zero and this may be interpreted as the final design is efficiently optimized. On the other hand, as seen in Figure 7-13 and Figure 7-14, the maximum value of constraints are starting from negative values and again converges to a nearly zero. This can also be interpreted that the starting point is over design and constraint values are lower than the defined constraint values. Design variables are continuously changed during optimization cycles according to search direction, and finally the optimizer finds the optimum design which satisfies all of the constraints with a minimum objective function.

The history graphics of each candidates can be seen in Appendix D.

When the results are further investigated, it is seen that the buckling constraint is much more dominant compared to the failure index constraint especially for the upper skin and after the optimization, the minimum buckling eigenvalues for the upper skin can be seen in below Figure 7-15.

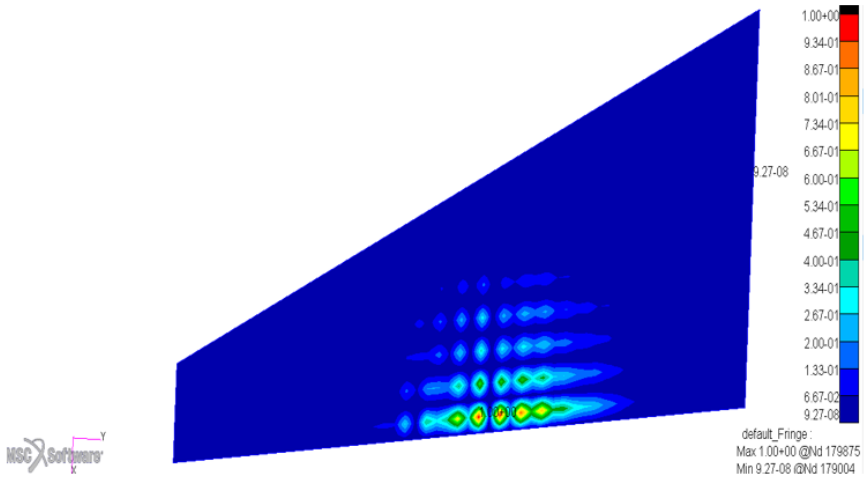

Figure 7-15 Minimum Buckling Eigenvalues for the Upper Skin after the Optimization

7.4 Optimization Including the Flutter Constraint

Flutter is the dynamic instability of any components subjected to the air flow in the aircraft and must be one of the most important concerns of the designers since it can result in a fatal accident when it is encountered during the flight. Flutter is commonly seen on the wings or the control surfaces including the aileron, the elevator and the rudder. It should be investigated at the earlier design stages as much as possible since it is a complicated phenomenon and related with the stiffness of the whole structure. Therefore, local design modifications such as increasing thickness after sizing according to the strength-only constraints may not generally lead to a flutter-free structure and it may require changing of the whole design.

A reliable minimum flutter speed for an aircraft is defined according to the certification requirements. The aircraft used in this study is a supersonic fighter and therefore, MIL-A-8870C [58] can be used to define the minimum flutter speed. As mentioned before in Section 6.4.2, according to the flight properties of the selected aircraft in this study, the minimum flutter speed of the wings must be greater than 510 m/s at the sea level.

7.4.1 Flutter Speeds of the Candidates

First of all, the flutter speeds of the design candidates which are sized with the strength-only constraints in the first stage of the optimization study should be investigated and for this purpose MSC NASTRAN Sol 145 is used. There are some parameters required for the flutter analysis such as the air density, the velocity set and the M-K pair sets. The load cases which are used in the trim analyses are at the sea level, therefore, the density ratio will be 1.0 representing the sea level. For the velocity set, the stall and the dive speeds of the aircraft are taken as references. However, higher speeds from the dive speed are also included in the velocity set. The spacing between the velocities where the flutter is expected is decreased in order to calculate the flutter speed more precisely. Finally, the M-K pair sets are prepared according to Equations 7.13 and 7.14 automatically by the MSC NASTRAN by using the input values.

$$k_{min} = \frac{2 \text{ x } \pi \text{ x } f_{min} \text{ x } c}{2 \text{ x } V_{max}} \tag{7.13}$$

$$k_{max} = \frac{2 \text{ x } \pi \text{ x } f_{max} \text{ x } c}{2 \text{ x } V_{min}} \tag{7.14}$$

where, c is the reference chord length, f is the frequency and V is the velocity. As a rule, f_{min} is entered as lower than frequency of the first bending mode and f_{max} is entered as higher than the first torsion mode of the wing since the flutter generally occurs between these two modes.

All used parameters for the flutter analyses can be seen in Table 7-6.

Table 7-6 Input Values for the Flutter Analyses

Density Ratio	1.0
Input Mach	1.3
Velocity Set ($x10^3$) [mm/s]	80 100 150 200 300 350 400 425 450 475 510 525 535 550 575 585 595 620 700 725 750 800
M-K Pair Set	0.087 0.358 0.629 0.900 1.172 1.443 1.714 1.985 2.256 2.798 2.827 3.069 3.340 3.611 3.882 4.153 4.424 4.695 4.967 5.238

The same aero model in the trim analysis is used for the purpose of the flutter analyses as well. For splining the aero model into the structural model, only nodes of the ribs and the spars which have stiffness in out-off plane direction are used.

The representation of the aero-structure coupled model for the wing v1_2 can be seen in Figure 7-16. It should be stated that, the same aero model is used for all of the candidates however the splines are different for each other as the structures are different.

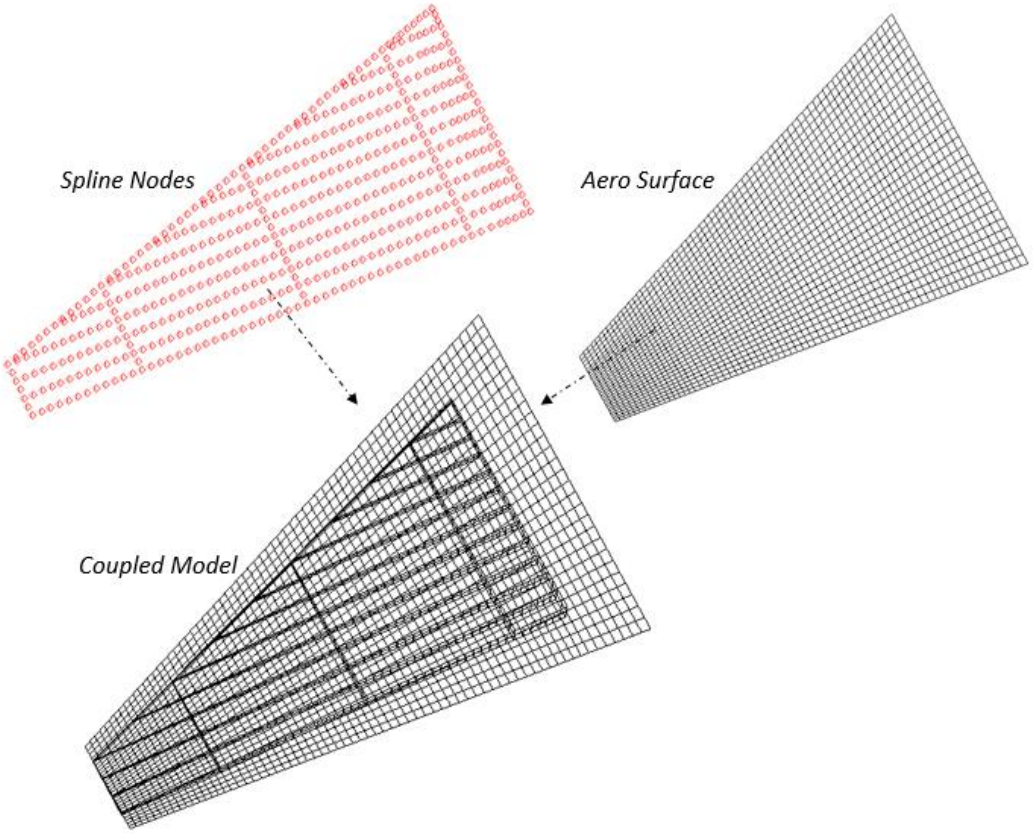

Figure 7-16 Aero – Structure Coupled Model

Finally, by using the models and the parameters all mentioned above and with the aid of MSC NASTRAN Sol 145, the flutter speed of each candidate wing with the sized properties are found. However, it should be noted that, the flutter speed cannot be determined directly within the analysis via MSC NASTRAN Sol 145. As mentioned before, the point at which the velocity-damping curve crosses the velocity-axis is accepted as the flutter speed. The velocity versus damping graphs defining the flutter speed of each candidate wing can be seen in Figure 7-17.

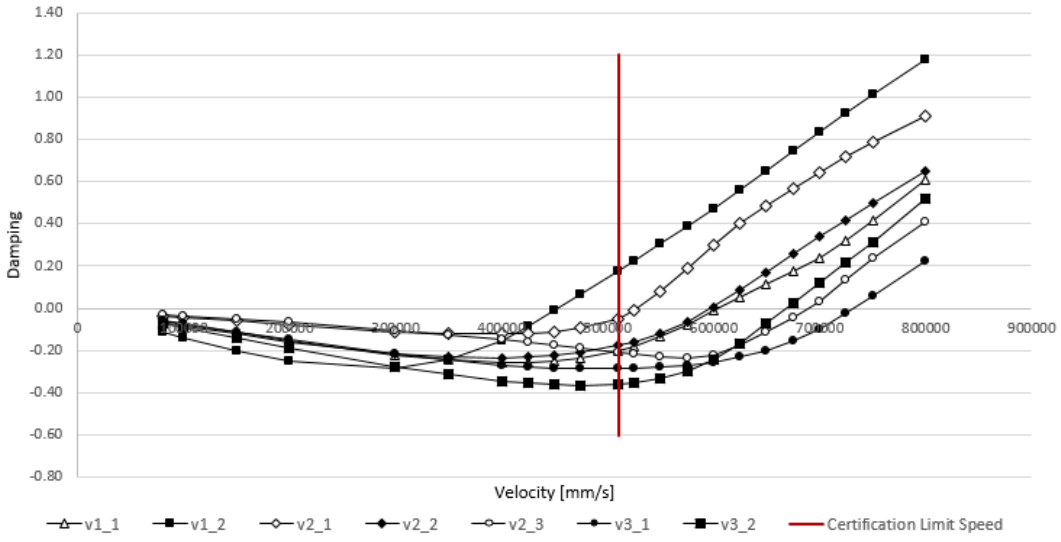

Figure 7-17 Velocity vs Damping Graphics for each Candidate

After investigating the velocity-damping graphs created for each candidate, the flutter speeds and the frequencies at the flutter together with the frequencies of the first bending and the first torsion modes are summarized in Table 7-7.

Table 7-7 Comparison of the Flutter Speeds of each Candidate

Candidate (Wing ID)	**1st Bending Mode [Hz]**	**1st Torsion Mode [Hz]**	**Frequency at Flutter [Hz]**	**Flutter Speed [m/s]**	**Weight [kg]**
v1_1	17.0	43.2	31.0	604.0	182.2
v1_2	16.5	44.7	25.3	453.8	114.7
v2_1	15.0	40.7	18.6	528.3	188.0
v2_2	15.2	40.5	28.4	597.2	149.7
v2_3	14.5	40.5	44.7	689.1	164.6
v3_1	15.9	47.5	32.4	731.6	156.8
v3_3	18.2	49.6	36.2	669.2	138.2

It is well known that the flutter speed is calculated after a complicated eigenvalue analyses and it depends on multiple factors such as stiffness, mass, density, etc. of the materials used in the structure of interest. All of the candidates are sized by considering the same constraints under the same loads with the same objective,

however after the optimization process, each of them has different weight and stiffness because of their different layouts. Although one cannot make rigorously generalizations about the flutter speeds of each candidate, it is possible to deduce reasonable results from each family.

First of all, in Table 7-7, it is clearly seen that the minimum flutter speed is obtained for the wing v1_2 which is also the "minimum weight design" after strength-only constraints. It can be said that v1_2 is the optimal design which carries the same loads compared with the other candidates, thereby, the stiffness of that design is low when it is compared to the others and it results as having the minimum flutter speed. Similarly, although the first bending and the first torsion natural frequency of the v1_1 is close to v1_2, it is heavier than the v1_2, therefore the flutter speed of that configuration is higher compared to that of the v1_2.

For the third family which consists of the candidate v3_1 and v3_2, it is inferred from Table 7-7 that the flutter speeds for the both candidates are quite high. There is a common belief that the flutter phenomenon takes place between the first bending and the first torsional modes of the structure and as the spacing between these two modes increases, the flutter appears to be at the higher speeds. Based on the results presented in Table 7-7, it can be clearly seen that the spacing between the first bending and the first torsion modes of the third family is greater than that of the others.

The main difference between the members of the second family is the number of the spars. By increasing the number of the spars, the stiffness becomes very high especially at the tip section of the wing where they are closely spaced. Therefore, the increase in the flutter speeds of the family two can be attributed to the increase in the number of the spars in candidate v2_1 to the one in v2_3.

After the general investigations for the flutter speeds of the candidates, it can be said that only one of the candidates does not satisfy the certification requirements for the flutter speed of minimum 510 m/s for the flight performance of the aircraft used in this study as seen from the Figure 7-17. Additionally, the minimum weight design

results in a more flexible structure and this type of flexibility also gives rise to the aeroelastic problems such as flutter at the lower speeds. Therefore, the second stage of the optimization with both strength and stiffness constraints are performed for only v1_2. At the following sections, the flutter speed of the wing v1_2 is aimed to be postponed by using two different methods. All of the constraints included in this particular optimization is summarized in below.

$$\left\{ \begin{array}{c} \frac{\sigma_{\text{max. von\_mises}}}{\sigma_{\text{allowable}}} \geq 1.0 \\ \text{FI}(x) \leq 1.0 \\ \min(\text{Buck.}) \geq 1.0 \\ g \leq 0 \end{array} \right\}$$

where, the FI(x) represents the failure index for the composite structures and the min(Buck.) is used to represent the minimum eigenvalue for the buckling constraint.

7.4.2 Results of the Optimization with Flutter Constraints

As abovementioned, the flutter speed of the minimum obtained weight design does not satisfy the lower limit of the certification requirement. In this section, multidisciplinary optimization capability of the MSC NASTRAN Sol 200 is used to postpone the flutter speed of the wing to the required level. As mentioned before in Section 6.4.2, the constraint is not directly given to the flutter speed, it is given to the damping value at the specified velocities.

After the optimization is performed with the constraints as specified in Section 6.4, the increment in the flutter speed can be clearly seen in the below Figure 7-18.

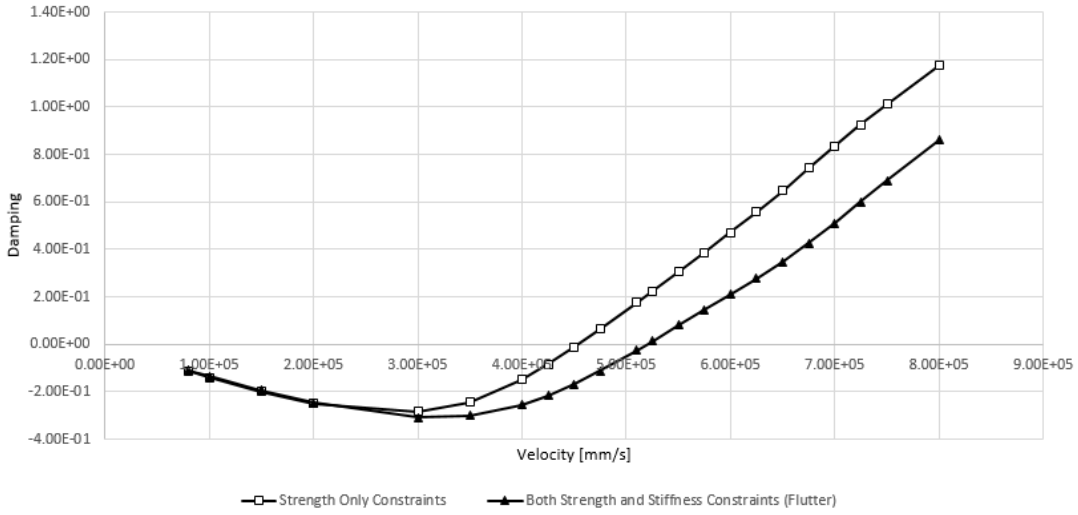

Figure 7-18 Velocity – Damping Curves Before and After Optimization with Both Strength and Stiffness (Flutter) Constraint

However, as expected, to provide a flutter speed at the intended level, the weight of the sized wing increases slightly as 10.4% from 114.7 kg to 126.6 kg as shown in Table 7-8.

Table 7-8 Comparison of Results for the both First and Second Stage Optimizations Including Flutter

Constraints for v1_2	**Flutter Speed [m/s]**	**Weight [kg]**
Strength-Only Constraints	453.8	114.7
Both Strength and Stiffness (Flutter) Constraints	519.4	126.6

In Figure 7-19, the change of the velocity – frequency curves for the first bending mode can be seen. As inferred, there is no significant change in the frequencies of the wing which is sized with the strength-only constraints and both strength and stiffness (flutter) constraints. Although the increment in the flutter speed is obtained successfully, it can be attributed to the increase in the weight of the structure.

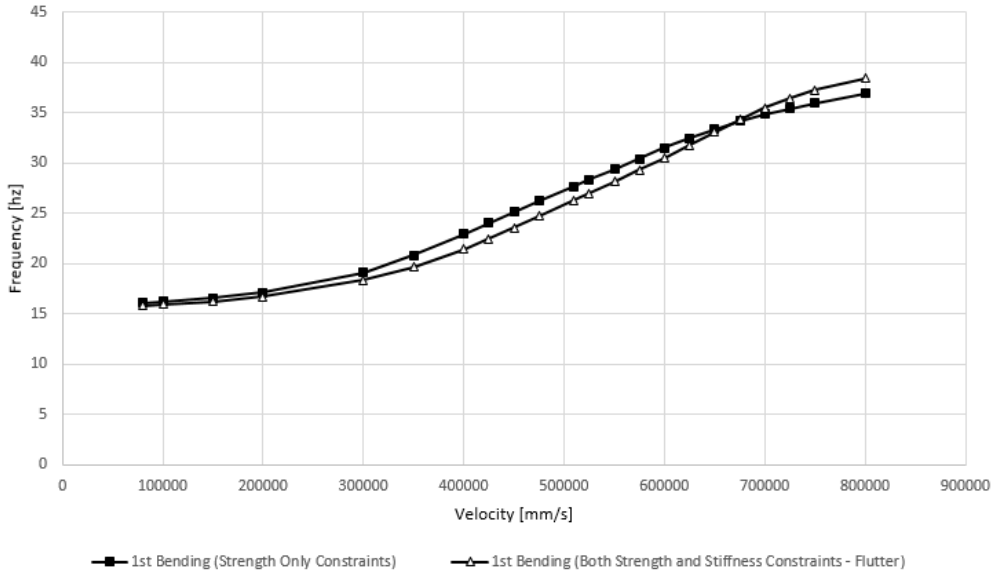

Figure 7-19 Velocity – Frequency Curves Before and After Optimization with Both Strength and Stiffness (Flutter) Constraint

When investigations on the further are performed for the percentages of the principal fiber directions in composite skin cases, while the fibers which are aligned in ±45 degrees, the fibers with 0 and 90 degrees for both the lower and the upper skin decreases as seen in Table 7-9. Therefore, it can be concluded that the sensitivity of the flutter response with respect to fibers in ±45 degrees is greater compared to that of 0 and 90 degrees in the optimization including the stiffness constraints.

Table 7-9 Change of Percentages of the Fibers in Composite Skin for Optimization with Both Strength and Stiffness (Flutter) Constraints compared with the Strength-Only Constraints

	Lower Skin			**Upper Skin**		
	0 degree	**±45 degree**	**90 degree**	**0 degree**	**±45 degree**	**90 degree**
Strength-Only Constraints	37.39 %	36.77 %	25.84 %	54.49 %	25.16 %	20.35 %
Both Strength and Stiffness (Flutter) Constraints	35.01 %	40.32 %	24.66 %	52.57 %	29.51 %	17.92 %

7.5 Optimization Including the Frequency Constraint

The second method which is used to postpone the flutter speed of the wing is the optimization including the frequency constraint in addition to the strength constraints. Similar to the optimization study performed in the previous section, the frequency constraint is only applied to wing v1_2.

It is well known that the classic flutter phenomenon occurs generally because of the elastic coupling of the first bending and first torsion modes of the wings. Therefore, the flutter speed of the wing is aimed to be postponed by separating the first bending and the first torsion natural frequencies which is obtained after the optimization with the strength-only constraints seen in Table 7-10.

Table 7-10 The First Bending and the First Torsion Modes of Wing v1_2

Wing ID	**1st Bending Mode [Hz]**	**1st Torsion Mode [Hz]**
v1_2	16.5	44.7

To see the effects of these modes of the wing and the separation of them on the flutter speed, several optimizations are performed at different frequency values. In the optimizations, the strength-only constraints and both strength and stiffness (frequency) constraints are considered. The frequency constraint is applied with two different ways; the first one is to apply the constraint on the first bending mode and the second one is to apply it on the spacing between the first bending and the first torsion modes as seen from the below scenarios in Table 7-11.

Table 7-11 Results after Optimization with Both Strength and Stiffness (Frequency) Constraints

Scenarios	1st Bending Mode [Hz]	Spacing [Hz]	Flutter Speed [m/s]	Weight of the Wing v1_2 [kg]
First	16.5	28	453	114.7
1	16.5	31	491	122.0
2	16.5	32	499	128.4
3	16.5	33	532	143.7
4	17.5	32	510	128.6
5	18.5	32	521	131.8

The first one is directly given to the natural frequency of the first bending. Three different frequency values are then tried as 16.5 Hz (i.e. the initial state) 17.5 Hz and 18.5 Hz. Finally, by using the DEQATN cards which are used for the writing of equations in the input file of MSC NASTRAN Sol 200, it is aimed to increase the gap between the first two modes.

As it can be inferred from Table 7-11, five different scenarios are performed in the structural optimization of the wing v1_2. In the first three scenarios, the first bending mode does not change, on the other hand, the gap between the first bending and the first torsion modes are increased one by one. In the last two scenarios, the first bending mode is also increased and the gap between these two modes is kept constant as 32 Hz.

The applied constraints for the optimizations in this section can be summarized as below which consist of both strength and stiffness constraints.

$$\left\{\begin{array}{c} \frac{\sigma_{\text{max. von Mises}}}{\sigma_{\text{allowable}}} \geq 1.0 \\ \text{FI}(x) \leq 1.0 \\ \min(\text{Buck.}) \geq 1.0 \\ \min(1^{st}\ \text{Bending Mode}) \geq \{16.5, 17.5, 18.5\ \text{Hz}\} \\ \min(1^{st}\ \text{Torsion Mode} - 1^{st}\ \text{Bending Mode}) \geq \{31, 32, 33\ \text{Hz}\} \end{array}\right\}$$

It is clearly seen that separating the natural frequencies of the first bending and the first torsion results in the increment for the flutter speed of the wing as expected. These results also support the argument for the third family which has a maximum gap between the first two modes.

As also seen in Table 7-11, the last three scenarios satisfy the requirement level of the flutter speed which is the minimum of 510 m/s. However, if the final weights obtained after the optimizations are investigated, it is seen that the most efficient scenario from the minimum weight point of view comes out as the fourth one and the increment of the flutter speed can be seen in Figure 7-20 from the velocity – damping curves.

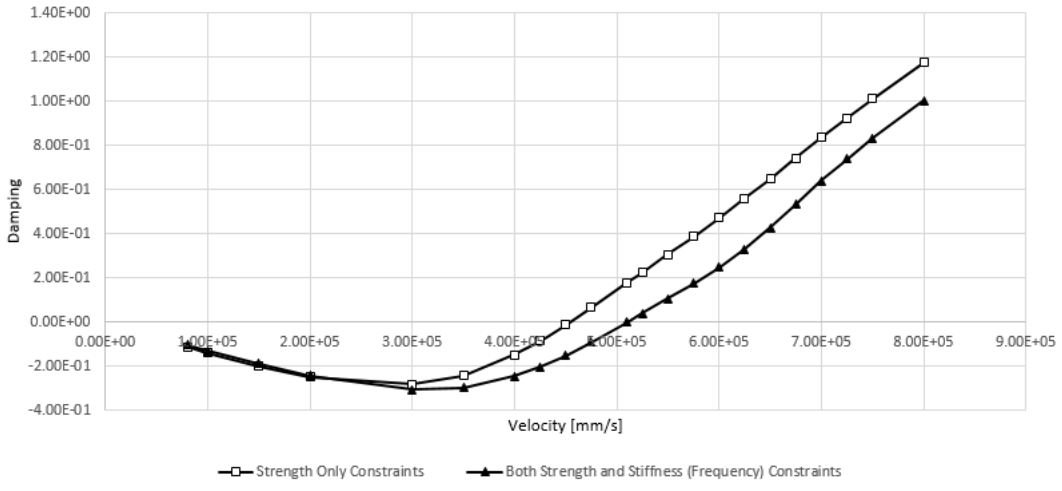

Figure 7-20 Velocity – Damping Curves Before and After Optimization with Both Strength and Stiffness (Frequency) Constraints

The results of the first stage (strength-only) and the second stage (both strength and stiffness) of the optimization including the frequency constraints are summarized in Table 7-12. Likewise, in the results with the flutter constraint, the ones with the frequency constraint result in a weight increment of 12.1%.

Table 7-12 Comparison of Results for Both the First and the Second Stage Optimizations Including Frequency Constraints

Constraints for v1_2	**Flutter Speed [m/s]**	**Weight [kg]**
Strength-Only Constraints	453.8	114.7
Both Strength and Stiffness (Frequency) Constraints	510.7	128.6

When the percentages of the principal fiber directions in the composite skin are investigated, an increment is also observed in the fibers with ±45 degree for both the lower and the upper skin as seen in Table 7-13 likewise the case in optimization with the flutter constraint. However, as distinct from the optimization with the flutter constraint, it is also observed an increment in the percent of the plies which are aligned in 0 degree especially for the lower skin and it can easily be attributed to the increase of the natural frequencies.

Table 7-13 Change of Percentages of the Fibers in Composite Skin for Optimization with Both Strength and Stiffness (Frequency) compared with the Strength-Only Constraints

	Lower Skin			**Upper Skin**		
	0 degree	**45 degree**	**90 degree**	**0 degree**	**45 degree**	**90 degree**
Strength-Only Constraints	37.39%	36.77%	25.84%	54.49%	25.16%	20.35%
Both Strength and Stiffness (Frequency) Constraints	45.66%	40.33%	14.01%	53.61%	35.59%	10.80%

7.6 Conclusion

In this chapter, the results of the developed multidisciplinary optimization approach are investigated by using different candidates having various layouts. First of all, the performance of the shape functions used for the design variable linking method are compared with each other and it is decided to use the quadratic 2D function for the composite skin and the linear functions for the ribs and the spars. The weights of all of the candidates are then compared with each other under the same aerodynamic load by using the strength-only constraints and this step is named as the first stage of the optimization. In the second stage of the optimization study, the flutter speed of each candidate with sized properties are calculated by using the MSC NASTRAN Sol 145 and it is observed that only one candidate could not manage to satisfy the minimum limit of the certification. Therefore, for that design candidate providing the minimum weight design after the first stage of the optimization, two different strategies are followed to postpone the flutter speed including both the flutter and the frequency constraints. Finally, the results reveal that an increment in the flutter speed by approximately 12% is obtained with the price of an approximately 10% increase in the weight of the both two approaches.

CHAPTER 8

CONCLUSIONS

8.1 General Conclusions

In this thesis, several optimization studies are performed on the different layouts which are subjected to the strength-only and both strength and stiffness constraints by adopting the design variable linking method. By investigating the results, the most suitable layout for the selected fighter wing geometry is found through the optimization capabilities of the MSC NASTRAN.

The aerodynamic loads acting on the wing surface are then obtained by using the trim analyses via the MSC FLDS and compared with the results of the Schrenk's Approximation and it is deduced that the aerodynamic loads obtained from the trim analyses are considered as satisfactory from the trustworthiness point of view as obtained with a less computational effort instead of using expensive CFD analyses.

In this thesis, as distinct from the other optimization studies, the design variable linking method is adopted mainly to decrease the total number of design variables and to obtain practical final designs which also consider the manufacturing issues. By comparing the results obtained from the constant, the linear, the quadratic 1D and the quadratic 2D shape functions in the variable linking method, it is seen that the thickness distribution of the composite skin are represented best with the quadratic 2D shape functions, and therefore the minimum weight is obtained from this particular optimization study where the skin thickness changes with the quadratic 2D

shape function making the change of the thickness both in the chord-wise and in the span-wise directions possible. Besides, it is also seen that the layout in which the spars are parallel to the rear spar shows the best performance from the lightweight point of view for the wing geometry used in this study between all of the candidates.

In this research study, the two-staged optimization methodology is adopted and the studies concerning the minimum flutter speed are included in the second stage. After sizing all of the candidates in the first stage of the optimization by considering the strength-only constraints, the minimum speeds at which the flutter occurs are calculated via MSC NASTRAN Sol 145 with P-K method. By investigating the obtained optimization results, it is inferred that the flutter speed is mostly affected by the torsional stiffness and the gap between the first bending and the first torsion modes of the wing.

In the second stage of the optimization study, two different methods are adopted to postpone the minimum flutter speed. One of them is to constrain the damping value and the other is to increase the gap between the first bending and first torsion modes. For both of the methods, the flutter speed is increased approximately by 12% for the price of approximately 10% increase in the weight. When these two methods are to be compared with each other, separating the first two modes from each other are said to be more practical from the computational effort and the high sensitiveness to the flutter speed point of view. Besides, comparing the results for the strength-only and both strength and stiffness constraints, it is seen that the percentage of the plies which are aligned in ±45 degree is increased for both of the methods used in the second stage of the optimization to postpone the flutter speed.

As a conclusion, it is proven that the design variable linking method is a very efficient method for especially in decreasing the total number of design variables and obtaining smooth thickness distributions by also overcoming the manufacturing issues. Besides, by using the multidisciplinary optimization tools by including both the strength and the stiffness related constraints at the same time, more reliable

designs can also be obtained with a minimum weight penalty in a much shorter computational time.

8.2 Recommendation for the Future Work

Following suggestions may be listed for future related studies as;

- Control surfaces are not included in this study. However, inclusion of them may change the whole vibration characteristics of the wing and therefore the flutter might be encountered at lower speeds. The same optimization studies might be re-performed by including the control surfaces as well.
- The flange elements may be included for the ribs and the spars. Therefore, in order to size the flange elements, a failure method of crippling might also be implemented in the MSC NASTRAN database.
- Another aeroelastic phenomena such as the divergence and the control surface reversal might also be investigated through the proposed optimization methodology.
- The aerodynamic loads are obtained through the rigid trim analyses. Flexible trim analysis where the deflection of the structure is also included might be performed as well.
- In this study, only the plies in the direction of 0°, ±45° and 90° are used. In order to investigate the effects of the fiber directions on the results of the optimization, different ply orientations might also be considered.
- Many more layouts including the multi-rib concepts might be experimented.
- On top of the pull-up maneuvers used in this study, analysis with different maneuvers such as roll with pull-up might also be performed.

REFERENCES

[1] A. J. McAndrew, “Consolidated FY2020 Flying Hour Aircraft Rates”, Office of the Under Secretary of Defence, 2019.

[2] I. Nicolin and B. A. Nicolin, “Analysis of modern military jet trainer aircraft,” *Int. Conf. Aerosp. Sci. “AEROSPATIAL 2018,”* vol. 10, no. 4, pp. 193–202, 2018, doi: 10.13111/2066-8201.2018.10.4.17.

[3] Wikipedia, https://en.wikipedia.org/wiki/Northrop_T-38_Talon (accessed Jun. 27, 2020).

[4] Quara, https://www.quora.com/In-your-opinion-which-would-make-a-better-replacement-for-the-F-16-in-the-USAFs-Thunderbirds-acrobatic-team-the-F-22-or-the-F-35 (accessed Jun. 27, 2020).

[5] D. W. Zingg, M. Nemec, and T. H. Pulliam, “A comparative evaluation of genetic and gradient-based algorithms applied to aerodynamic optimization,” *Eur. J. Comput. Mech.*, vol. 17, no. 1–2, pp. 103–126, 2008, doi: 10.3166/REMN.17.103-126.

[6] J. Arora, *Introduction to Optimum Design*. Elsevier Researcher Academy, 4th Edition, 2016.

[7] N. Corporation and A. Division, “ASTROS - A Multidisciplinary Automated Structural Design Tool,” *AIAA J.*, 1990.

[8] J. Larson, M. Menickelly, and S. M. Wild, “Derivative-free optimization methods,” *Acta Numer.*, vol. 28, pp. 287–404, 2019, doi: 10.1017/S0962492919000060.

[9] L. Cao, L. Xu, and E. D. Goodman, “A Guiding Evolutionary Algorithm with Greedy Strategy for Global Optimization Problems,” *Comput. Intell. Neurosci.*, vol. 2016, 2016, doi: 10.1155/2016/2565809.

[10] H. Zhang, X. Zheng, and Z. Liu, “Optimization of composite wing using genetic algorithm,” *ICCM Int. Conf. Compos. Mater.*, vol. 2017-Augus, no. August, pp. 20–25, 2017.

[11] M. S. Beato, I. Capua, and D. Alexander, “Optimization of Aeroelastic Composite Structures using Evolutionary Algorithms,” vol. 27, no. 02, pp. 146–168, 2010.

[12] MSC Software Corporation, *MSC Nastran 2012 Design Sensitivity and Optimization User’s Guide*. 2011.

[13] X. Chen and M. M. Kostreva, “Methods of feasible directions: A Review,” *Kluwer Acad. Publ.*, pp. 205–206, 2000.

[14] S. Guo, D. Li, and Y. Liu, “Multi-objective optimization of a composite wing subject to strength and aeroelastic constraints,” *Proc. Inst. Mech. Eng. Part G J. Aerosp. Eng.*, vol. 226, no. 9, pp. 1095–1106, Sep. 2012, doi: 10.1177/0954410011417789.

[15] D. Chen, R. T. Britt, K. Roughen, and D. Stuewe, “Practical application of multidisciplinary optimization to structural design of next generation supersonic transport,” in *13th AIAA/ISSMO Multidisciplinary Analysis and Optimization Conference 2010*, 2010, doi: 10.2514/6.2010-9311.

[16] D. Li, J. Xiang, S. Guo, and R. Xu, “Optimization of composite wing structure for a flying wing aircraft subject to multi constraints,” *Collect. Tech. Pap. - AIAA/ASME/ASCE/AHS/ASC Struct. Struct. Dyn. Mater. Conf.*, pp. 1–11, 2013.

[17] MSC Software Corporation, “MSC Nastran 2012 Aeroelastic Analysis User’s Guide,” 2012.

[18] H. Djojodihardjo, “Optimization of Tapered Wing Structure with Aeroelastic Constraints”, 22nd International Congress Of Aeronautical Sciences, January 2014, 2000.

[19] Wikipedia, https://en.wikipedia.org/wiki/Handley_Page_Type_O (accessed May 01, 2020).

[20] M. Hasan, “Multidisciplinary Design and Optimization of a Composite Wing Box,” Phd. Thesis, Middle East Technical University, 2003.

[21] N. S. Khot and J. V. Zweber, “Design of Flutter Characteristics of Composite Wings Using Frequency Constraint Optimization,” *J. Aerosp. Eng.*, vol. 16, no. 1, pp. 19–30, Jan. 2003, doi: 10.1061/(ASCE)0893-1321(2003)16:1(19).

[22] S. Janardhan and R. V. Grandhi, “Multidisciplinary optimization of an aircraft wing/tip store configuration in the transonic regime,” *Eng. Optim.*, vol. 36, no. 4, pp. 473–490, Aug. 2004, doi: 10.1080/03052150410001686512.

[23] M. Sensmeier and J. Samareh, “A Study of Vehicle Structural Layouts in Post-WWII Aircraft,” *AIAA J.*, Apr. 2004, doi: 10.2514/6.2004-1624.

[24] The-Blueprints, https://www.the-blueprints.com/index.php?search/Mig-31/ (accessed Apr. 26, 2020).

[25] The-Blueprints, https://www.the-blueprints.com/search/f-22/.

[26] The-Blueprints, https://www.the-blueprints.com/search/f-16/.

[27] V. Weissberg, A. Green, and H. Mey-Paz, “Towards a fastenerless all composite wing,” *27th Congr. Int. Counc. Aeronaut. Sci. 2010, ICAS 2010*, vol. 3, pp. 2443–2452, 2010.

[28] T. Yao and M. Fujikubo, “Buckling/Plastic Collapse Behavior and Strength of Rectangular Plate Subjected to Uni-Axial Thrust,” in *Buckling and Ultimate Strength of Ship and Ship-Like Floating Structures*, Elsevier, 2016,

pp. 75–155.

[29] V. Soloshenko, “Conceptual design of civil airplane composite wingbox structures,” *29th Congr. Int. Counc. Aeronaut. Sci. ICAS 2014*, 2014.

[30] J. H. Jang and S. H. Ahn, “FE modeling methodology for load analysis and preliminary sizing of aircraft wing structure,” *Int. J. Aviat. Aeronaut. Aerosp.*, vol. 6, no. 2, 2019, doi: 10.15394/ijaaa.2019.1301.

[31] MSC . Software Corporation, “MSC SimCompanion - Interface To MSC Nastran Preference Guide Volume 1: Structural Analysis,” 2014. [Online]. Available: https://simcompanion.mscsoftware.com/infocenter/index?page=content&id=DOC9219&cat=PATRAN_DOCUMENTATION_2008_R1&actp=LIST.

[32] Hexcel, “Allowables of Hexply AS4/8552/RC34/AW134.” https://www.hexcel.com/Products/Resources/1664/hextow-laminate-properties-in-hexply-8552 (accessed Apr. 27, 2020).

[33] Battelle Memorial Institute, “Metallic Materials Properties Development and Standardization (MMPDS-12),” 2017.

[34] Z. Xin, Y.-B. Liu, P. Chen, F. Shen, S.-J. Zhang, and X.-R. Fu, “Flutter frequency based on bending - torsion coupling theory,” *8th Int. Conf. Comput. Methods*, 2017.

[35] D. Eagle and J. Ausman, “Integration of MSC.FlightLoads and Dynamics at Lockheed Martin Aeronautics Company”, MSC. Software 3rd Worldwide Aerospace Conference and Technology Showcase, Paper No: 2001-31, 2001.

[36] M. Mert, “A Preliminary Sizing Tool For Minimum Weight Aircraft,” Msc. Thesis, Middle East Technical University, 2018.

[37] MSC . Software Corporation, “MSC.FlightLoads and Dynamics User’s Guide

Version 2006," 2006.

[38] E. Albano and W. P. Rodden, "A doublet-lattice method for calculating lift distributions on oscillating surfaces in subsonic flows," *AIAA J.*, vol. 7, no. 2, pp. 279–285, May 1969, doi: 10.2514/3.5086.

[39] Ping-Chih Chen and D. D. Liu, "A Harmonic Gradient Method for Unsteady Supersonic Flow Calculations," vol. 22, no. 5, 1985.

[40] Ü. Gülçat, "Fundamentals of Modern Unsteady Aerodynamics," in *Fundamentals of Modern Unsteady Aerodynamics*, Springer Singapore, 2016, pp. 1–24.

[41] P. Arendsen, "The B2000 Doublet Lattice Processor : B2DL", National Aerospace Laboratory, October 2002.

[42] J. K. S. DILLINGER, "Static Aeroelastic Optimization of Composite Wings with Variable Stiffness Laminates," Msc. Thesis, Delft University of Technology, 2014.

[43] J. Woo, "Static Aeroelastic Response of an Aircraft With Asymmetric Wing Planforms Representative of Combat Damage," p. 76, 1993.

[44] MSC . Software Corporation, "MSC . Flightloads and MSC . Aeroelasticity," 2005.

[45] M. V. Cook, *Flight Dynamics Principles*, vol. 53, no. 9. 2007.

[46] MSC Software Corporation, "MSC Nastran 2019 Quick Reference Guide," 2019.

[47] "Design Loads for Future Aircraft," Research And Technology Organisation, Rto Technical Report 45, 2002.

[48] O. Schrenk, "A simple Approximation Method for Obtaining the Spanwise Lift Distribution," no. 1, pp. 1–9, 1940.

[49] E. Stein, The History of Theoretical, Material and Computational Mechanics, Lecture Notes in Applied Mathematics and Mechanics 1, doi: 10.1007/978-3-642-39905-3_22

[50] E. Wilson, “Isoparametric Elements.” http://www.edwilson.org/BOOK-Wilson/05-iso.pdf (accessed May 01, 2020).

[51] B. I. G. Brian C. Hoskin, “An Introduction to Use of Isoparametric Elements with Examples from Torsion Problem,” 1978.

[52] Singiresu S. Rao, *The Finite Element Method in Engineering*, 4th ed., no. December. Elsevier, 2004.

[53] C. Hua, “An inverse transformation for quadrilateral isoparametric elements: Analysis and application,” *Finite Elem. Anal. Des.*, vol. 7, no. 2, pp. 159–166, 1990, doi: 10.1016/0168-874X(90)90007-2.

[54] (EASA) European Aviation Safety Agency, “Certification Specifications for Normal, Utility, Aerobatic, and Commuter Category Aeroplanes CS-23 Amendment 3,” *Opt. Eng.*, vol. 36, no. Amendment 3, p. 482, 2012, doi: 10.1002/9780470664797.

[55] J. J. Zipay, C. T. Modlin, and C. E. Larsen, “The ultimate factor of safety for aircraft and spacecraft – its history, applications and misconceptions,” *57th AIAA/ASCE/AHS/ASC Struct. Struct. Dyn. Mater. Conf.*, 2016, doi: 10.2514/6.2016-1715.

[56] C. T. Modlin and J. J. Zipay, “The 1.5 & 1.4 Ultimate Factors of Safety for Aircraft & Spacecraft - History, Definition and Applications,” *NESC Factor Saf. TIM; 23-24 Sep. 2014*, pp. 1–26, 2014, doi: 10.1109/WCSE.2009.314.

[57] P. Hajela, “A root locus-based flutter synthesis procedure,” *J. Aircr.*, vol. 20, no. 12, pp. 1021–1027, 1983, doi: 10.2514/3.48206.

[58] “MIL-A-8870C Military Specification,” 1987.

[59] M. Şahin and O. Adıgüzel, “Statik Kısıtlar Altında Bir Jet Uçağı Kanadının Değişkenleri Birbirlerine Bağlama Metodu Yardımıyla Optimizasyonu”, 5. Ulusal Havacılık Teknolojisi ve Uygulamaları Kongresi, 2020.

APPENDICES

A. Mesh Convergence Studies

To see the results of the finite element analysis free from mesh density, for each candidate, four different model which have different mesh sizes from coarse to the finest are created. Max. tip displacements and first three natural frequencies are compared with each other. For the linear static analysis to see the tip displacement, all models are loaded from mid chord length of tip section with 3000 N which is in –z direction. For this purpose, RBE3 (rigid body element) elements have been used. Besides, modal responses of the wing in this study is very important. Therefore, in addition to tip displacement results, modal analyses are performed for all models and the first three natural frequencies are compared in below tables.

Table 8-1 Max. Tip Displacements and First Three Natural Frequencies of the Wing v1_1

Mesh Type	**Mesh Size [mm]**	**Element Number**	**Node Number**	**Max. Tip Disp. [mm]**	**1st Mode [Hz]**	**2nd Mode [Hz]**	**3rd Mode [Hz]**
Coarse	200	270	181	162.97	12.89	45.74	72.23
Fine	100	1084	875	164.60	12.90	45.10	71.59
Finer	55	2485	2157	164.73	12.89	44.36	69.16
Finest	40	7389	6806	164.86	12.89	44.25	68.94

In below Figure 8-3, Figure 8-2, Figure 8-3 and Figure 8-4, the maximum tip displacement under 3000N tip force in –z direction can be seen for the wing v1_1 with a coarse, fine, finer and finest mesh densities respectively.

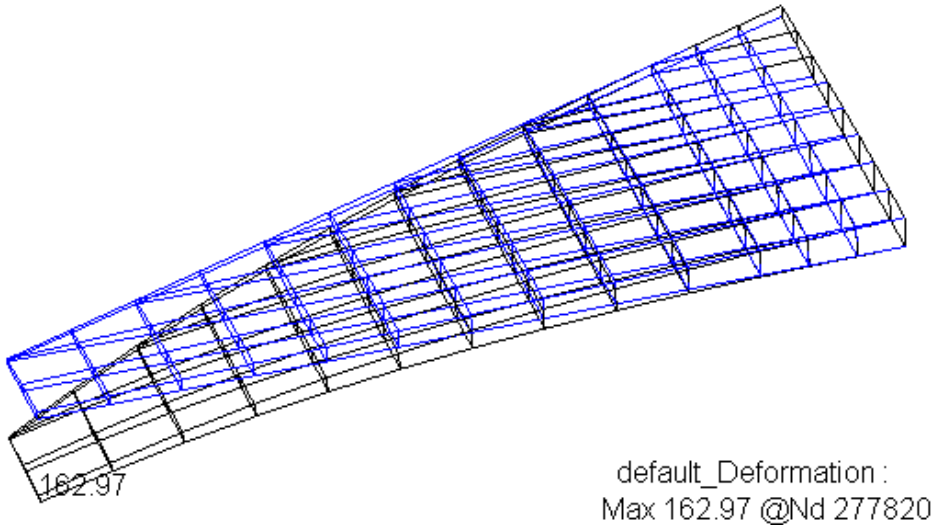

Figure 8-1 Max. Tip Displacement of Wing v1_1 with Coarse Mesh

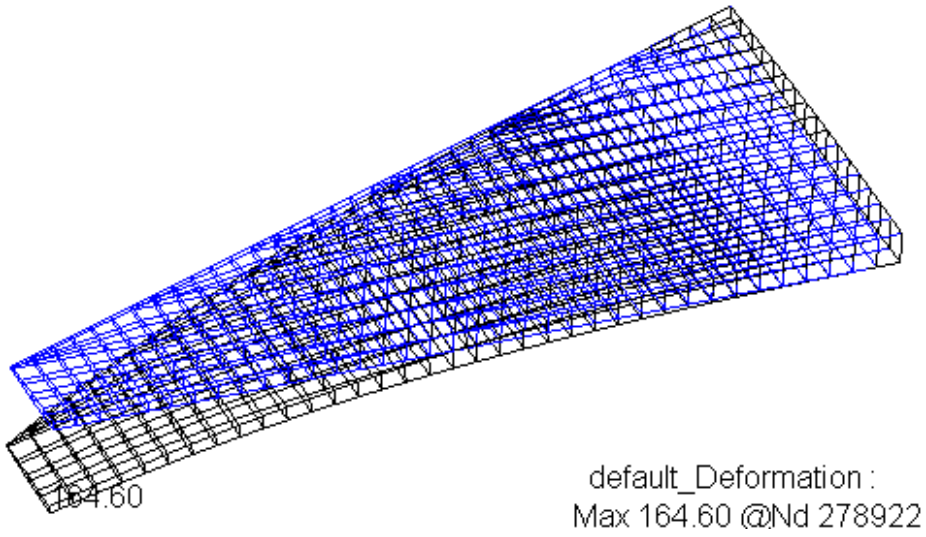

Figure 8-2 Max. Tip Displacement of Wing v1_1 with Fine Mesh

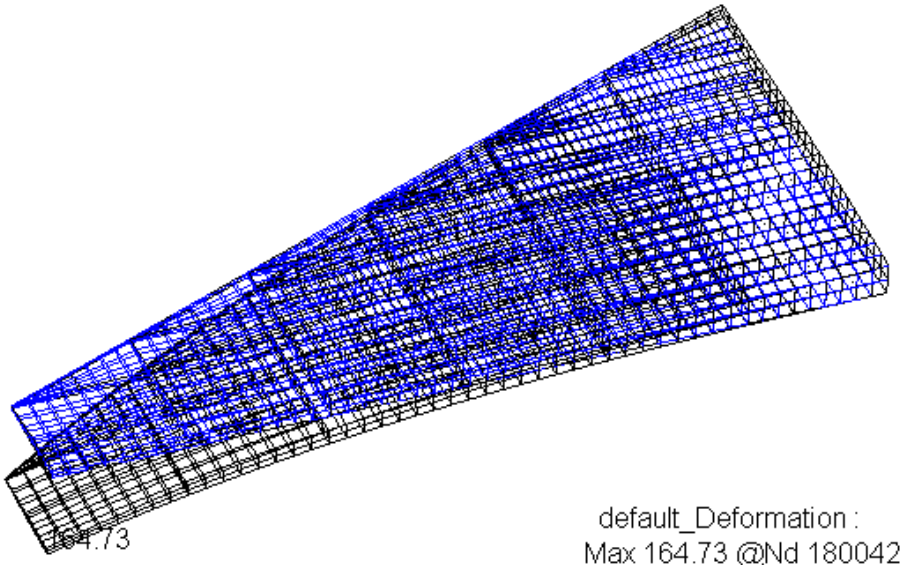

Figure 8-3 Max. Tip Displacement of Wing v1_1 with Finer Mesh

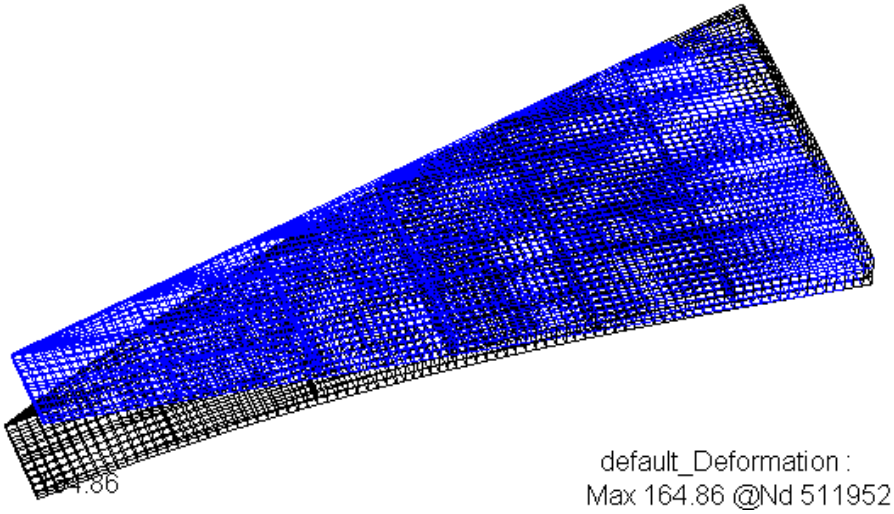

Figure 8-4 Max. Tip Displacement of Wing v1_1 with the Finest Mesh

Table 8-2 Max. Tip Displacements and First Three Natural Frequencies of the Wing v1_2

Mesh Type	Mesh Size [mm]	Element Number	Node Number	Max. Tip Disp. [mm]	1st Mode [Hz]	2nd Mode [Hz]	3rd Mode [Hz]
Coarse	200	506	694	233.77	10.58	37.36	59.59
Fine	100	1348	1082	234.58	10.58	37.42	59.62
Finer	55	2930	2465	235.09	10.58	37.21	59.66
Finest	40	5106	4491	235.20	10.57	37.17	59.62

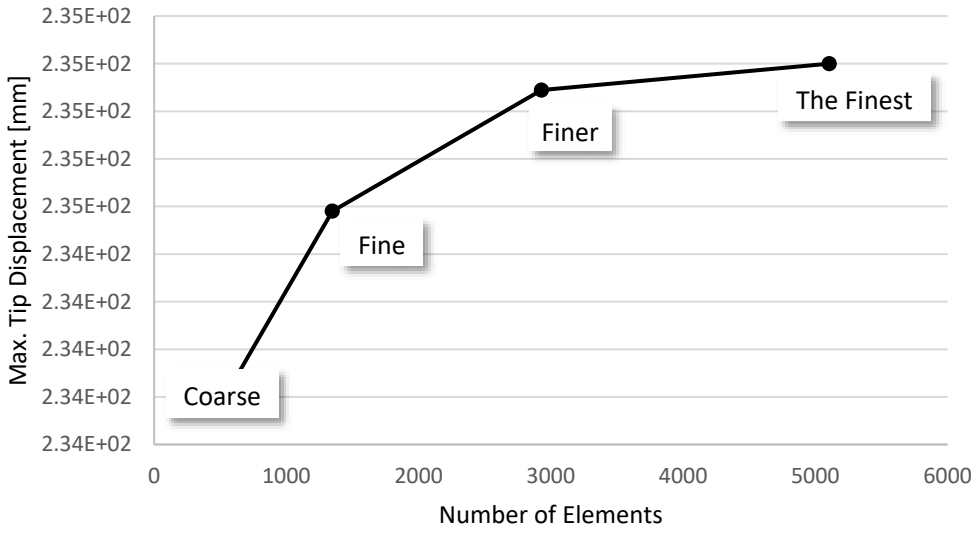

Figure 8-5 Mesh Convergence Results for Wing v1_2

Table 8-3 Max. Tip Displacements and First Three Natural Frequencies of the Wing v2_1

Mesh Type	Mesh Size [mm]	Element Number	Node Number	Max. Tip Disp. [mm]	1st Mode [Hz]	2nd Mode [Hz]	3rd Mode [Hz]
Coarse	200	511	463	247.38	10.22	12.62	13.88
Fine	100	1519	1431	248.36	10.21	12.78	13.98
Finer	55	4515	4357	248.68	10.21	12.89	14.10
Finest	40	7965	7753	248.76	10.22	12.92	14.13

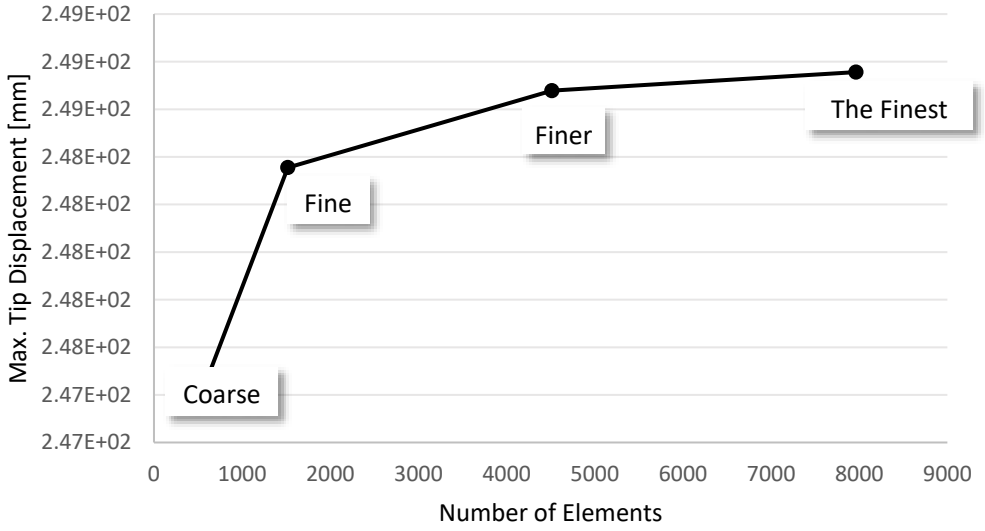

Figure 8-6 Mesh Convergence Results for Wing v2_1

Table 8-4 Max. Tip Displacements and First Three Natural Frequencies of the Wing v2_2

Mesh Type	Mesh Size [mm]	Element Number	Node Number	Max. Tip Disp. [mm]	1st Mode [Hz]	2nd Mode [Hz]	3rd Mode [Hz]
Coarse	200	558	491	243.84	10.38	21.95	23.28
Fine	100	1518	1397	245.27	10.39	22.17	23.49
Finer	55	4652	4630	245.50	10.39	22.58	23.71
Finest	40	7614	7325	245.55	10.39	22.68	23.77

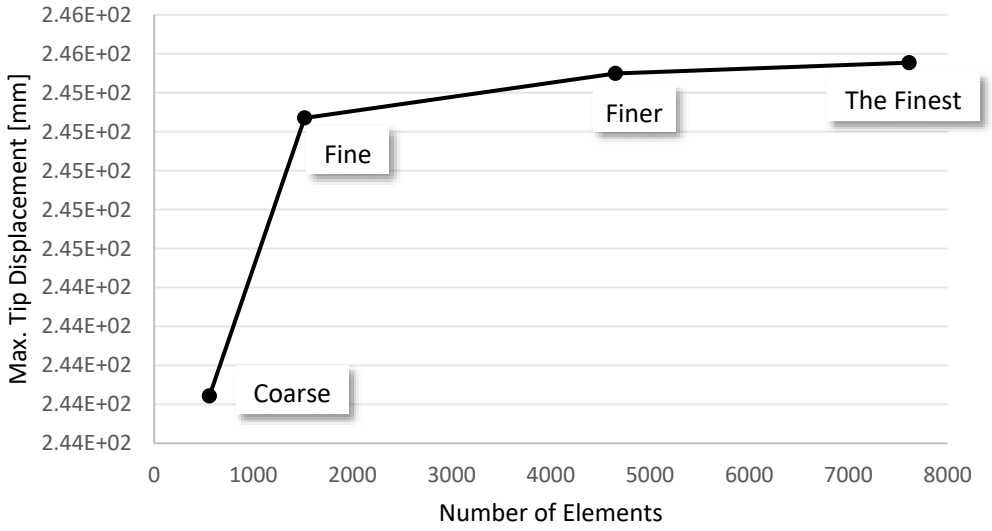

Figure 8-7 Mesh Convergence Results for Wing v2_2

Table 8-5 Max. Tip Displacements and the First Three Natural Frequencies of the Wing v2_3

Mesh Type	Mesh Size [mm]	Element Number	Node Number	Max. Tip Disp. [mm]	1st Mode [Hz]	2nd Mode [Hz]	3rd Mode [Hz]
Coarse	200	540	452	238.90	10.46	31.05	34.97
Fine	100	1672	1507	241.79	10.38	30.52	33.85
Finer	55	4476	4190	242.99	10.38	31.05	34.35
Finest	40	7920	7538	243.05	10.38	31.24	34.37

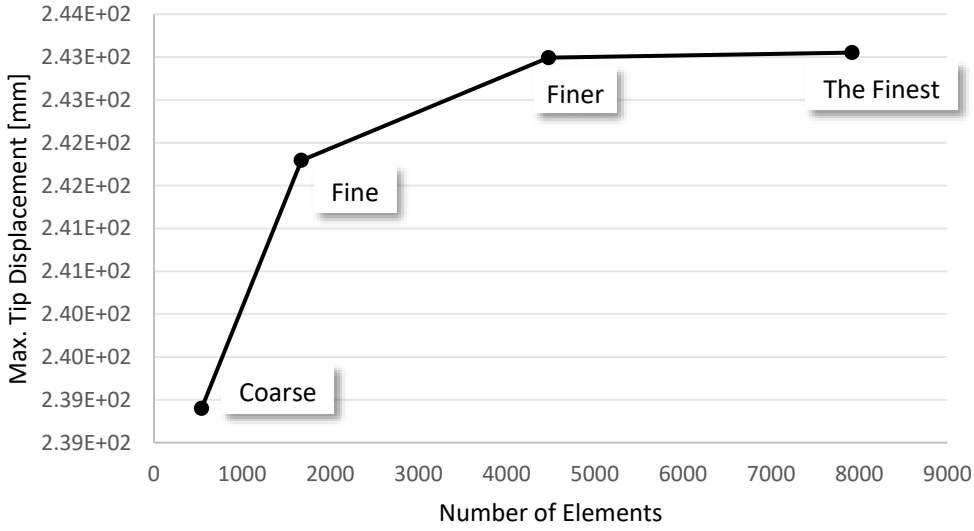

Figure 8-8 Mesh Convergence Results for Wing v2_3

Table 8-6 Max. Tip Displacements and First Three Natural Frequencies of the Wing v3_1

Mesh Type	Mesh Size [mm]	Element Number	Node Number	Max. Tip Disp. [mm]	1st Mode [Hz]	2nd Mode [Hz]	3rd Mode [Hz]
Coarse	200	500	423	242.05	10.31	32.56	34.59
Fine	100	1265	1125	243.58	10.39	32.66	35.26
Finer	55	4460	4355	245.88	10.40	32.69	35.73
Finest	40	7991	7605	246.90	10.46	32.75	35.84

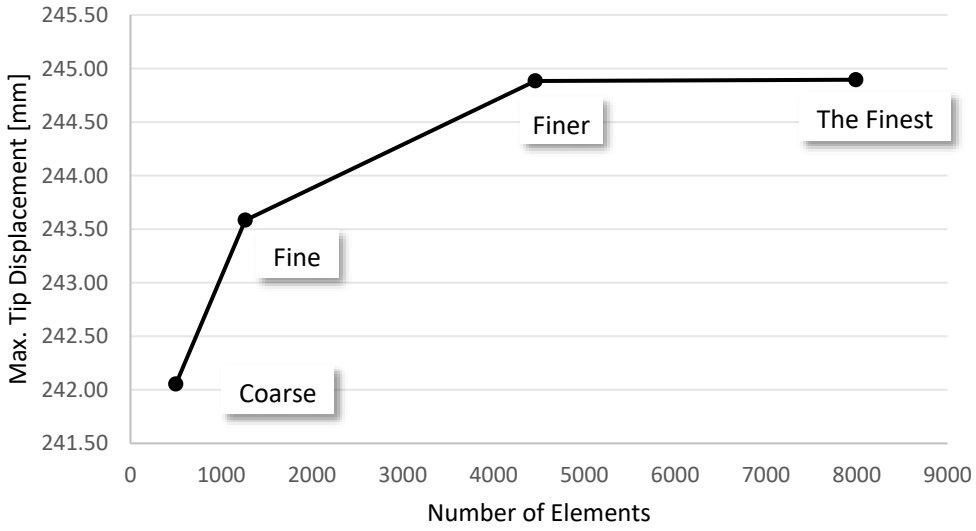

Figure 8-9 Mesh Convergence Results for Wing v3_1

Table 8-7 Max. Tip Displacements and First Three Natural Frequencies of the Wing v3_2

Mesh Type	Mesh Size [mm]	Element Number	Node Number	Max. Tip Disp. [mm]	1st Mode [Hz]	2nd Mode [Hz]	3rd Mode [Hz]
Coarse	200	510	423	246.66	10.19	35.32	39.75
Fine	100	1284	1121	244.95	10.28	35.46	40.33
Finer	55	4692	4366	244.07	10.32	35.65	40.30
Finest	40	8322	7887	242.83	10.34	35.62	41.87

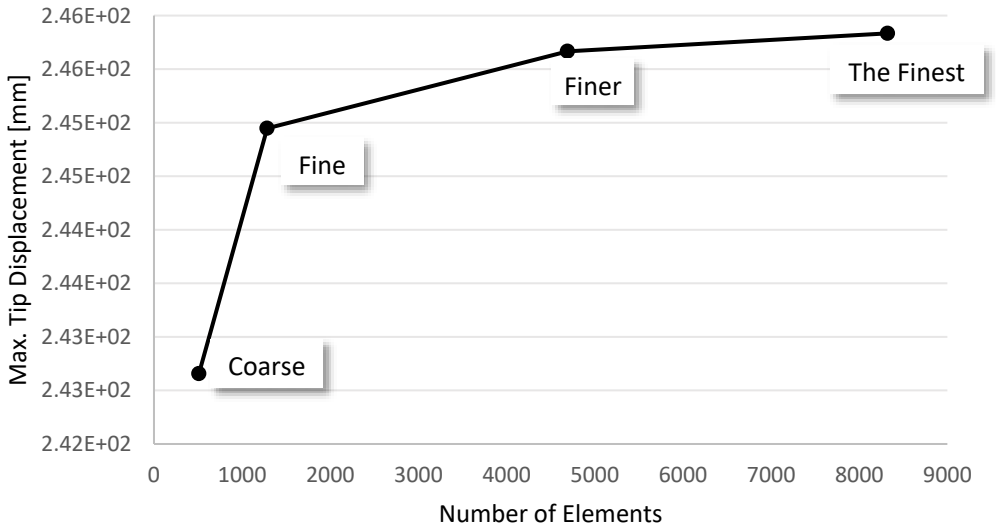

Figure 8-10 Mesh Convergence Results for Wing v3_2

Mesh convergence study for aero model

Table 8-8 Station Loads for the Coarse Aero Mesh

0.6 Mach – 7 g (Coarse Aero Mesh)						
Station	**F_x [N]**	**F_y [N]**	**F_z [N]**	**M_x [Nmm]**	**M_y [Nmm]**	**M_z [Nmm]**
1	-6.7×10^{2}	-2.3×10^{3}	4.0×10^{4}	-3.7×10^{7}	8.2×10^{6}	-1.4×10^{5}
2	-5.8×10^{2}	-2.0×10^{3}	3.5×10^{4}	-2.7×10^{7}	7.6×10^{6}	-8.8×10^{3}
3	-6.1×10^{2}	-2.1×10^{3}	3.7×10^{4}	-2.5×10^{7}	7.2×10^{6}	-1.5×10^{3}
4	-6.0×10^{2}	-2.1×10^{3}	3.6×10^{4}	-2.1×10^{7}	6.3×10^{6}	4.0×10^{3}
5	-5.5×10^{2}	-1.9×10^{3}	3.3×10^{4}	-1.7×10^{7}	5.0×10^{6}	9.0×10^{3}
6	-4.8×10^{2}	-1.7×10^{3}	2.9×10^{4}	-1.3×10^{7}	4.0×10^{6}	1.8×10^{4}
7	-3.1×10^{2}	-1.1×10^{3}	1.8×10^{4}	-6.9×10^{6}	2.8×10^{6}	4.5×10^{4}
Total	-3.8×10^{3}	-1.3×10^{4}	2.3×10^{5}	-1.5×10^{8}	4.1×10^{7}	-7.6×10^{5}

Table 8-9 Station Loads for the Fine Aero Mesh

0.6 Mach – 7 g (Fine Aero Mesh)						
Station	**F_x [N]**	**F_y [N]**	**F_z [N]**	**M_x [Nmm]**	**M_y [Nmm]**	**M_z [Nmm]**
1	-6.6×10^{2}	-2.3×10^{3}	4.0×10^{4}	-3.7×10^{7}	8.1×10^{6}	-1.5×10^{5}
2	-6.0×10^{2}	-2.1×10^{3}	3.6×10^{4}	-2.8×10^{7}	7.5×10^{6}	-8.3×10^{3}
3	-6.4×10^{2}	-2.2×10^{3}	3.8×10^{4}	-2.6×10^{7}	6.9×10^{6}	-1.5×10^{3}
4	-6.0×10^{2}	-2.1×10^{3}	3.6×10^{4}	-2.1×10^{7}	5.8×10^{6}	4.1×10^{3}
5	-5.3×10^{2}	-1.8×10^{3}	3.2×10^{4}	-1.6×10^{7}	4.7×10^{6}	8.7×10^{3}
6	-4.6×10^{2}	-1.6×10^{3}	2.7×10^{4}	-1.2×10^{7}	3.8×10^{6}	1.8×10^{4}
7	-3.1×10^{2}	-1.1×10^{3}	1.8×10^{4}	-7.0×10^{6}	2.8×10^{6}	4.5×10^{4}
Total	-3.8×10^{3}	-1.3×10^{4}	2.3×10^{5}	-1.5×10^{8}	4.0×10^{7}	-8.1×10^{5}

Table 8-10 Difference Between Coarse and Fine Aero Mesh

Difference as a Percentage						
Station	**F_x [N]**	**F_y [N]**	**F_z [N]**	**M_x [Nmm]**	**M_y [Nmm]**	**M_z [Nmm]**
1	-0.59%	-0.59%	0.59%	-0.68%	1.84%	-3.04%
2	-3.85%	-3.85%	3.85%	-3.64%	0.99%	-6.17%
3	-3.79%	-3.79%	3.79%	-3.12%	3.90%	-4.77%
4	-0.59%	-0.59%	0.59%	-0.49%	8.54%	1.05%
5	-3.53%	-3.53%	3.53%	-4.60%	7.43%	3.86%
6	-6.15%	-6.15%	6.15%	-6.62%	4.24%	2.42%
7	-0.18%	-0.18%	0.18%	-0.20%	0.18%	0.13%

B. Comparison of the Loads for Subsonic and Supersonic Conditions

0.6 Mach – 7 g (Sea Level)						
Station	**F_x [N]**	**F_y [N]**	**F_z [N]**	**M_x [Nmm]**	**M_y [Nmm]**	**M_z [Nmm]**
1	-6.7×10^{2}	-2.3×10^{3}	4.0×10^{4}	-3.7×10^{7}	8.2×10^{6}	-1.4×10^{5}
2	-5.8×10^{2}	-2.0×10^{3}	3.5×10^{4}	-2.7×10^{7}	7.6×10^{6}	-8.8×10^{3}
3	-6.1×10^{2}	-2.1×10^{3}	3.7×10^{4}	-2.5×10^{7}	7.2×10^{6}	-1.5×10^{3}
4	-6.0×10^{2}	-2.1×10^{3}	3.6×10^{4}	-2.1×10^{7}	6.3×10^{6}	4.0×10^{3}
5	-5.5×10^{2}	-1.9×10^{3}	3.3×10^{4}	-1.7×10^{7}	5.0×10^{6}	9.0×10^{3}
6	-4.8×10^{2}	-1.7×10^{3}	2.9×10^{4}	-1.3×10^{7}	4.0×10^{6}	1.8×10^{4}
7	-3.1×10^{2}	-1.1×10^{3}	1.8×10^{4}	-6.9×10^{6}	2.8×10^{6}	4.5×10^{4}
Total	-3.8×10^{3}	-1.3×10^{4}	2.3×10^{5}	-1.5×10^{8}	4.1×10^{7}	-7.6×10^{5}

Table 8-11 Station Loads for the Supersonic Flight Condition

1.3 Mach - 5.6 g (10000 ft)						
Station	**F_x [N]**	**F_y [N]**	**F_z [N]**	**M_x [Nmm]**	**M_y [Nmm]**	**M_z [Nmm]**
1	-5.2×10^{2}	-1.8×10^{3}	3.1×10^{4}	-1.6×10^{7}	2.7×10^{6}	-1.1×10^{5}
2	-4.7×10^{2}	-1.6×10^{3}	2.8×10^{4}	-1.1×10^{7}	3.1×10^{6}	-9.1×10^{3}
3	-5.1×10^{2}	-1.8×10^{3}	3.0×10^{4}	-1.1×10^{7}	3.1×10^{6}	-4.0×10^{3}
4	-5.2×10^{2}	-1.8×10^{3}	3.1×10^{4}	-9.7×10^{6}	2.8×10^{6}	-7.1×10^{2}
5	-5.1×10^{2}	-1.8×10^{3}	3.0×10^{4}	-8.0×10^{6}	2.4×10^{6}	2.6×10^{3}
6	-4.9×10^{2}	-1.7×10^{3}	2.9×10^{4}	-6.6×10^{6}	2.1×10^{6}	1.4×10^{4}
7	-3.2×10^{2}	-1.1×10^{3}	1.9×10^{4}	-4.4×10^{6}	2.1×10^{6}	4.7×10^{4}
Total	-3.3×10^{3}	-1.2×10^{4}	2.0×10^{5}	-6.7×10^{7}	1.8×10^{7}	-6.5×10^{5}

C. Optimization Results with Different Initial Design Variables

Table 8-12 Results for the Wing v1_1 with Different Initial Points

Starting from	Number of Iterations	Weight [kg]	Difference from Mid [%]
Min	21	182.19	N/A
Mid	16	187.57	2.95%
Max	21	190.32	4.46%

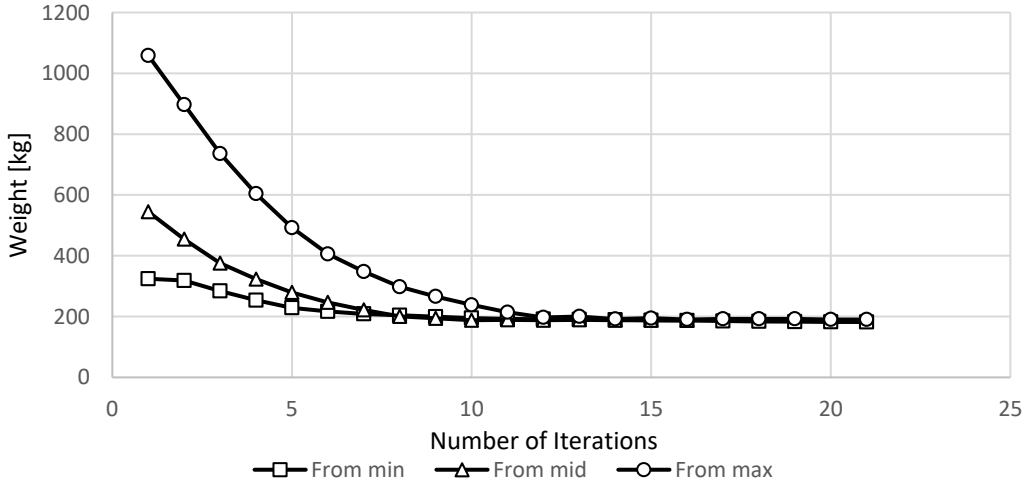

Figure 8-11 Convergence History for Wing v1_1 with Strength-Only Constraints

Table 8-13 Results for the Wing v2_1 with Different Initial Points

Starting from	Number of Iterations	Weight [kg]	Difference from Mid [%]
Min	25	190.35	1.25%
Mid	39	188.00	N/A
Max	45	188.46	0.24%

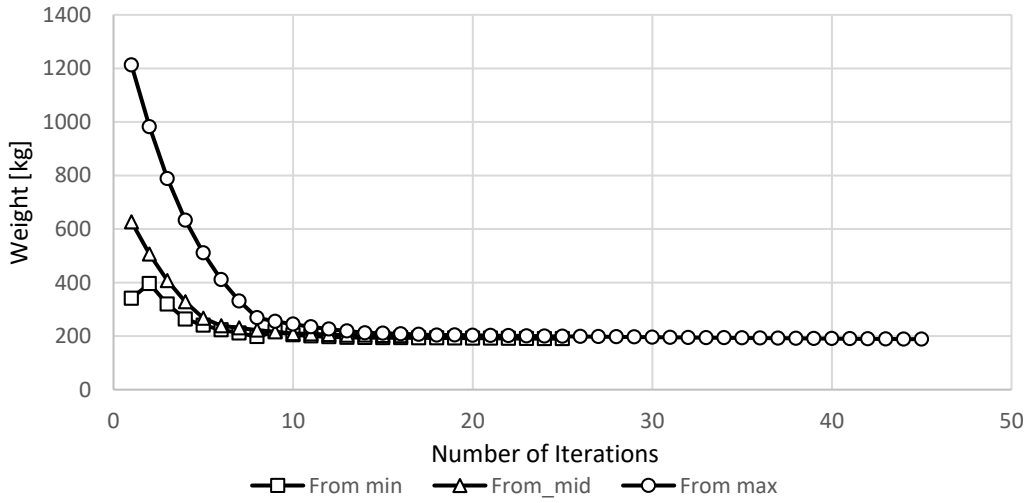

Figure 8-12 Convergence History for Wing v2_1 with Strength-Only Constraints

Table 8-14 Results for the Wing v2_2 with Different Initial Points

Starting from	Number of Iterations	Weight [kg]	Difference from Mid [%]
Min	44	149.69	0.01%
Mid	52	149.67	N/A
Max	60	150.17	0.33%

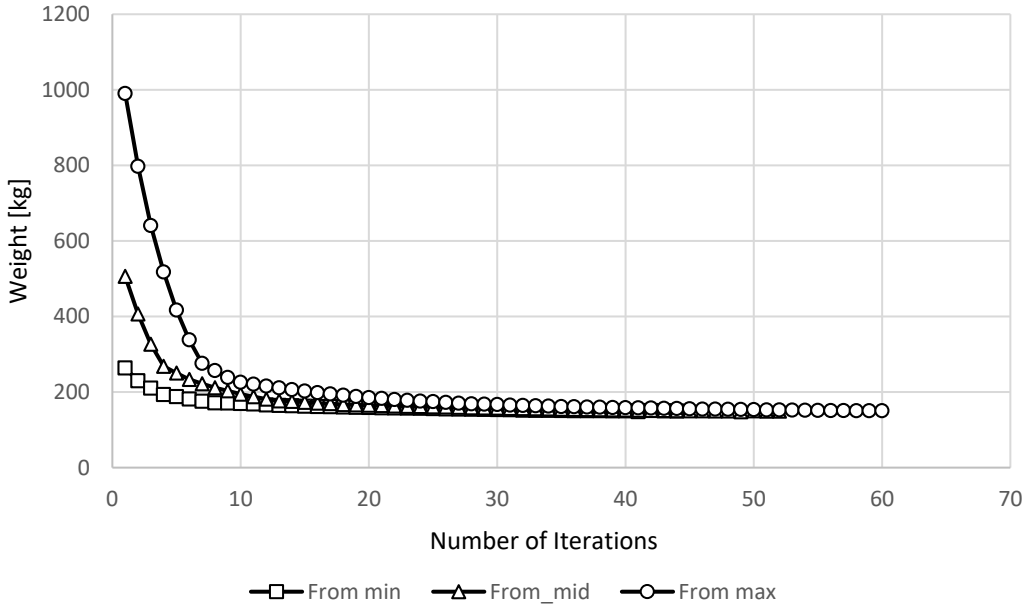

Figure 8-13 Convergence History for Wing v2_2 with Strength-Only Constraints

Table 8-15 Results for the Wing v2_3 with Different Initial Points

Starting from	Number of Iterations	Weight [kg]	Difference from Mid [%]
Min	13	167.15	1.55%
Mid	43	164.60	N/A
Max	21	166.69	1.27%

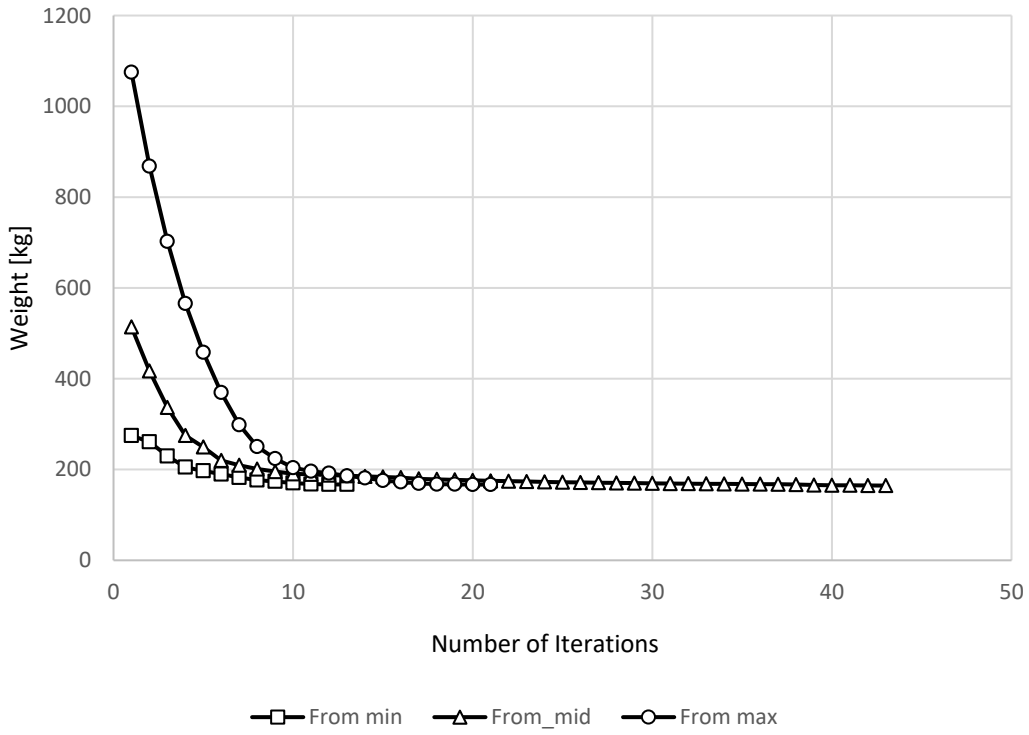

Figure 8-14 Convergence History for Wing v2_3 with Strength-Only Constraints

Table 8-16 Results for the Wing v3_1 with Different Initial Points

Starting from	Number of Iterations	Weight [kg]	Difference from Mid [%]
Min	22	157.31	0.33%
Mid	19	158.44	1.05%
Max	31	156.79	N/A

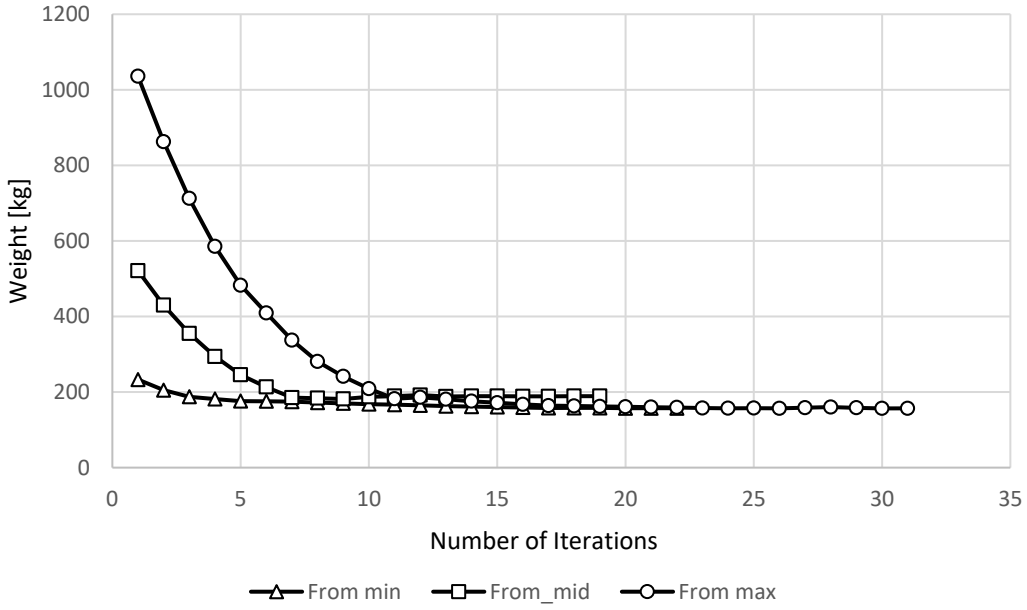

Figure 8-15 Convergence History for Wing v3_1 with Strength-Only Constraints

Table 8-17 Results for the Wing v3_2 with Different Initial Points

Starting from	Number of Iterations	Weight [kg]	Difference from Mid [%]
Min	25	140.90	1.93%
Mid	45	140.68	1.77%
Max	27	138.23	N/A

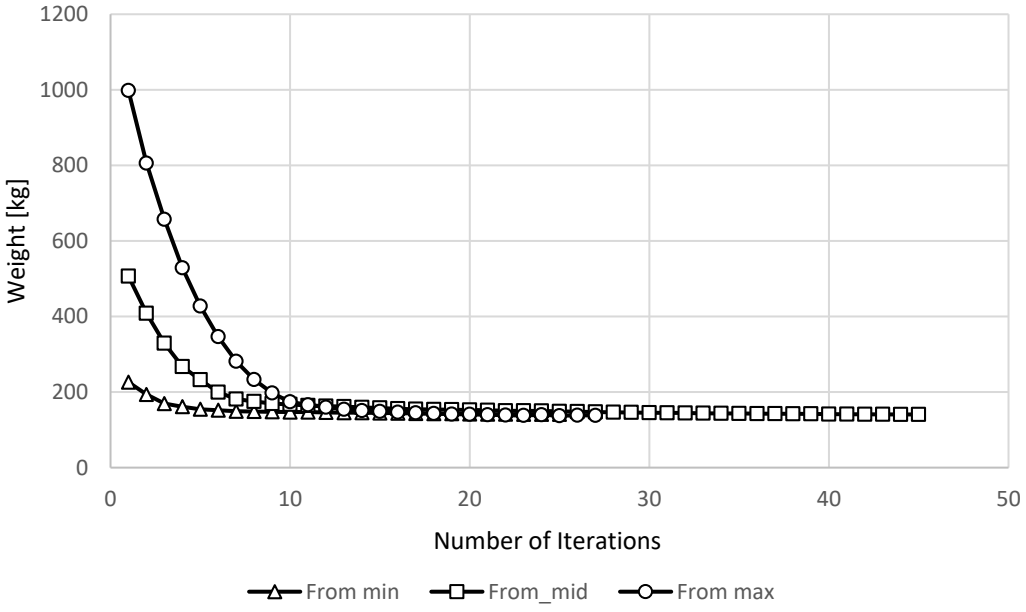

Figure 8-16 Convergence History for Wing v3_2 with Strength-Only Constraints

D. History of the Maximum Value of the Constraints

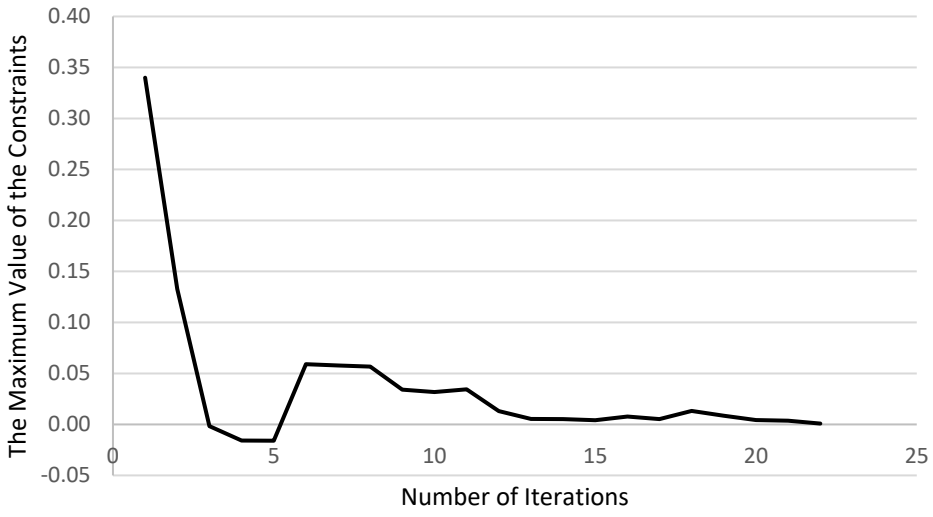

Figure 8-17 The Maximum Value of the Constraints vs Number of Iterations for Wing v1_1

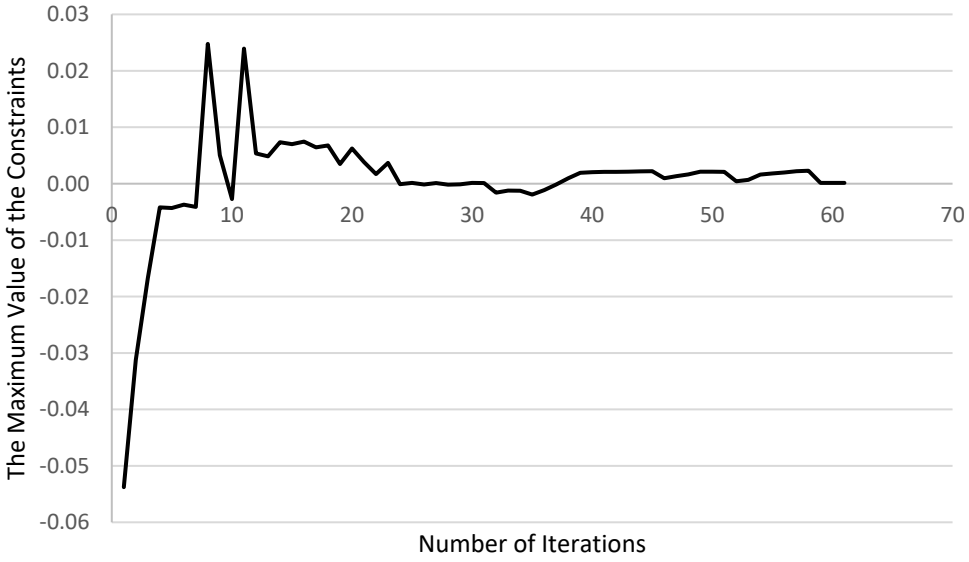

Figure 8-18 The Maximum Value of the Constraints vs Number of Iterations for Wing v2_1

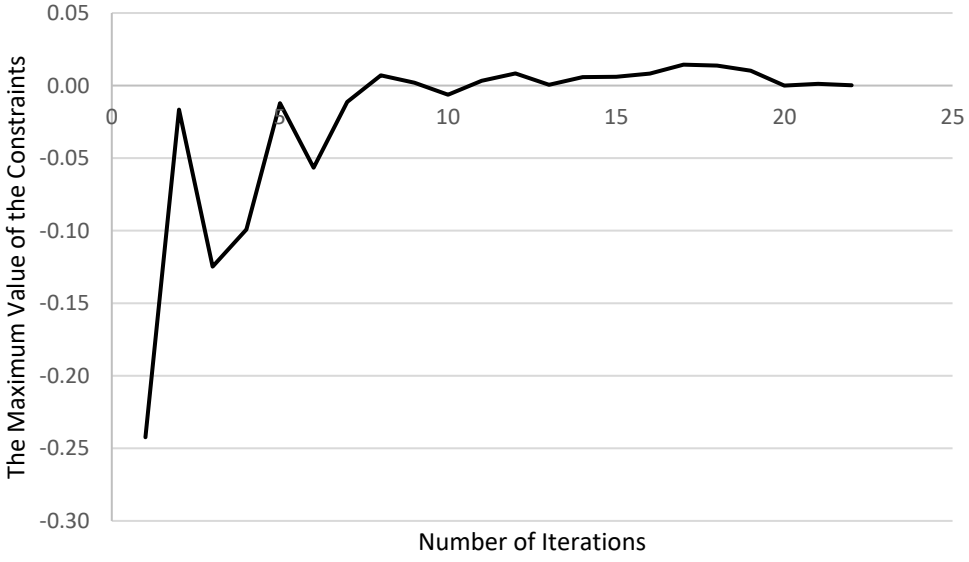

Figure 8-19 The Maximum Value of the Constraints vs Number of Iterations for Wing v2_2

Figure 8-20 The Maximum Value of the Constraints vs Number of Iterations for Wing v2_3

Figure 8-21 The Maximum Value of the Constraints vs Number of Iterations for Wing v3_1

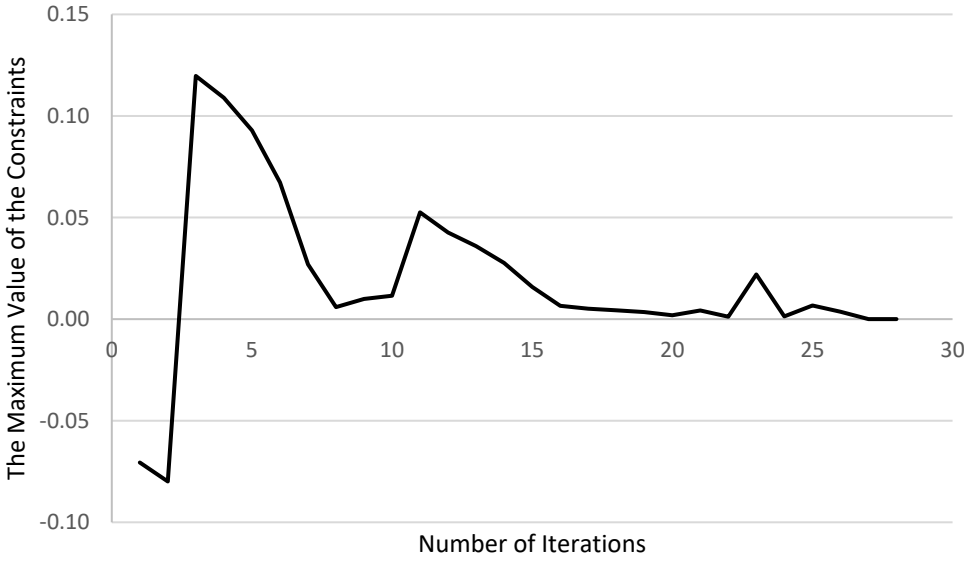

Figure 8-22 The Maximum Value of the Constraints vs Number of Iterations for Wing v3_2